Biomimetic Design of an Under-Actuated Leg Exoskeleton For Load-Carrying Augmentation

by

Conor James Walsh

B.A.I, B.A. Mechanical and Manufacturing Engineering (2003)

Trinity College Dublin

Submitted to the Department of Mechanical Engineering in Partial Fulfillment of the requirements for the Degree of

Master of Science in Mechanical Engineering

at the

Massachusetts Institute of Technology

February 2006

Signature of Author:...
Department of Mechanical Engineering
January 19th, 2006

Certified by:...
Hugh Herr
Associate Professor of Media Arts and Sciences
Thesis Supervisor

Certified by:...
Derek Rowell
Professor of Mechanical Engineering
Thesis Supervisor

Accepted by:...
Lallit Anand
Professor of Mechanical Engineering
Chairman, Department Committee on Graduate Students

Biomimetic Design of an Under-Actuated Leg Exoskeleton
For Load-Carrying Augmentation

by

CONOR JAMES WALSH

Submitted to the Department of Mechanical Engineering on
January 19th, 2006 in partial fulfillment of the requirements for the
Degree of Master of Science in Mechanical Engineering

Abstract

Metabolic studies have shown that there is a metabolic cost associated with carrying a load (Griffin et al, 2003). Further studies have shown that by applying forward propulsive forces a person can walk with a reduced metabolic rate (Farley & McMahon, 1992 and Gottschall & Kram, 2003). Previous work on exoskeleton design has not considered the passive dynamics of walking and has focused on fully actuated systems that are inefficient and heavy. In this thesis, an under-actuated exoskeleton is presented that runs parallel to the human leg. The exoskeleton component design is based on the kinematics and kinetics of human walking. The joint components of the exoskeleton in the sagittal plane consist of a force-controllable actuator at the hip, a variable-damper mechanism at the knee and a passive spring at the ankle. A state-machine control strategy is written based on joint angle and ground-exoskeleton force sensing. Positive, non-conservative power is added at the hip during the walking cycle to help propel the mass of the human and payload forward. At the knee, the damper mechanism is turned on at heel strike as the exoskeleton leg is loaded and turned off during terminal stance to allow knee flexion. The spring at the ankle engages in controlled dorsiflexion to store energy that is later released to assist in powered plantarflexion.

Kinetic and metabolic data are recorded from human subjects wearing the exoskeleton with a 75lb payload. These data are compared to data recorded from subjects walking without the exoskeleton. It is demonstrated that the exoskeleton does transfer loads to the ground with a 90% and higher load transfer depending on the phase of gait. Further, exoskeleton wearers report that the exoskeleton greatly reduces the stress on the shoulders and back. However, although a significant fraction of the payload is transferred through the exoskeleton structure, the exoskeleton is found to increase metabolic economy by 74%. By comparing distinct exoskeleton configurations, the relative effect of each exoskeleton component is determined. Metabolic data show that the variable-damper knee and ankle spring mechanisms increase metabolism by only 32%, whereas a non-actuated exoskeleton (no motor, variable-damper, or spring) increases walking metabolism by 62%. These results highlight the benefit of ankle elastic energy storage and knee variable-damping in exoskeleton design, and further the need for a lighter, more efficient hip actuator.

Thesis Supervisor: Hugh Herr
Title: Associate Professor of Media, Arts and Sciences

Acknowledgments

My time spent working on this thesis has been both interesting and enjoyable. This is due to the fact that I have gained tremendously as a result of having worked alongside many interesting and dedicated colleagues. In particular, I would like to thank Professor Herr for having given me the opportunity to work in the Biomechatronics Group and for his constant assistance and motivation. I would also like to thank 'Dr.' Daniel Paluska and Dr. Ken Pasch for their advice and mentoring during the period which I spent working on my thesis. I have gained a lot of knowledge from the both of them. Thanks also to Professor Rowell for his advice and guidance.

May I also offer thanks to those in the Biomechatronics Group with whom I have worked for making it such an exciting working environment. Goutham Reddy for all his electronics advice and techno beats. Sam Au for all his control help and runs along the banks of the river Charles. Bruce Deffenbaugh for his constant willingness to help on any topic and for all the late night cups of tea. Peter Dilworth for his design advice and life-saving chokes. William 'Guillermo' Grand for being the most dedicated person I have ever met and the late nights in Johnson track during the summer. Waleed Farahat for his help with anything related to Matlab and for always looking at the theoretical side of things. Russ Tedrake for onsite PC104 technical support. Ernesto Martinez for his sensor advice and for the headphones. Andrea Chew for the GUI help and for her phone charger. Thanks also to all other friends and staff at MIT who have made life so enjoyable and fulfilling for me.

Thanks also to Mum and Dad and to my brothers Damien and Niall for always keeping my ego in check. Thanks also to the lads at *chez Jay* and *chez Elm,* life is all the better when you're living with good friends. And finally, my thanks to that special lady - you know who you are!

This research was done under Defense Advanced Research Projects Agency (DARPA) contract #NBCHC040122, 'Leg Orthoses for Locomotory Endurance Amplification'.

Table of Contents

List of Figures

List of Tables

1 Introduction

When compared to wheeled vehicles, exoskeleton-based assistive devices have several advantages, such as allowing the user to traverse irregular terrain. Individuals employed in specific recreational, occupational and military pursuits often carry heavy loads using a variety of backpack systems. Recreational hikers and backpackers commonly carry subsistence and comfort items in backpacks (Fletcher, 1994). Fire fighters and other emergency personnel carry oxygen tanks for breathing and other equipment using backpack systems (Louhevaara *et al.,* 1985). Still further, foot soldiers often carry extremely heavy backpack loads and walk long distances across rough terrain (Fletcher, 1994).

A leg exoskeleton could benefit people who engage in load carrying by increasing load bearing capacity, speed and endurance, lessening the likelihood of injury, improving efficiency and reducing the perceived level of difficulty. Exoskeletons have been developed that amplify the strength of the wearer, apply assistive torques to the wearer's joints and support a payload for the wearer. Several exoskeleton design approaches have employed hydraulic actuators to power hip, knee and ankle joints in the sagittal plane. Such an exoskeleton design demands a great deal of power, requiring a heavy power supply to achieve system autonomy. For example, the Bleex developed at the University of California, Berkeley (Chu *et al.,* 2005) consumes approximately 2.27kW of hydraulic power, 220 Watts of electrical power, and has a total system weight of 100 lbs. This approach leads to a noisy device that has a very low payload to system weight ratio. Further, this type of exoskeleton is heavy and, if failure were to occur, could cause significant harm to the wearer.

This thesis examines biomechanical data from human walking and outlines the design of an alternative, more efficient exoskeleton that uses both passive and active elements. The exoskeleton actuation in the sagittal plane consists of a non-conservative actuator at the hip, a variable-damper mechanism at the knee, and springs at the ankle. The actuator at the hip allows power to be added at desired instances throughout the gait cycle to propel the wearer forward and to reduce the effects of exoskeleton mass.

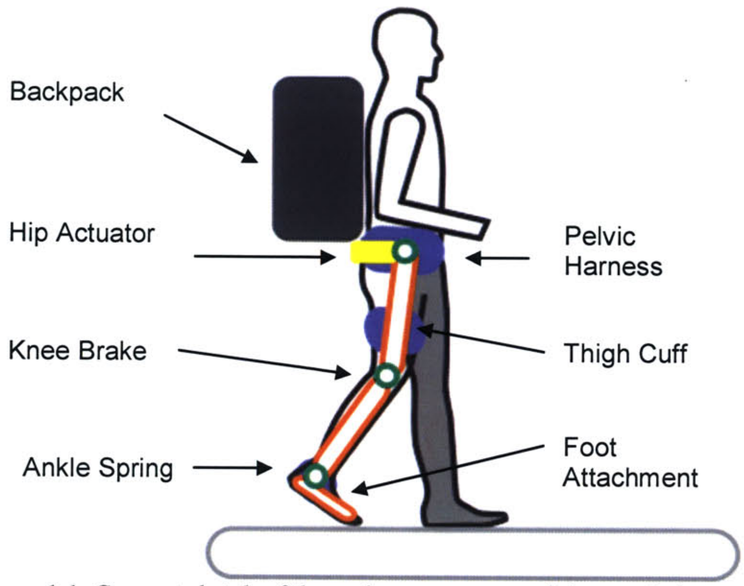

Figure 1.1 Concept sketch of the main components of the exoskeleton.

A state-machine control strategy is written based on joint angle sensing as well as ground-exoskeleton interaction sensing. When the human foot is on the ground, the exoskeleton transfers the forces from the loaded backpack to the ground. Using the force-controllable actuator at the hip, positive power is added at the hip during the stance phase to propel the mass of the human and payload forward, and to cancel the mass of the human and exoskeleton leg during the swing phase. The variable-damper mechanism at the knee is turned on during early stance to provide support for the load and is then switched off during terminal stance and swing to minimize resistance at the knee joint. The passive spring at the ankle engages in controlled dorsiflexion to store energy that is later released to assist in powered plantarflexion.

1.1 Metabolic effect of forces applied to the human during walking

Walking metabolism is set by muscles that act to perform work on the center of mass, swing the legs relative to the center of mass, and support the body weight. A number of researchers have performed metabolic experiments where external loads were applied to the body in vertical and horizontal directions. The results of these experiments are summarized below in Figure 1.2.

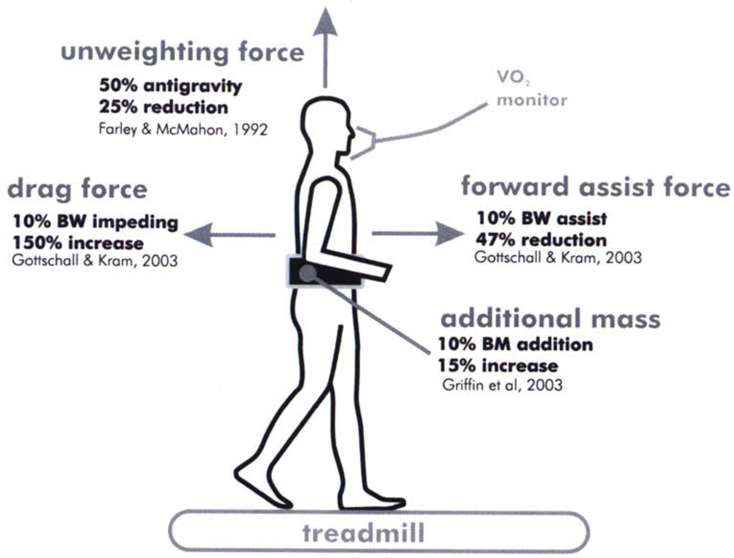

Figure 1.2 Summary of results from metabolic studies while exerting external forces on the human (Figure courtesy of Daniel Paluska).

One set of experiments recorded metabolic data while various levels of assistive and impeding external horizontal forces were applied to the waist of a subject walking on a treadmill (Gottschall and Kram, 2003). A 47% reduction in metabolic rate was found when an aiding horizontal force equal in magnitude to 10% body weight was applied to a person. Further, the study showed that the 10% value was optimal and that a larger assisting force increased metabolic demands.

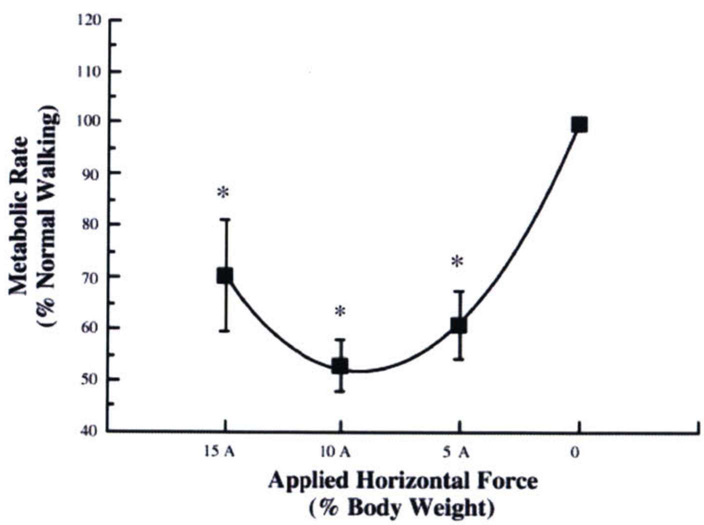

Figure 1.3 Results showing an optimal forward assistive force of 10% when walking (Gottschall and Kram, 2003).

Other metabolic experiments have been performed to examine the effect of load carrying on metabolic rate. In these investigations, it was found that net metabolic rate increased as subjects carried heavier loads and the percent increase due to loading was found to be similar at all speeds. Further, Pandolf *et al.* (1978) found that when a human carried a load equivalent to 40% of body weight, the rate of energy consumption during walking increased by approximately 40%. Griffen *et al.* (2003) found a similar result. When subjects carried loads equal to 30% of their body mass, the net metabolic rate increased 47 +- 17% above their unloaded rate.

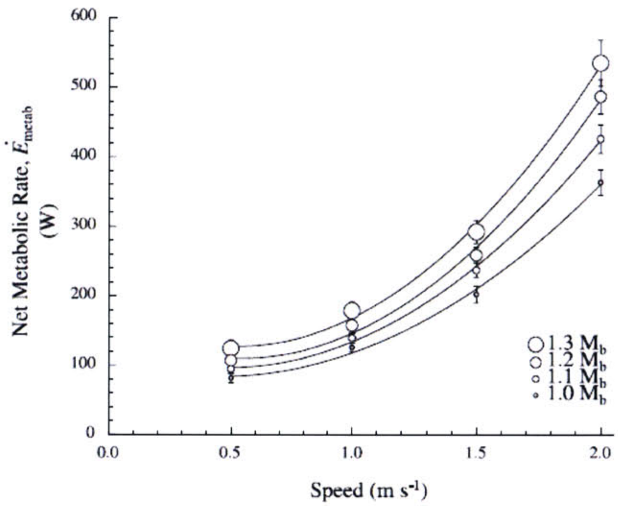

Figure 1.4 Increasing metabolic rate with increasing payload and speed (Griffen *et al.*, 2003).

Researchers have also performed experiments to examine the effect of gravity on the metabolic rate of walking (Farley and McMahon, 1992). In this investigation, a series of steel springs were used to apply a nearly constant upward force to the body through a bicycle saddle. This reduced the force that the muscles had to generate to support the weight of the body. These researchers discovered that by reducing gravity by 50%, the metabolic rate reduced by 25%.

1.2 Biomechanics of Load Carrying

There has been much research on the biomechanics of human gait published in the literature. However, there has only been a very small proportion of research published on load carrying biomechanics. Much of the work that has been done in the area has been carried out by the Military due to its relevance to soldiers carrying heavy backpack loads for long periods of time. Many associated medical injuries have been reported involving tissue damage under straps, back problems and lower limb injuries (Jones, 1983; Knapik *et al.*, 1996). Another common injury is metatarsalgia which results from the foot rotating anteroposteriorly around the distal ends of the metatarsal bones for prolonged periods of time. Other common injuries include stress fractures in the lower limb, knee pain and lower-back injuries. In one study 50% of the soldiers who were unable to complete a strenuous 20-km walk reported problems associated with the back (Knapik *et al.,* 1992). Dalen *et al.* (1978) reported a 15% incidence (17 cases out of 114) of knee pain during load-carriage from subjects walking for long periods of time. These studies all showed that backpack load carrying caused significant stress on the shoulders, back and leg joints.

During load-carrying, propulsive, braking and vertical ground reaction forces increase in proportion to increasing load carried (Harman *et al.,* 2000). In a study they found that for a body plus mass increase by 40%, ankle peak plantarflexion torque increased by 38%, knee peak extension torque increased by 98% and hip peak extension torque increased by 47%. The forward inclination of the trunk also increased significantly with load, helping to keep the body plus pack center of mass over the feet. Other adaptations to load included greater knee flexion after impact (which aids in shock absorption), reduced pelvic rotation and increased foot rotation in the sagittal plane. These results all indicate that it is likely that a load-carrying exoskeleton could reduce the injuries associated with the back and lower limbs. Further, such an exoskeleton also has the potential to reduce walking metabolism compared to unassisted load carrying.

1.3 Exoskeleton Concept and Background

Exoskeletons have been developed that amplify the strength of the wearer, apply assistive torques to the wearer's joints and support a payload being carried by the wearer. General Electric developed and tested a prototype man-amplifier, a master-slave system called the Hardiman (General Electric, 1968). It consisted of a set of overlapping exoskeletons worn by the human operator and the outer exoskeleton followed the motions of the operator. Difficulties in human sensing, stability of the servomechanisms, safety, power requirements and system complexity kept it from walking.

The Berkeley Lower Extremity Exoskeleton attached to the human foot and back. The hip, knee and ankle joints were powered in the sagittal plane with linear hydraulic actuators (Chu *et al.,* 2005). The system was powered with an internal combustion engine that was also supported by the exoskeleton. Sarcos Inc. developed a similar exoskeleton with rotary hydraulics at the joints (Huang, 2004). Both systems sensed the intent of the wearer and the robotic legs tracked the human legs so the wearer did not 'feel' the exoskeleton. Other researchers are also developing a prototype of an exoskeleton to support a payload (Liu et *al.,* 2004).

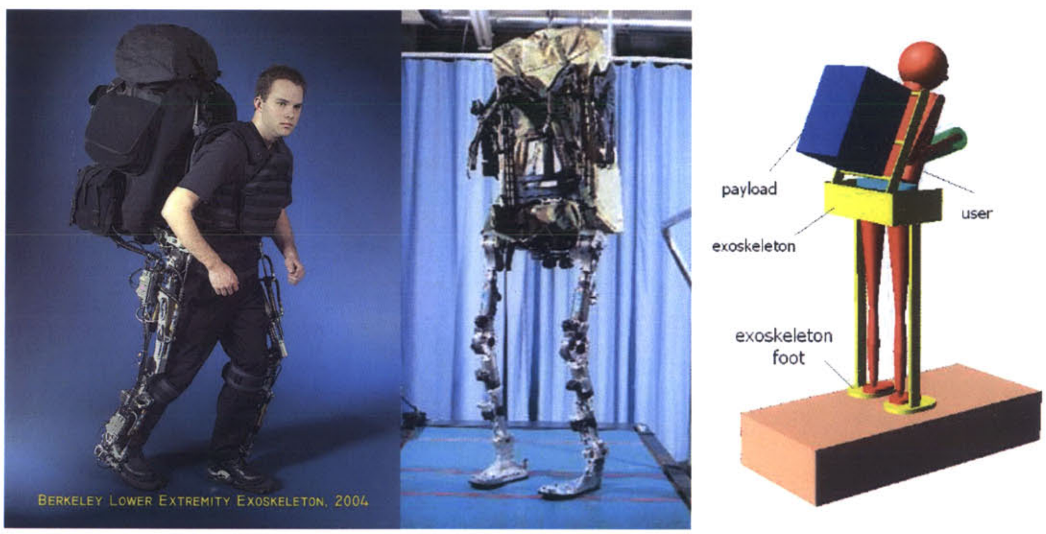

Figure 1.5 Load-Carrying Exoskeletons. In a), the Berkeley Lower Extremity Exoskeleton is shown with an IC engine attached on the back powering linear hydraulic actuators (Kazerooni *et al.*, 2005). In b), the Sarcos, Inc. exoskeleton is shown with rotary hydraulic actuators and backpack (Huang, 2004), In c), a concept sketch of another exoskeleton in development is shown (Liu *et al.*, 2004).

Vukobratović *et al.* (1990) developed exoskeletons to aid walking for paraplegics. They assisted patients to walk by commanding the exoskeleton to track pre-defined trajectories. They had limited success in assisting subjects to walk, partly due to the fact that the devices were greatly limited by material, actuation and battery technology at the time. Researchers at the University of Tsukuba in Japan developed an exoskeleton power assist system to aid people with a gait disorder to walk (Sankai, 2004). They measured the joint angles, ground contact force and myoelectrical signals of the muscles and used these signals to control the actuation applied to the wearer. The RoboWalker was developed to augment or replace muscular functions of the lower extremities (Pratt *et al.*, 2004). This was done by powering the human hip and knee joints using series elastic actuators.

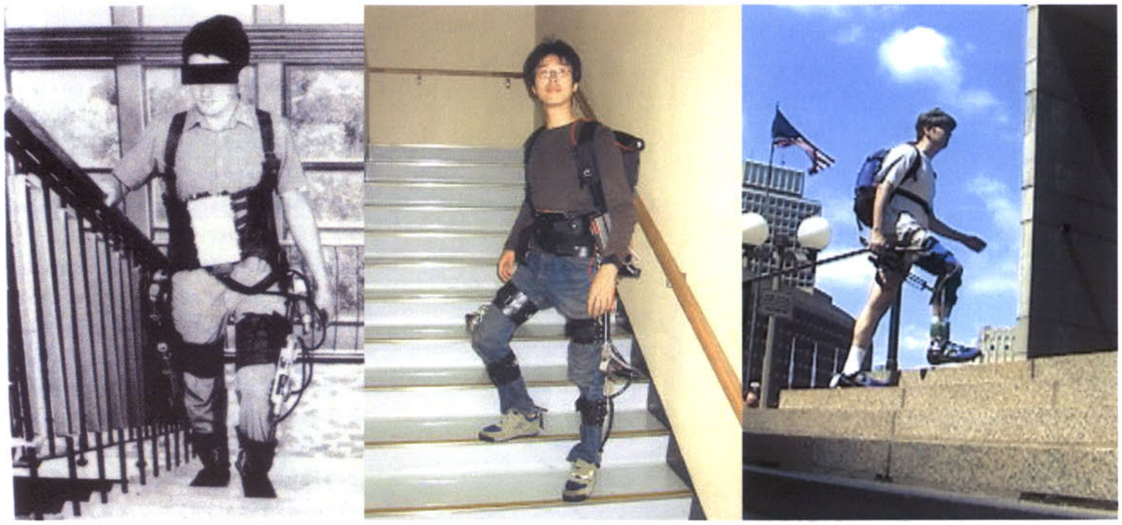

Figure 1.6 Assistive Exoskeletons. In a), a subject is shown with leg weaknesses stair climbing using an exoskeleton (Vukobratovic *et al.*, 1990). In b), the exoskeleton from the University of Tsukuba is shown. DC motors were used to power the hip and knee joint of the wearer (Sankai, 2004), In c), the RoboWalker from Yobotics Inc. is shown. It used series elastic actuators to power the joints (Pratt *et al.*, 2004)

1.4 Motivation for a Semi-Active Approach

Evidence from biology (Farley and Ferries, 1998) and passive walkers (McGeer, 1990) suggest that legged locomotion can be very energy efficient. The exchange between potential and kinetic energy suggests that walking may be approximated as a passive mechanical process. Passive walkers reinforce this fact. In such a device, a human-like pair of legs settles into a natural gait pattern generated by the interaction of gravity and inertia. Although a passive walker requires a modest incline to power its movements, researchers have enabled these robots to walk on level ground by adding just a small amount of energy at the hip or ankle joint (Wisse, 2004). Figure 1.7 shows some examples of actuated passive walkers. MIKE was a 2D pneumatically activated biped with knees, weighing only 6 kg. The actuation is realized with McKibben muscles at the hip joints. Denise is from the University of Delft and stands 1.5 m tall, weighs 8 kg, and walks with a velocity of 0.4 m/s. The hip joint was actuated and consisted of a bisecting mechanism which linked the two legs to each other. The ankles and knees were completely passive, except that the knee was provided with a controllable latch. The

Cornell biped was actuated at the ankle where it pushed off to restore energy lost, mostly due to heel strike collisions (Collins *et al.*, 2005). The hip joint was fully passive and a latch at each knee passively locked the shank throughout stance.

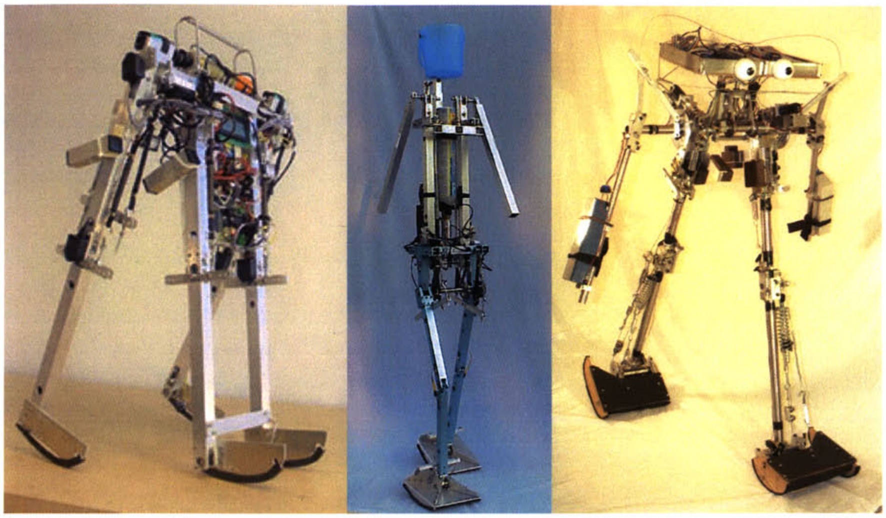

Figure 1.7 Passive Dynamic Walkers. In a), a 2D pneumatically activated biped with knees, MIKE, is shown (Wisse, 2004). In b), Denis, a powered passive walker from Delft is shown. The robot is only actuated at the hip and can walk with a human like gait (Wisse, 2004). Lastly, in c), the Cornell biped is shown. It is actuated at the ankle only (Collins *et al.*, 2005).

Recent evidence suggests that elastic energy storage is also critical for efficient bipedal ambulation. Palmer (2002) characterized the human ankle during the stance phase of walking in terms of simple mechanical spring elements. He showed that the sagittal plane dynamics of a normal ankle can be reproduced at least at slow to moderate walking speeds. Further, researchers have studied the placement of appropriate springs in parallel with the human (van den Bogert, 2004). It was shown in numerical simulation that an exoskeleton using passive elastic devices substantially reduced the muscle force and metabolic energy in walking.

1.5 Contributions

This thesis presents an alternative architecture to a fully actuated exoskeleton. Specifically, human walking data was analyzed and design specifications for actuation at the hip, knee and ankle joints were extracted. A controller was written that controls actuation at the hip and knee that allows the exoskeleton to support a payload and apply assistive torques to the wearer. The hypotheses guiding this research effort follow.

1.6 Hypotheses

The following are the specific hypotheses of this research effort:

1. An under-actuated leg exoskeleton consisting of a force-controllable actuator at the hip, a variable-damper mechanism at the knee and a spring at the ankle will improve metabolic walking economy for carrying a 75lb load compared with unassisted loaded walking.
2. The same exoskeleton will improve metabolic walking economy for carrying a 75lb load compared with a minimal mass non-actuated exoskeleton (no motor, no variable-damper or spring).
3. An under-actuated exoskeleton will transfer its own weight and that of a payload to the ground during walking.

1.7 Thesis Outline

Chapter 2 provides background on some of the terms associated with human walking. It also examines human walking data at the hip, knee and ankle joint in the sagittal plane and provides design specifications for the exoskeleton. Chapter 3 describes the mechanical design of the exoskeleton and the characterization of the components used for actuation whilst Chapter 4 outlines the implementation of the electronics test-bed for sensing and control as well as describes the state-machine controller used to control the hip and knee. Chapter 5 details the experimental methods and metrics for quantifying the metabolic cost and Chapter 6 presents and discusses the results. Chapter 7 summarizes the conclusions of this work and Chapter 8 provides recommendations for future work.

2 Biomechanical Gait Analysis

This chapter provides background on describing human walking biomechanics and introduces the relevant terminology used in examining it. The energetics of walking is described and the significant regions of positive and negative power of the three main leg joints during a single walking cycle are highlighted. From this description, specifications for joint actuation in the sagittal plane are extracted.

2.1 Human Gait

Walking uses a repetitious sequence of limb motion to move forward while simultaneously maintaining stance stability. The beginning of the gait cycle is represented as initial contact of one foot with the gait surface, usually termed heel strike (Perry, 1992). Walking is three dimensional but this thesis focuses only on the sagittal plane as the largest motions, torques and powers are in this plane.

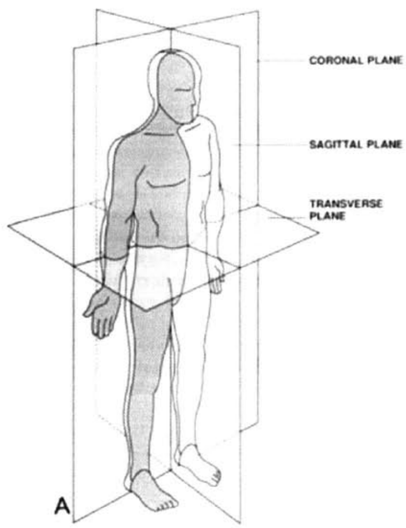

Figure 2.1 Reference planes of body in standard anatomic position (Inman *et al.*, 1981).

The sign convention that is used is that each joint angle is measured as the positive counterclockwise displacement of the distal link from the proximal link (zero in standing position) with the person orientated as shown in Figure 2.2. In the position shown, the hip angle is positive whereas both the knee and ankle angles are negative. Torque is measured as positive acting counterclockwise on the distal link.

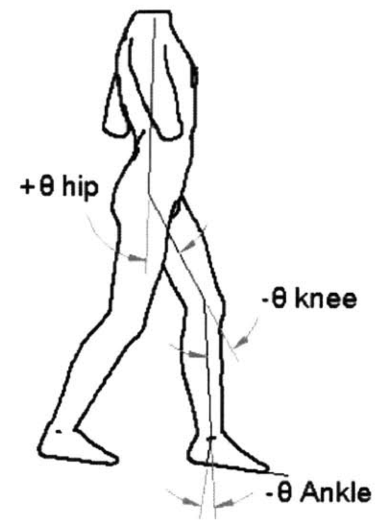

Figure 2.2 Sign convention used for joint angles. Each joint angle is measured as the positive counterclockwise displacement from the distal link to the proximal link (Chu *et al.*, 2005).

Very simply, walking can be thought of as two phases, a stance phase and a swing phase. During the stance phase the muscles at the hip, knee and ankle generally act to decelerate and stabilize the body. At the end of the stance phase the ankle is in powered plantarflexion where it provides the energy to power the body forward. At the start of the swing phase, the hip gives a burst of energy to raise the leg and swing it forward. Figure 2.3 outlines the eight main phases of the walking cycle.

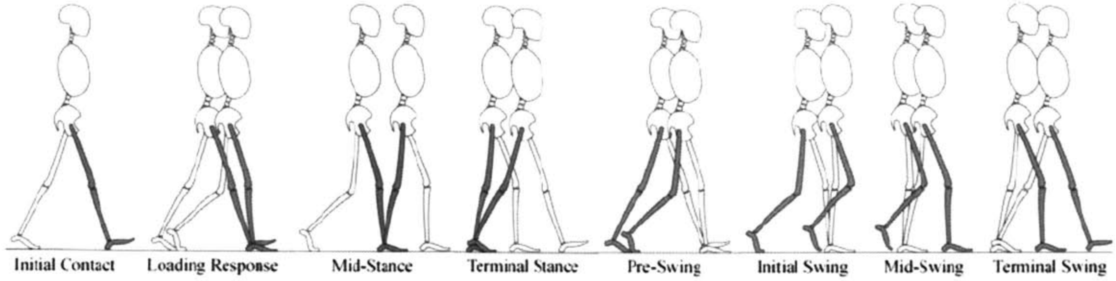

Figure 2.3 The eight main phases of the walking cycle from heel strike to heel strike (Perry, 1992).

The kinetic and gravitational potential energy of the center of mass of the human are approximately 180 degrees out of phase in walking. At mid-stance in walking, the gravitational potential energy is at its maximum and the kinetic energy is at its minimum. Because these energies are approximately 180 degrees out of phase with each other and their fluctuations are similar in magnitude, substantial pendulum-like energy exchange occurs. In human walking, as much as 60-70% of the mechanical energy required to lift and accelerate the center of mass is conserved by this energy transfer mechanism (Farley and Ferris, 1998). Mechanical energy savings are maximized at moderate walking speeds, and fall toward zero at very low and very high walking speeds. This energy transfer mechanism in walking is often referred to as the "inverted pendulum mechanism".

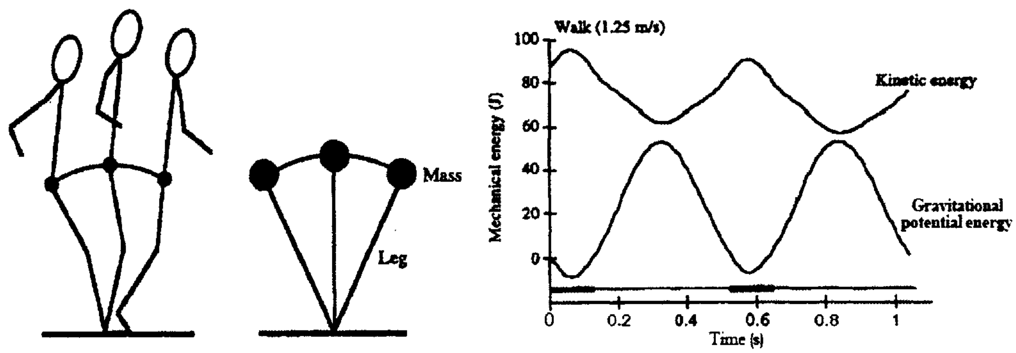

Figure 2.4 A simple model of walking. In a), an illustration of the inverted pendulum type motion of the human during walking is shown. In b), the potential and kinetic energy fluctuations during walking are shown (Farley and Ferris, 1998).

2.2 Muscle Activity in Gait

Many muscles responsible for walking contract isometrically to allow for maintenance of upright posture against gravity. Brief bursts of more energy expensive contraction of muscle are added when needed to provide power for forward motion (Inman *et al.,* 1981). Positive work is performed when a muscle is concentrically contracting whilst negative work is said to be performed when a muscle is eccentrically contracting. Much muscle activity in walking is isometric or eccentric. Negative work allows the limbs to absorb energy while resisting the pull of gravity, yet remain metabolically efficient. Positive work of muscles during walking allows acceleration of limbs and powers such activities as flexion of the hip during pre-swing.

Figure 2.5 illustrates the significant regions of positive and negative power during the gait cycle. The red and blue circles highlight regions of positive and negative power respectively at the hip, knee and ankle joints at various instances of the gait cycle. The majority of positive power during a gait cycle comes from H1 and H3 at the hip and A2 at the ankle. The knee largely dissipates energy apart from the K2 region as the body's center of mass is raised. The regions A1 at the ankle and H2 at the hip are instances of significant negative power as the muscles control the body's forward movement against gravity.

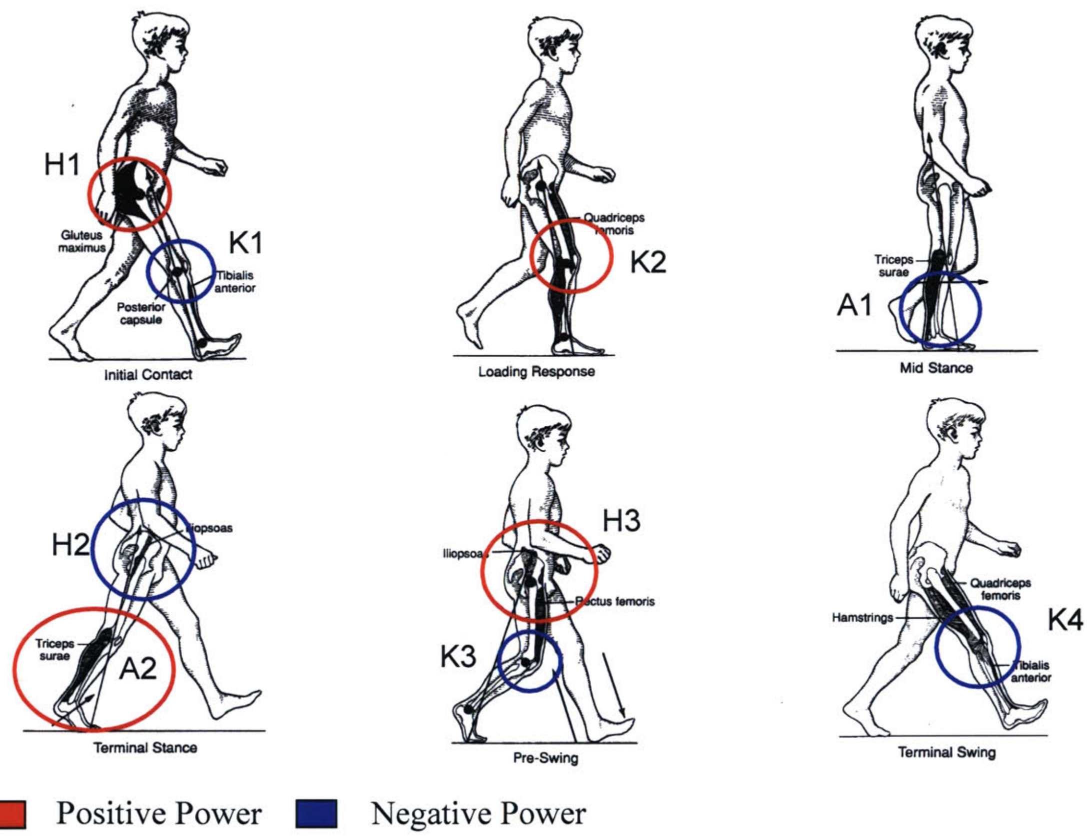

Figure 2.5 Significant regions of positive and negative work in walking. The instances labeled here are referred to later in this paper when examining human walking data. (Adapted from Inman *et al.*, 1981)

The regions of positive and negative power highlighted in Figure 2.7 are well documented in the literature and can generally be seen in any set of walking data (Inman *et al.*, 1981). However, there is a large amount of variation in the magnitude and duration of the regions across different subjects and different walking speeds.

2.3 Human Walking Biomechanics in the sagittal plane

In this thesis, human walking data were used in order to specify the design requirements for the components at the exoskeleton joints. The power profiles for the hip, knee and ankle in the sagittal plane were plotted for a number of sets of gait data (Kirtley, 1998 (old and young); Linskell, 1997; van den Bogert, 2004). The biomechanical data presented in this thesis come from studies where camera systems tracked markers placed on a subject's legs while they walked on a set of force plates. The marker position data and the force plate data are then used to calculate the kinematics and kinetics of movement. Joint power is the dot-product of the moment at the joint and the angular velocity of the distal segment with respect to the proximal segment. Depending on the direction of the movement and the direction of the angular velocity, the power can be either positive or negative. In the biomechanics literature, positive power is called 'power generated', and negative power is called 'power absorbed'.

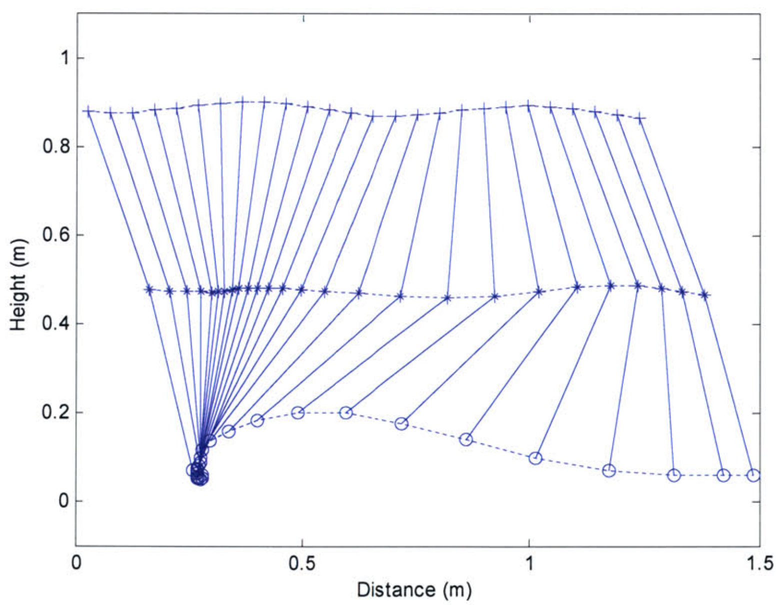

Figure 2.6 A plot of the gait data showing the trajectory of the hip, knee and ankle joint (Data from Kirtley, 1998 (old)).

A conservative estimate of the weight of the exoskeleton and payload was chosen to be 60kg and the normative data were scaled to a 60kg person in order to estimate the torques and powers required at the joints of the exoskeleton. In estimating the torque and power requirements at the hip joint of the exoskeleton, the normative data were scaled to a

135kg person. This was due to the fact that the design goal was to have the actuator at the hip assist the exoskeleton (60kg) as well as the human (75kg). The human was assisted by means of a thigh cuff attachment between the human and exoskeleton thigh. The pelvic tilt angle was added to the hip angle to yield a single angle which represented the angle between the human torso and the thigh in the sagittal plane. The goal was to design an exoskeleton to assist in load carrying at slow walking speeds. As a result, the data used to extract specifications for actuation at the joints were that for a walking speed of 0.8m/s (Kirtley, 1998).

A number of assumptions were made in the application of the human biomechanical data to the design of the exoskeleton. The first was that the exoskeleton carried its own weight, power supply and payload. The second assumption was that joint torques and joint powers scaled linearly with mass. This second assumptions seemed reasonable given that increases in vertical ground reaction force have been found to be proportional to increases in the load being carried (Llyod, 2000). The third assumption was that the exoskeleton would not greatly affect the gait of the wearer.

2.3.1 Hip Kinematics and Kinetics

During normal walking, the human hip joint follows an approximate sinusoidal pattern as can be seen in Figure 2.7. The thigh is flexed forward on heel strike and then the hip moves through extension during stance as the body is pivoted over the stance leg in a pendulum-like motion. The range of motion of the hip joint can be seen to vary between -20 to 45 degrees.

At heel strike there is a sharp increase in hip torque as the leg accepts the weight of body to begin the stance phase. A peak negative hip torque of approximately 130Nm is experienced as the leg accepts load and the body's center of mass is raised. A maximum positive torque of about 100Nm occurs during the swing phase as the hip muscles provide energy to swing the leg forward.

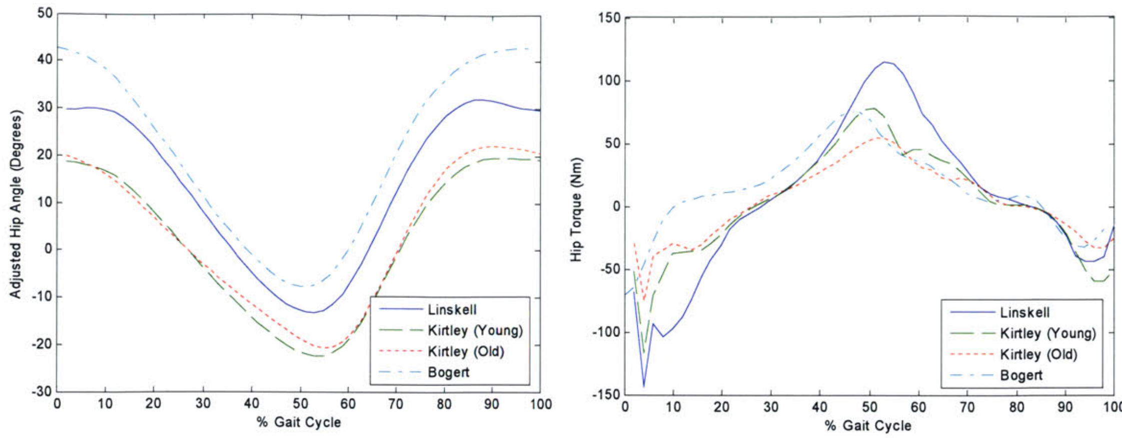

Figure 2.7 Hip angle and torque profiles scaled for a 135kg person.

The power profile at the hip as a function of gait cycle is shown in Figure 2.8. On heel strike the hip abductors move from eccentric to isometric to concentric activity, elevating the pelvis in preparation for swing. During mid-stance, eccentric hip flexor activity controls the body being carried forward by momentum. The hip contributes to propulsion as it shifts from eccentric to concentric activity which will advance the extremity into the swing phase by lifting the leg and swinging it forward. This region is the muscular system's second largest contribution of propulsive power during the gait cycle and is often referred to as 'pull-off'.

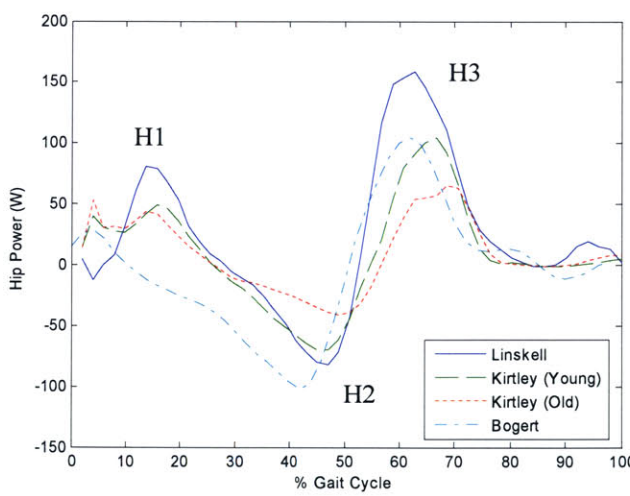

Figure 2.8 Hip joint power profile scaled for a 135kg person as a function of the gait cycle. H1 is a small region of positive power, not always present, which corresponds to concentric hip extensor activity during loading response. H2 is a region of negative power, corresponding to eccentric hip flexor activity during mid-stance. Lastly, H3 is a region of positive power, corresponding to concentric activity in the hip flexors during pre-swing and initial swing.

The hip joint is the preferred location for a non-conservative actuator as proximal mass is less expensive metabolically in walking than distal mass. An actuator could assist by adding power in the H1 and H3 regions. The maximum positive power required is approximately 150W and this occurs as the leg is beginning the swing phase. Also from Figure 2.8 it can also be seen that a spring placed at the hip joint could absorb the negative energy in H2 and release it during H3 to assist in swinging the leg forward. In Figure 2.9 an approximate linear relationship can be seen between the hip torque and angle during the stance phase of the walking cycle. The spring constant for such an "extension spring" was estimated as 115Nm/rad.

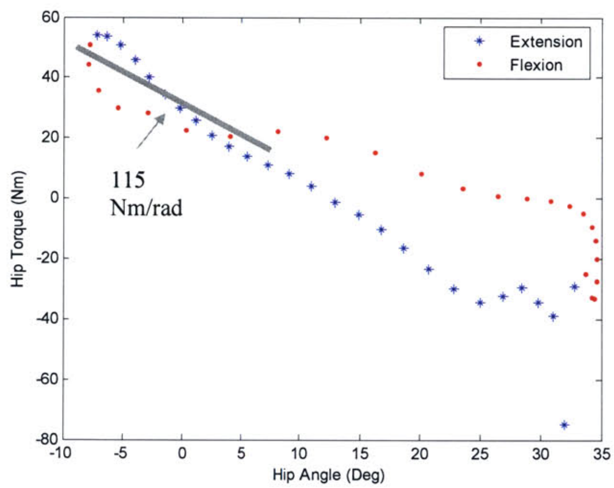

Figure 2.9 The hip angle plotted versus hip torque for a walking speed of 0.8m/s (Kirtley, 1998 (old)).

A summary of the specifications for actuation at the hip joint of the exoskeleton are shown in Table 2.1. The approach taken in this thesis was to use a non-conservative actuator at the hip. Although a non-conservative actuator at the hip is heavier than a simple spring, it was believed that it would not be too detrimental to walking metabolism as the mass was proximal. A possible hybrid approach might be to use a small motor in conjunction with the spring in the stance phase to aid the leg further in the swing phase.

Range of Motion	-20 deg to 45 deg
Max Joint Velocity	4 rad/s
Max Joint Torque	130 Nm
Max Joint Power	150 Watts
Extension Spring Constant	115 Nm/rad

Table 2.1 Specifications for the hip joint of the exoskeleton that were extracted from the gait data

2.3.2 Knee Kinematics and Kinetics

Figure 2.10 shows plots of the angle and torque profile of the knee joint as a function of gait cycle. In early stance there is initial flexion-extension of the knee to help maintain a near horizontal trajectory of the body's center of mass. After the initial flexion-extension the knee remains locked for the remainder of the stance phase. The knee then undergoes flexion of approximately 60 degrees to allow for foot clearance during the swing phase. On heel strike, the knee bends slightly while exerting a maximum negative torque of 30Nm as the leg accepts the weight of the human. This is followed by a large positive extension torque of approximately 50Nm that keeps the knee from buckling during early stance and also assists in straightening the leg.

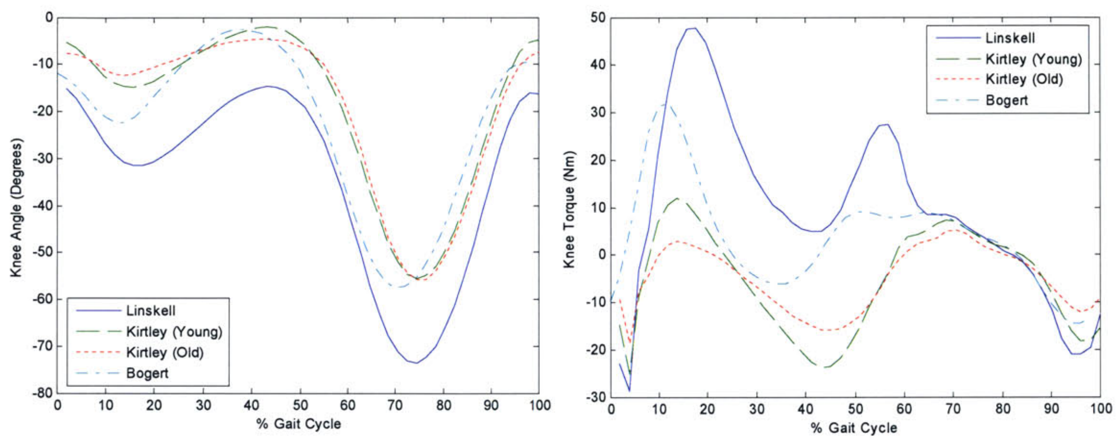

Figure 2.10 Knee angle and torque profiles scaled for a 60kg person.

Figure 2.11 outlines the power of the knee as a function of gait cycle. It can be seen that the power is largely negative indicating that the knee absorbs power for the majority of the gait cycle. At heel strike there is a region of negative power followed by a period of positive power as the knee goes through stance flexion-extension. This is followed by a period of negligible joint power as the knee is passively extended. Here the quadriceps are inactive and it is the ground reaction forces, as well as activity in the ankle plantar flexors, that keep the knee stabilized in extension. For a large part of the swing phase the leg has a pendulum like motion with the knee varying the damping to control the swing leg duration.

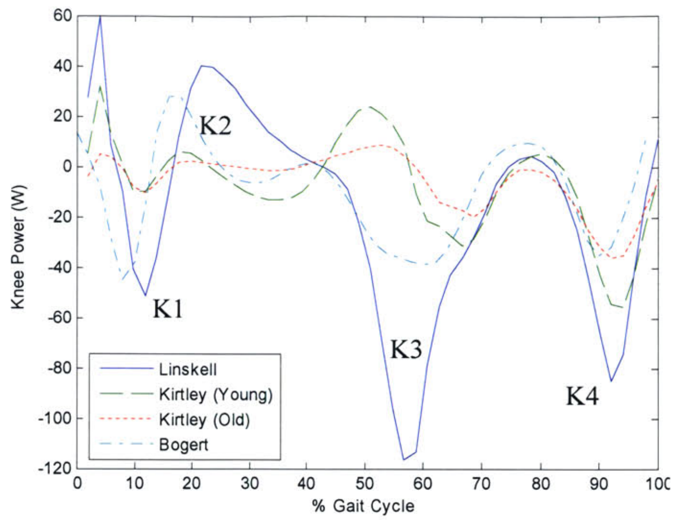

Figure 2.11 Knee joint power profile scaled for a 60kg person as a function of gait cycle. K1 is a region of negative power, corresponding to eccentric knee extensor activity during the loading response K2 is a region of positive power, corresponding to concentric knee extensor activity during mid-stance. K3 is a region of negative power, corresponding to eccentric activity in the rectus femoris during pre-swing. K4 is a region of negative power, corresponding to eccentric activity in the hamstrings during terminal swing.

It can be seen in Figure 2.11, that during flexion-extension during early stance, the knee behaves like a spring as there is a region of negative energy followed by a region of positive energy of similar size. Figure 2.12 shows a plot of knee angle vs. torque and a linear relationship can be seem during the stance phase. For the remainder of the gait cycle, the knee acts like a variable-damper to control leg during the swing phase.

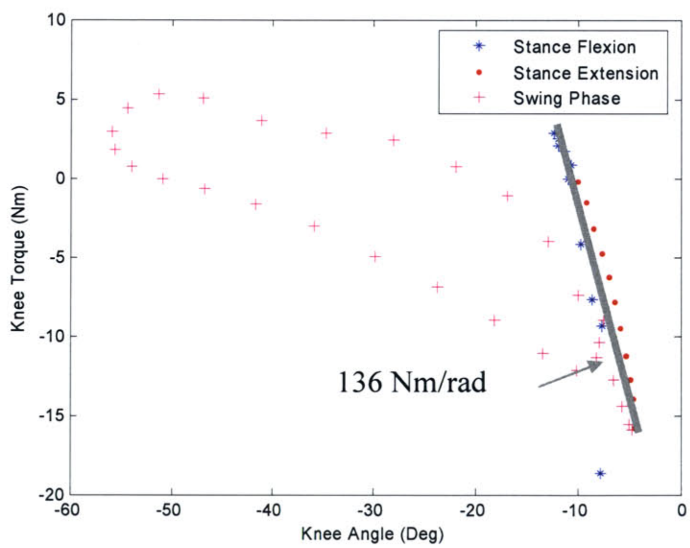

Figure 2.12 A plot of knee angle versus knee torque for the walking cycle. During the stance phase there is a linear relationship between torque and angle. It can be seen that the knee behaves primarily as a variable-damper throughout the gait cycle (Kirtley, 1998 (old)).

From the gait data it appears that the ideal actuator for the knee of the exoskeleton is a spring with a variable-damper. The spring would provide a resistive torque at the knee on heel strike as energy is absorbed and this energy is then released to aid in knee extension during stance. During the swing phase, the variable-damper would be engaged to control the swinging of the leg. It should be noted, for walking on a decline or down stairs, the variable-damper would be required during the stance phase to dissipate energy. However, for this thesis a variable-damper mechanism was used without the spring. The damper was able to provide the necessary resistive torque during stance but the negative energy was dissipated as heat.

Range of Motion	0 deg to 90 deg
Max Braking Torque	50 Nm
Stance Spring Constant	136 Nm/rad

Table 2.2 Specifications for the knee joint of the exoskeleton that were extracted from the gait data.

2.3.3 Ankle Kinematics and Kinetics

The ankle joint experiences a range of motion of approximately 15 degrees in both directions during normal human walking. During the mid and late stance phases of walking the ankle eccentric plantar flexor activity creates negative joint torque as the ankle controls the forward movement of the center of mass. The peak torque experienced by the ankle is approximately 90Nm.

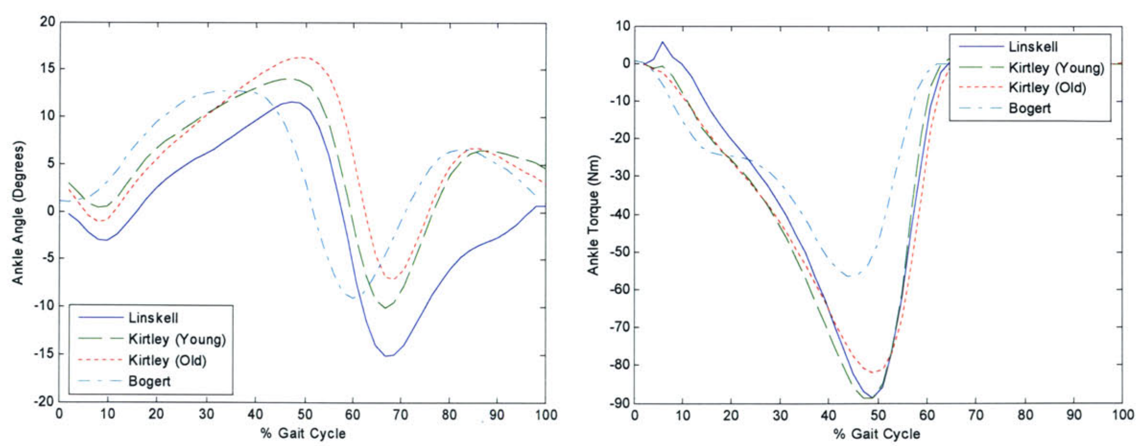

Figure 2.13 The ankle angle and torque profile scaled for a 60kg person are shown.

The power as a function of gait cycle for the ankle is shown in Figure 2.14. For slow walking the region of negative work, A1, is approximately equal to the region of positive power, A2 suggesting that a spring at the ankle is be a good choice for actuation at the ankle. At faster walking speeds, A2 is significantly larger indicating that a non-conservative actuator is required. However, a heavy actuator at the ankle would be detrimental to walking metabolism due to the large distal mass.

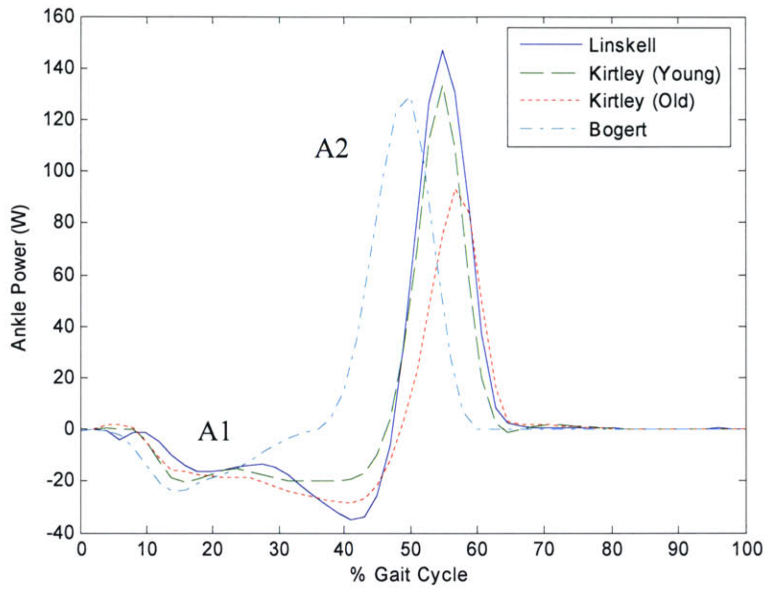

Figure 2.14 Ankle joint power profile scaled for a 60kg person as a function of gait cycle. A1 is a region of negative power, corresponding to eccentric plantar flexor activity at the ankle during mid-stance and terminal stance. A2 is a region of positive power, corresponding to the concentric burst of propulsive plantar flexor activity during pre-swing.

Figure 2.15 shows the ankle torque plotted vs. angle for walking at 0.8m/s. A linear fit yields a spring constant for the ankle of approximately 301Nm/rad for this walking speed. This implies that, for slow walking, a spring could be placed at the ankle of the exoskeleton to store the negative energy during controlled dorsiflexion and later release this to assist in powered plantarflexion. Further, the energy released from such a spring could also help to minimize the negative effects of distal exoskeleton mass.

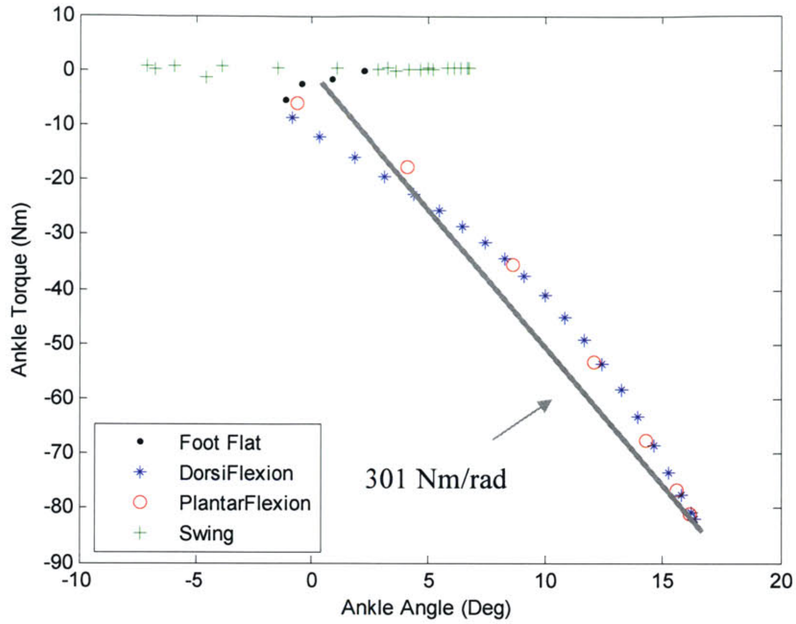

Figure 2.15 Plot of ankle angle versus ankle torque for the walking cycle. It can be seen that the ankle behaves like a spring during stance at a walking speed of 0.8m/s (Kirtley, 1998 (old)).

The summary of the specifications for the ankle joint are shown in Table 2.3. For slow walking speeds a spring is the ideal choice for actuation at the ankle as the energy absorbed during dorsiflexion is almost equal to the positive energy generated during controlled plantarflexion. Based on the ankle data in Figure 2.15 the total energy that is absorbed and then later released is approximately 9J. At faster walking speeds the positive power becomes increasing large and in this case a hybrid actuation approach may be beneficial where a small motor is used in conjunction with the spring. The focus of this thesis is slow walking only.

Range of Motion	-15 deg to 15 deg
Max Joint Torque	90 Nm
Ankle Spring Constant	301 Nm/rad

Table 2.3 Specifications for the ankle joint of the exoskeleton that were extracted from the gait data.

3 Electro-Mechanical Design of Exoskeleton

The exoskeleton was designed to provide a parallel load path that transferred the weight of the backpack directly to the ground. The exoskeleton had sufficient degrees of freedom to minimize kinematic constraints experienced by the wearer. Component design and selection for the hip, knee and ankle joints was based on the specifications outlined in Chapter 2. The main components of the exoskeleton are shown in Figure 3.1.

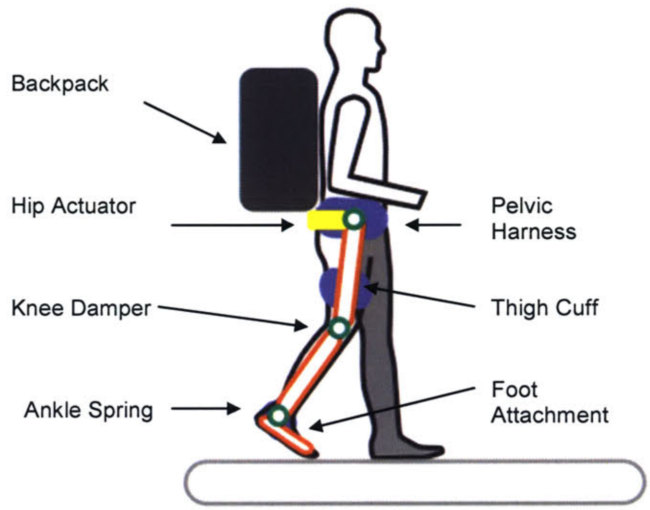

Figure 3.1 The main components of the exoskeleton.

3.1 Functional Requirements

It can be concluded, from the information outlined in Section 1.1 that there is an advantage to supporting a load that a person is carrying as well as providing them with a forward propulsive force. From the results of the metabolic experiments discussed, as well as the practical considerations of power requirement and noise level, a number of functional requirements for the exoskeleton can be listed. They are,

- The structure must support load of payload
- The structure must be lightweight and in particular have low distal mass
- The architecture must be wearable and not conflict substantially with gait
- The exoskeleton must use minimum power
- The exoskeleton must be as quiet as possible
- The actuation must apply torques at the joints of exoskeleton and human

3.2 Exoskeleton Structure

The design of the exoskeleton structure had to address the fact that the structure's primary function was to support the payload and provide the mechanical interface to the operator. A parallel orthotic structure was the basic framework used to transfer the load from the backpack to the ground. The main structural elements consisted of standard prosthetic aluminum tubing. This tubing was used since it is lightweight, rated for human use, and interfaced with standard prosthetic connectors and components.

The criteria for sizing the structural elements had to take into consideration the stresses, and also the structural stiffness. Minimizing the size and weight of the structural elements was traded off against maintaining structural stiffness so that the payload could be adequately supported. The strength to weight ratio of the exoskeleton components was maximized using finite element analysis. Free body diagrams were used to determine the boundary conditions that were applied in performing the analysis. Figure 3.2 shows graphical results of a stress analysis in the exoskeleton shank and thigh.

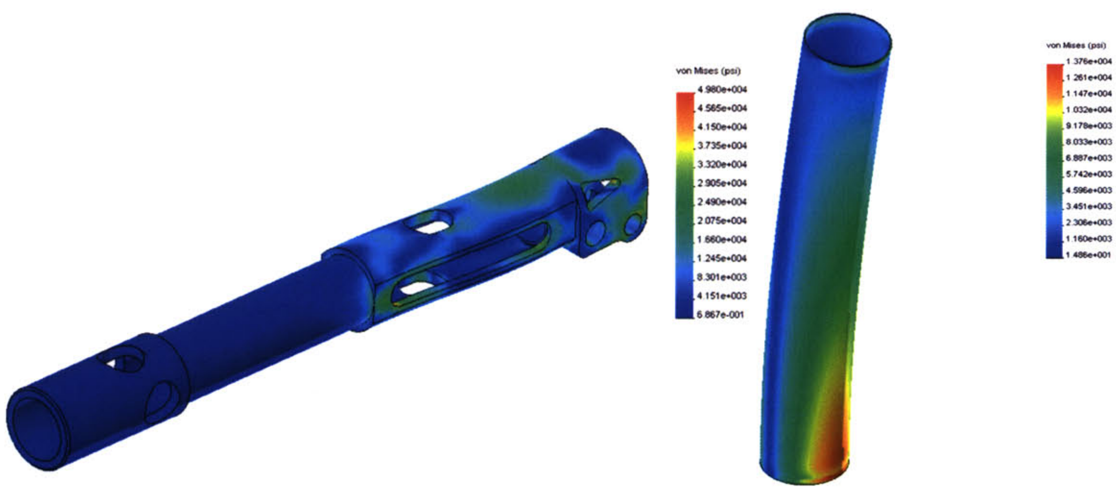

Figure 3.2 Finite element results from testing the exoskeleton thigh and shank.

3.3 Exoskeleton Degrees of Freedom

The exoskeleton was implemented with three degrees of freedom at the hip, one at the knee, and two at the ankle. The joint ranges of motion accommodated normal human walking.

Table 3.1 shows the degrees of freedom of the exoskeleton. The approach taken in the design of the exoskeleton in this thesis was to collocate the exoskeleton and human joints in the sagittal plane. This maximized comfort for the wearer.

Joint	DOF	Description
Hip	3	Flexion and extension, abduction and adduction, medial and lateral rotation
Knee	1	Flexion
Ankle	2	Flexion and extension, Inversion and eversion

Table 3.1 Exoskeleton degrees of freedom.

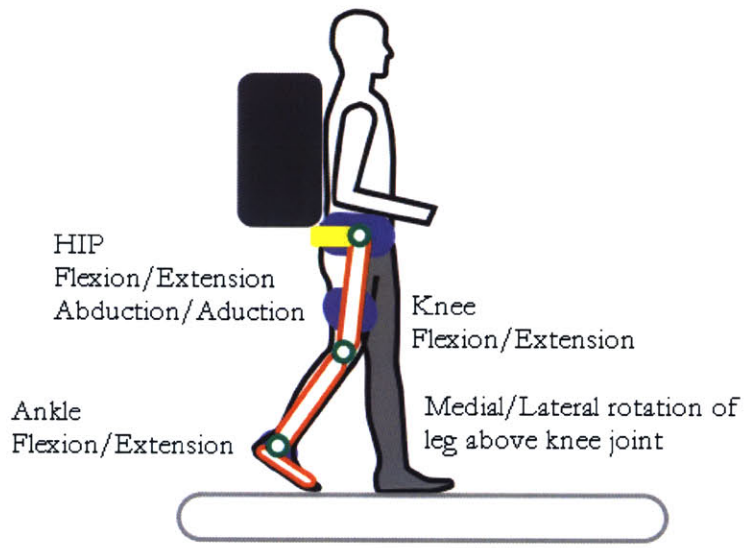

Figure 3.3 Schematic of exoskeleton structure and degrees of freedom of exoskeleton.

Flexion and extension of the exoskeleton hip was accomplished using a reali-slim Kaydon bearing in a custom housing. A cam mechanism was implemented at the hip joint to enable hip abduction and adduction (Valiente, 2005). The cam mechanism automatically adjusted the exoskeleton leg length so that the human leg could freely abduct and adduct. Medial-lateral rotation of the exoskeleton leg was allowed by means of a rotary joint just above the knee joint. The knee joint of the exoskeleton was a revolute joint. A revolute joint at the ankle allowed for movement in the sagittal plane and a flexible spring steel attachment allowed relative motion between the human and exoskeleton foot in the coronal plane.

3.4 Exoskeleton interface to the human

The exoskeleton interfaced to the human via shoulder straps, a waist belt, thigh cuffs, and a shoe connection. A compliant belt interfaced the lower torso to the backpack frame and the backpack's shoulder straps interfaced to the upper torso. The physical connection between the exoskeleton and the human enabled the exoskeleton to passively track the human's leg motion and kept the exoskeleton and human leg joints collocated. A standard military issued backpack, Alice Pack, carried the load. The exoskeleton was attached to the standard military backpack through a harness. The hip joints of the exoskeleton legs were mounted to the harness. There was sufficient clearance between the pelvic harness and the wearer to minimize disturbance to the wearer's gait.

3.4.1 Carbon Fiber Harness

The exoskeleton was attached to the standard military backpack using a harness that allowed for mounting the hip joints of the exoskeleton. The structure was made from carbon fiber and was attached to the backpack such that it maximized stiffness of the structure. Interfacing the exoskeleton to the human was a difficult problem, making it necessary to construct mockups to determine the correct geometry to ensure that the disturbance of gait was minimized.

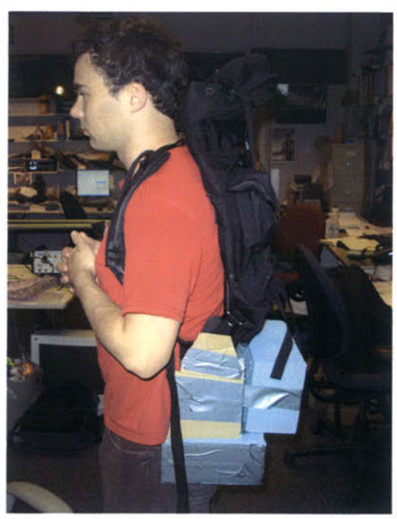

Figure 3.4 Foam mockup of the exoskeleton harness being tested.

The harness connected rigidly to the backpack frame to transfer the load from the backpack to the exoskeleton. The pelvic harness was made from carbon fiber and the stiffness to weight ratio was optimized using finite element analysis. The finite element analysis was used in an iterative design process until the regions of stress concentration were minimized and the desired stiffness was obtained. The structure consisted of a hollow core with 1/16th inch thick layer of carbon fiber over it. A box was also incorporated into the harness for electronic part storage while at the same time increasing structural integrity.

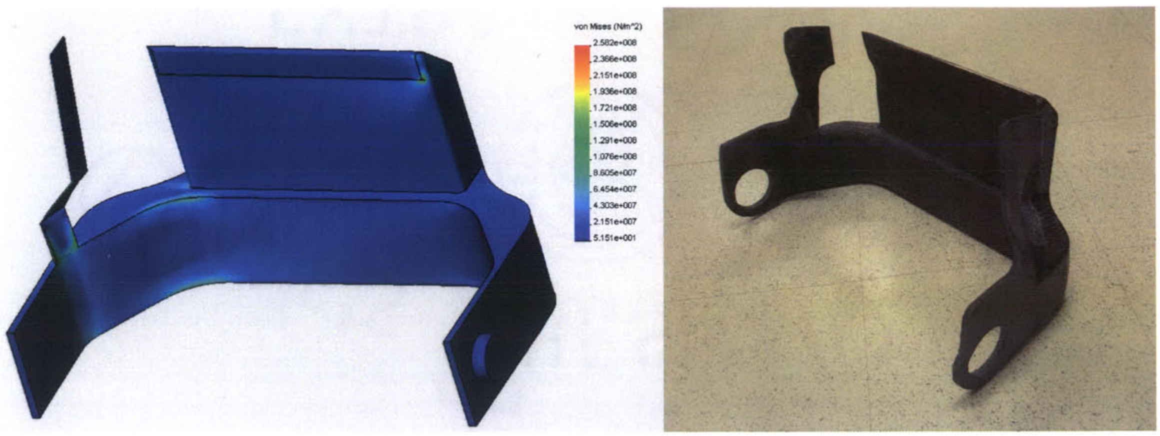

Figure 3.5 The stiffness to weight ratio of the carbon fiber harness was maximized using finite element analysis. In a), finite element result for stress in the carbon fiber harness is shown. In b), the structure consisting of a hollow core with 1/16th inch thickness of carbon fiber layer over it is shown.

3.4.2 Thigh brace

To enable the exoskeleton track the human leg and for requisite torques to be applied to the human thigh, a thigh brace was required. This allowed the exoskeleton knee to remain collocated with the human knee and also forced the exoskeleton leg to follow the human leg movement in the coronal plane during abduction and adduction. The custom thigh brace had molded vertical flat sides to allow for attachment to the exoskeleton leg. The cuff was padded and Velcro was used to secure it. A spring steel plate between the exoskeleton leg and the thigh cuff was compliant in the coronal plane and this allowed for small misalignments between the human and exoskeleton leg. The thigh brace was connected to the yaw joint that allowed for medial-lateral rotation of the exoskeleton leg ensuring that it rotated with the human leg.

3.4.3 Foot attach

The exoskeleton foot was attached to the human foot with two pieces of spring steel. The connection was sufficiently rigid so that it kept the exoskeleton foot in line with the human foot and also allowed movement between it and the human foot, increasing comfort during walking.

3.5 Final Assembly

The components for the exoskeleton, excluding the actuators for the hip joint, are shown in Figure 3.6. The carbon fiber harness was attached to the backpack and a waist belt secured it to the wearer. The thigh cuffs attached the exoskeleton thigh to the human thigh and the shimano bike shoes were worn by the wearer.

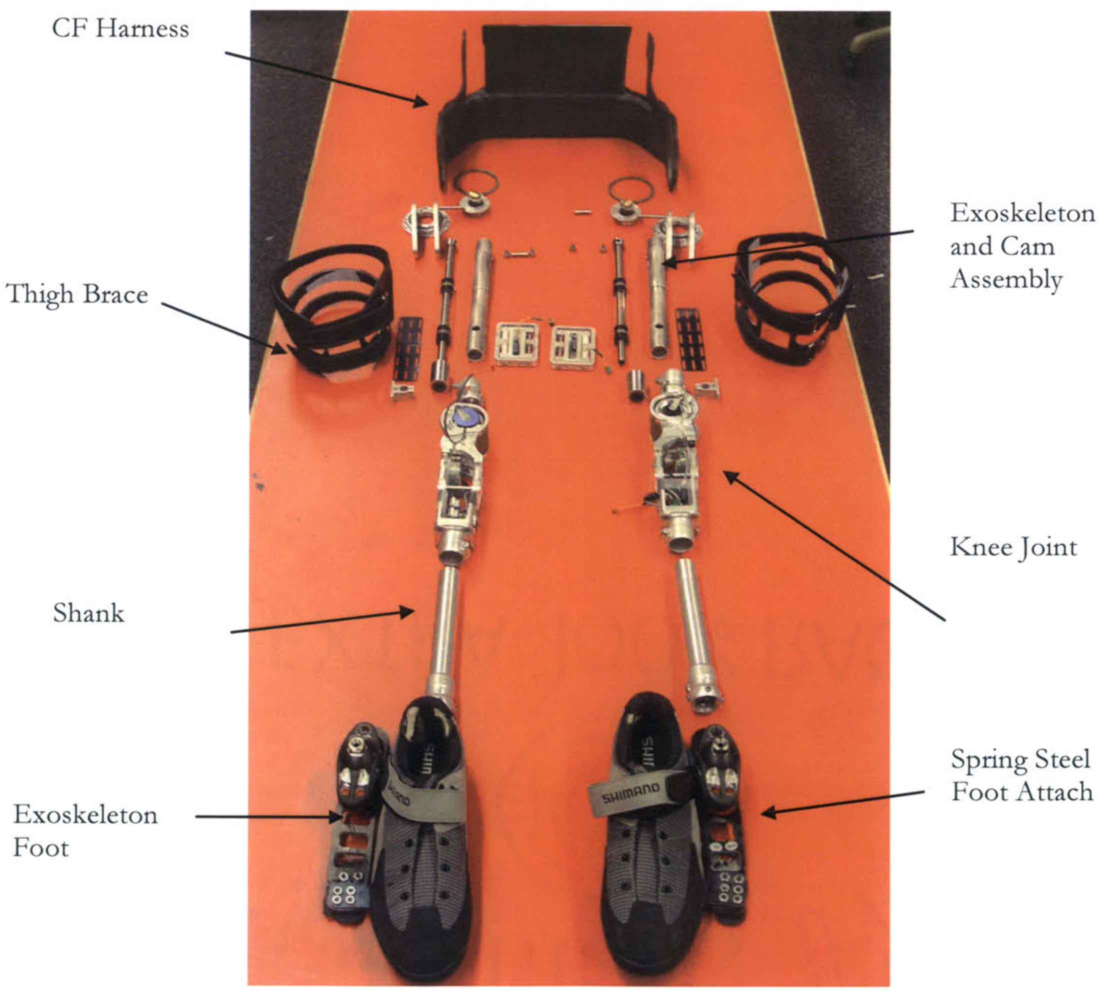

Figure 3.6 Exoskeleton components prior to assembly.

3.6 Actuation

This section describes the design and characterization of the actuation of the exoskeleton joints in the sagittal plane. A linear series elastic actuator with a DC brushed motor was used for the hip joint, a magnetorheological damper was used for the knee joint and a compression spring was used for the ankle joint. A passive spring for adduction at the hip joint was designed to counter moments from the exoskeleton leg on the wearer.

3.6.1 Hip Series Elastic Actuator Design

Series elastic actuators (Pratt *et al.*, 1995) were used as they provided a means for implementing lightweight and inexpensive force control in a bandwidth similar to that of natural muscle. The SEA uses a spring in series with the output of the motor as shown schematically in Figure 3.7. The spring acts as a sensor, filter and impedance limiter. For the actuator described in this thesis the ball screw nut was coupled to the output through four compression die-springs and the spring compression was measured with a linear potentiometer.

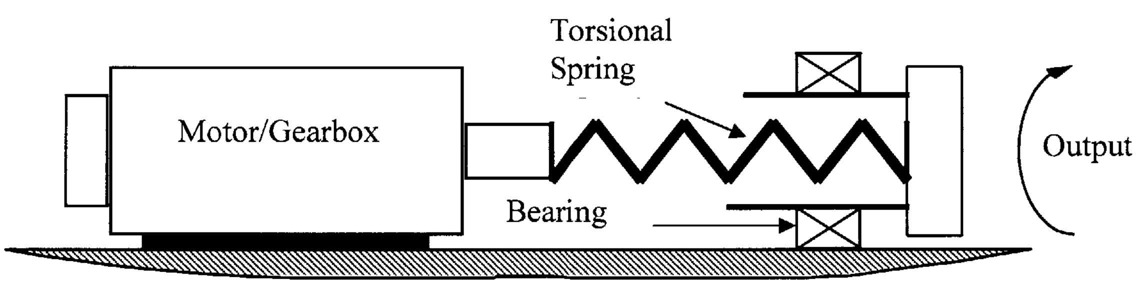

Figure 3.7 Rotary series elastic actuator schematic.

The specifications for actuation at the exoskeleton hip joint outlined in Section 2.3.1 were used to design the series elastic actuator. A 150W Maxon RE40 motor was chosen for its power to weight ratio. The ball screw and nut were Nook Industries products and the springs used were die springs from Century Spring. Since a linear actuator was used, the moment arm at the hip joint and the force output of the actuator determine the hip torque. The actuator had a brushed DC motor driving a 3mm lead ball screw via a 2:1 reduction belt drive. Figure 3.8 shows the main components of the actuator.

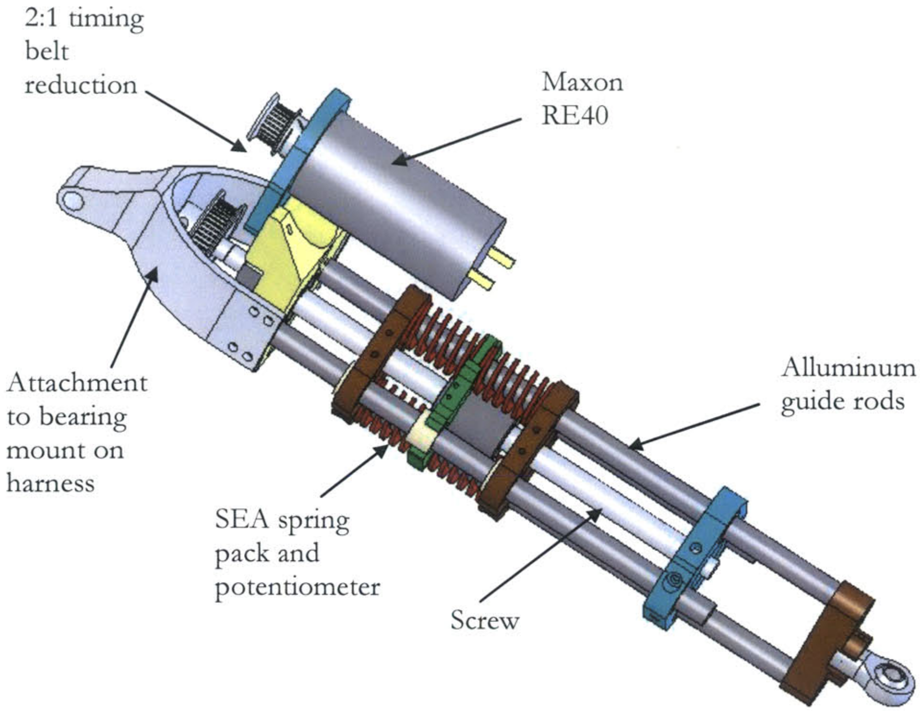

Figure 3.8 CAD model of the linear series elastic actuator showing the key components.

Table 3.2 below shows the effect of the belt drive and ball screw transmission on the motor output and the resulting maximum hip torque and velocity obtained for the exoskeleton.

Belt Drive Reduction	**Transmission**	**Torque**	**Angular Velocity**	
		(Nm)	**(rpm)**	**(rad/s)**
Maxon RE40 Specifications	none	2.5	8200	858
After Belt Drive	2	5	4100	429
Lead Screw Reduction	**Lead**	**Force**	**Linear Velocity**	
	(m/rev)	**(N)**	**(m/s)**	
Ball Screw Lead	0.003	1667	0.21	
Joint Moment Arm	**Moment Arm**	**Torque**	**Angular Velocity**	
	(m)	**(Nm)**	**(rpm)**	**(rad/s)**
Actuator Moment Arm	0.0762	127	161	17

Table 3.2 Maximum torque and angular velocity calculations for hip joint.

3.6.1.1 Actuator Characterization

An actuator used at the hip of the exoskeleton experienced two operational boundary conditions. The actuator either interacted with the environment, or it was connected to a freely moving inertial load. These boundary conditions represent the stance and swing phase of the walking cycle, respectively. During the stance phase, the load position can be considered a fixed position source, and in the swing phase, the load position is defined as a function of the force in the spring and the load mass. These boundary conditions were addressed separately in order to determine the performance of the actuator for each case.

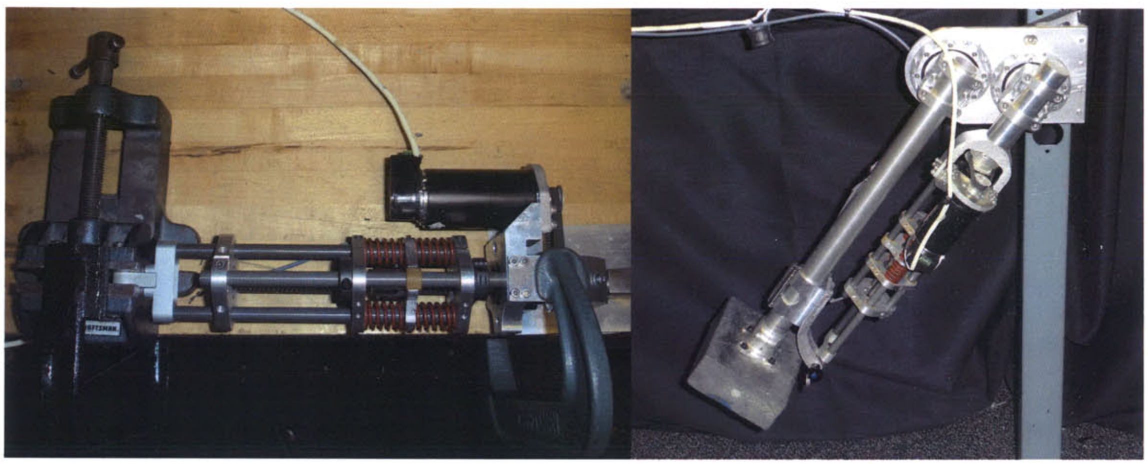

Figure 3.9 Testing the hip actuators for two different boundary conditions. For the first case a), the actuator output is fixed (clamped). In the second case b), the actuator is free and loaded with a mass of 16lbs attached to the end which is equivalent to the inertia of the human and exoskeleton leg.

3.6.1.2 Modeling of Series Elastic Actuator

The motor model in the power domain consists of a motor amplifier, motor mass and a viscous friction element. The motor amplifier sends a current based on a signal from the controller, which creates a force on the motor mass. In the model it is assumed that the electrical dynamics are fast enough so that they are negligible.

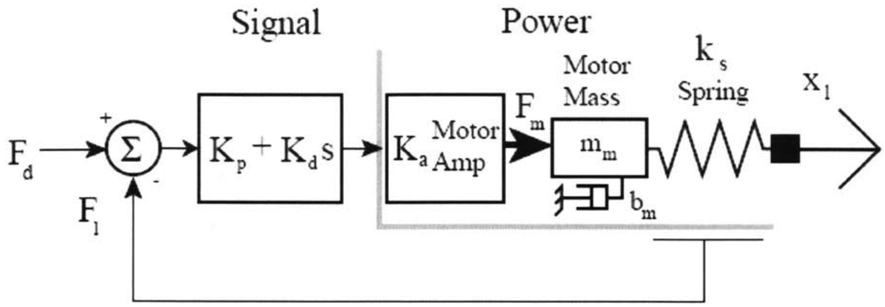

Figure 3.10 Actuator model showing controller and lumped parameter model (Robinson, 2000).

The lumped mass m_m includes the dynamic motor mass and the mass of the transmission elements as seen through the transmission. The motor friction is also seen through the transmission. The reflected inertia and reflected viscous friction are N^2 the actual values where N is the transmission reduction. The motor was controlled in torque mode and the power domain model of the system using linear force and components is shown in Figure 3.11. Feedback control of the actuator was provided by measuring the deflection of the spring pack, which implies the force output on a load, F_l, of the actuator. The open loop dynamic equation for the force F_l in the spring as a function of motor force and load motion was derived using a lumped parameter model (Robinson 2000).

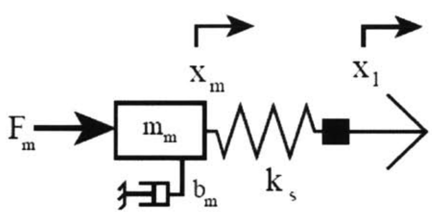

Figure 3.11 Lumped parameter model for the actuator (Robinson, 2000).

Equation (3.1) is the open loop transfer function for the general case. Two cases were considered for the end condition. One was the case when the end condition is fixed (X_l is zero) and the other was when the actuator is moving a load mass (m_l). The open loop equations for the two cases are shown in equations (3.2) and (3.3).

$$F_l(s) = \frac{F_m(s) - (m_m s^2 + b_m s)X_l(s)}{\frac{m_m}{k_s} s^2 + \frac{b_m}{k_s} s + 1} \tag{3.1}$$

Fixed end condition

For this case the desired transfer function was obtained by setting X_l to zero. The resulting transfer function between the force on the load and the force on the motor mass is shown in equation (3.2).

$$\frac{F_l(s)}{F_m(s)} = \frac{1}{\frac{m_m}{k_s}s^2 + \frac{b_m}{k_s}s + 1} \qquad \textbf{(3.2)}$$

Free end condition with a load mass

Figure 3.12 shows the change to the model for the case with the load mass on the end.

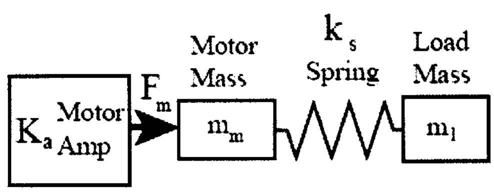

Figure 3.12 Model of the actuator showing the load mass on the end (Robinson 2000).

The transfer function was derived relating the input force on the motor mass to the force on the load. The equation is similar to that for the case when the end condition is fixed and as m_l goes to infinity the transfer functions are the same.

$$\frac{F_l(s)}{F_m(s)} = \frac{s}{\frac{m_m}{k_s}s^3 + \frac{b_m}{k_s}s^2 + (\frac{m_l+m_m}{m_l})s + \frac{b_m}{m_l}} \qquad \textbf{(3.3)}$$

The series elastic actuator was tested experimentally in the fixed end condition configuration in order to estimate the coefficients of the transfer function. A chirp signal was applied directly to the motor to measure the frequency response of the system. The chirp had an amplitude of 2A and varied from 0.1Hz to 50Hz in 50 seconds. The input command and the output force were recorded. Figure 3.13 shows the chirp input in blue and the output force in red. The force associated with the input current was calculated from the motor specifications and the transmission ratio. The output force was obtained by measuring the deflection of the series spring pack.

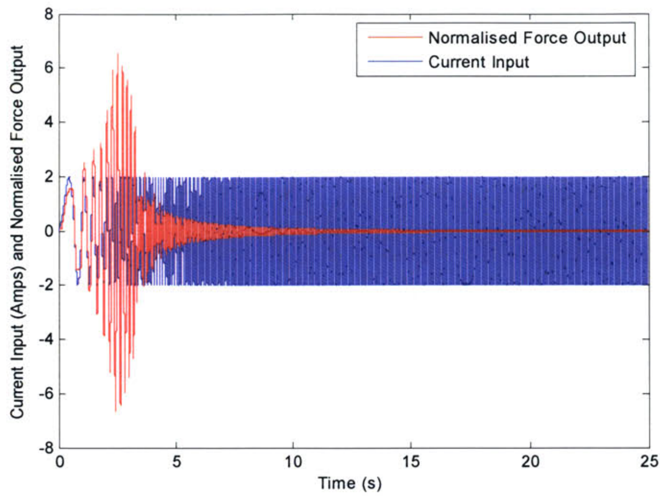

Figure 3.13 Output response (red) to an input chirp signal (blue). A 2A current chirp was commanded starting at 0.1Hz and finishing at 50Hz.

An open loop Bode plot was plotted for the system based on the input – output values from the chirp command. The open loop response to a step was also obtained and plots of the experimental results are shown below in Figure 3.14.

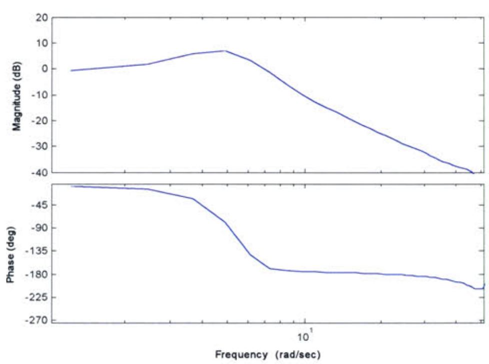

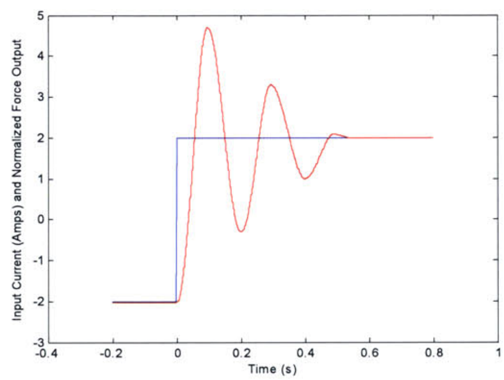

Figure 3.14 Experimental open loop response for the fixed end condition. In a), the open loop Bode plot of system and b), the response to step input of 4A.

The magnitude of peaking in the frequency domain, M_p and the frequency at which it occurs, ω_p were determined from the Bode plot. Assuming a second order system, this allowed the natural frequency, ω_n and damping coefficient, ς to be estimated. The system had 19.3 degrees of phase margin at 43.6rad/s. The step response of the open loop system resembles an under damped spring-mass system as can be seen in Figure 3.14. The peak overshoot, P_o and the damped natural frequency, ω_d were measured and ς and ω_n were again estimated. So an average value for ς and ω_n were calculated from the two methods and the values are listed in Table 3.3

Frequency Response				Step Response				Average	
M_p	2.71	ω_n	31.3	P_o	1.68	ω_n	32.2	ω_n	31..7
ω_p	30.7	Σ	0.19	ω_d	31.9	Σ	0.12	ς	0.16

Table 3.3 Experimentally obtained system parameters and calculated natural frequency and damping coefficient. All frequencies are in rad/s.

From the values obtained for ω_n and ς the parameter values of the lumped parameter model of the physical system were estimated and are listed in Table 3.4.

Equivalent mass, m_m (kg)	311.9
Spring constant, k_s (kN/m)	31.3
Equivalent damping, b_m (kNs/m)	3.1

Table 3.4 Physical values of the elements in the lumped parameter model.

A comparison of the experimental and theoretical open loop Bode plots for the system with the fixed end condition is shown in Figure 3.15a. There is some discrepancy between the model and the experimental data and this can be attributed to the fact that the system was not a perfect second order system. However, the model was sufficient for the design of a controller to control the force of the actuator. Experimental data are not shown for the free end condition with a load mass but the theoretical Bode plot is shown based on the physical parameters in Table 3.4 and an estimated load mass of 350kg.

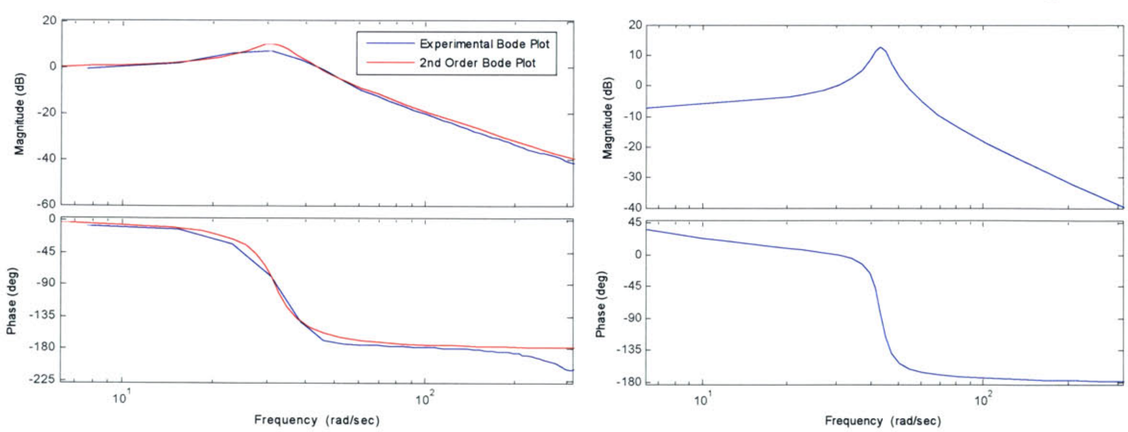

Figure 3.15 In a), the experimental and theoretical Bode plots for the series elastic actuator for the fixed end condition are shown. In b), the theoretical Bode plot for the load mass end condition is shown.

3.6.1.3 Closed Loop Force Control and Characterization

The controller design principles used for the closed loop control of the SEA were obtained from Robinson (2000). A PD controller is suggested as the means to control the output force of the SEA where the deflection of the series spring pack is measured with a linear potentiometer. Figure 3.10 showed the closed loop system and output force being fed back and subtracted from the desired force.

It was possible to control the actuator with a pure proportional controller alone. This worked well for the free end condition but did not work well for the case where the end is fixed. With pure P control if the system hit a hard boundary it bounced back due to the large impact force seen in the sensor (spring) and the resulting large error signal with opposite sign. Further, using purely proportional control it was observed that the actuator would limit cycle if it was held up against the end stop of the actuator. However, for a controllable actuator it was desired that the actuator be stable at the point where a collision occurred.

The chosen solution was to have a feed-forward term in conjunction with a PD controller where the D term was a band limited differentiator with a cutoff at 100Hz. It was found that the controller performed well for both the free and fixed boundary conditions. A disadvantage of this was that the performance of the free movement of the actuator was degraded. The P and D gains could only be increased so far before the high frequency noise in the sensor signal was amplified. The force feedback signal from the linear potentiometer was also filtered with an analog low pass filter and a digital median filter which are discussed in chapter 4.

Closed loop performance with fixed end condition

In order to determine the closed-loop bandwidth of the actuator the end of the actuator was fixed and a sine wave chirp in force was applied from 1Hz to 100Hz. Figure 3.16 shows both the experimental and theoretical closed loop Bode plots. The experimental and theoretical -3dB points are very close and are at approximately 226/rad/s (36Hz).

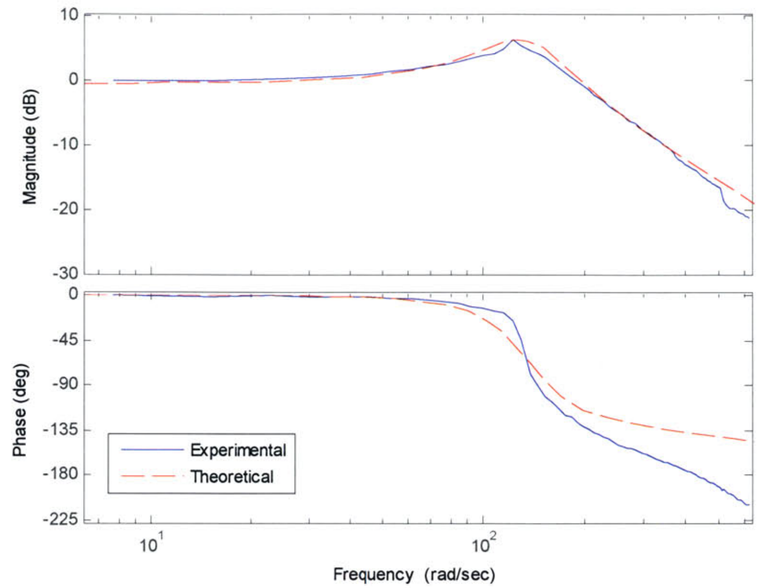

Figure 3.16 Experimental and theoretical closed loop Bode plot of the actuator for the fixed end condition. Experimentally the actuator was found to have a closed loop bandwidth of 226 rad/s (36Hz).

The proportional and derivative gains of the controller were tuned experimentally by examining the step response of the actuator and the ability of the actuator to track a sine wave in force. Figure 3.17 shows the response to a step of 1600N and the actuator tracking a sine wave in force of 1600N at 5Hz.

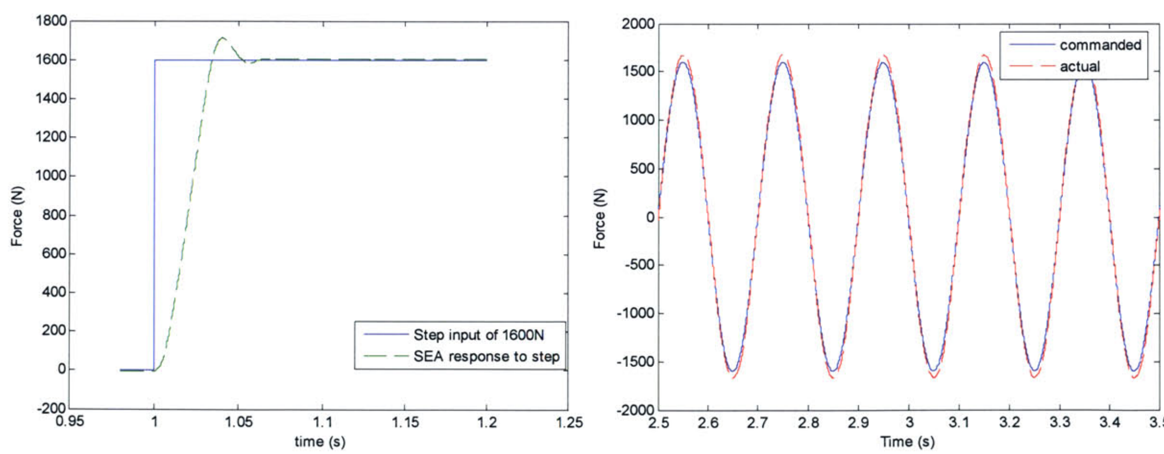

Figure 3.17 Closed loop testing of actuator. In a), the response to a step of 1600N. In b), tracking a sine wave of 1600Nm at 5Hz. 1666N (375lbs) is the max force that the actuator is designed to output.

Due to the mass-spring resonance, and limited voltage and current, a series elastic actuator is limited in its ability to command large forces at high frequencies. The resonance defines the frequency at which the actuator begins to decrease in large force performance. To examine this, the actuator was commanded to oscillate through the frequency spectrum at 1600N with the output end of the actuator fixed. Figure 3.18 shows the results of the experiment with the actuator performance dropping off at about 50rad/s (8Hz).

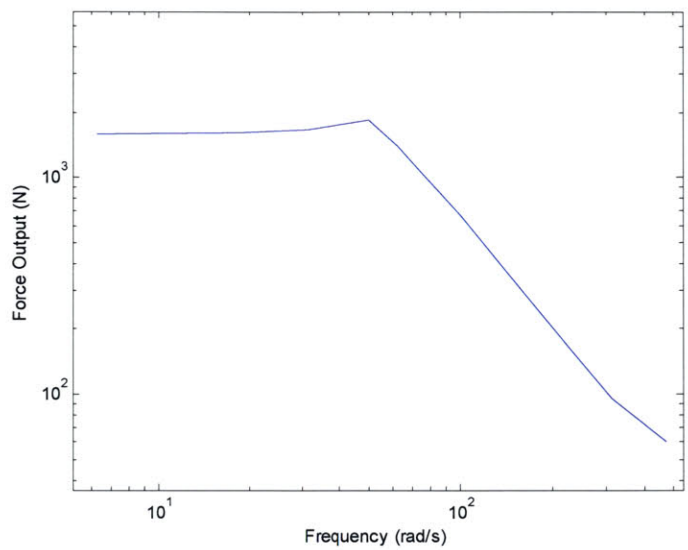

Figure 3.18 Large force bandwidth of actuator. As the magnitude of oscillation increases, the motor saturation dominates the large force capabilities of the actuator.

Closed loop performance with load mass

The actuator was required to apply a torque to the human and exoskeleton leg during the swing phase of the walking cycle. As a result, an experiment was performed to determine the closed loop bandwidth of the actuator for the case of applying a force to a free load mass in space. Shown in Figure 3.19 are the experimental and theoretical closed loop Bode plots of the actuator with the free load mass end condition. The -3dB point for the experimental curve is 253rad/s (40.3Hz) and the theoretical model is 230rad/s (36Hz). The plots are not as well matched as the case for the fixed end-condition. This is likely due to errors in the estimates of the physical parameters of the system, unmodelled dynamics as well as excessive compliance and backlash in the experimental setup.

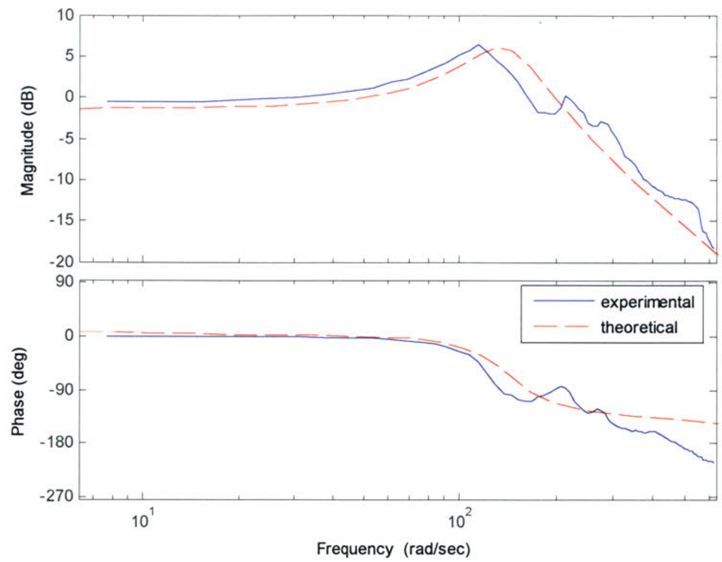

Figure 3.19 Experimental and theoretical closed loop Bode plot of the actuator with an equivalent load mass of 350kg. Experimentally the actuator is found to have a closed loop bandwidth of 253rad/s (40.3Hz).

It was shown in Section 3.6.1.2 that the case of applying a force to a large mass in space is similar to the case of the fixed end condition for large masses. This is true because the actuator was used at an articulated joint and the linear equivalent of the rotary inertia is scaled by the square of the moment arm. In order to validate this theory a number of simple tests were performed. Below is a plot showing the actuator tracking a hip torque of 100Nm at a frequency of 5Hz with an equivalent mass to the human and exoskeleton leg. The experimental setup is shown in Figure 3.9b.

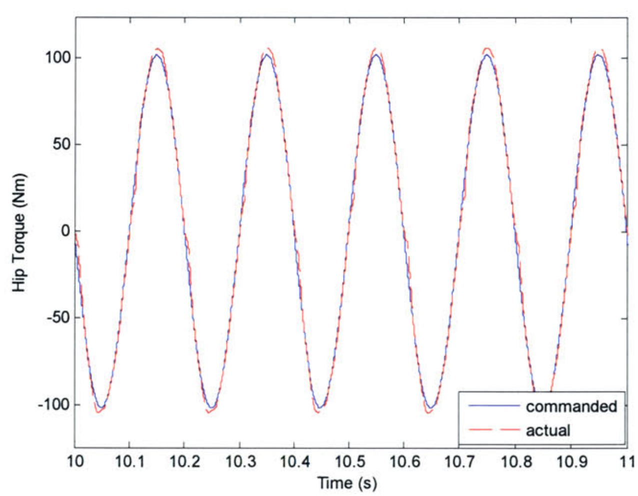

Figure 3.20 Closed loop testing of actuator. The actuator was mounted on the test arm with a mass of 7.2kg on the end. It was then commanded to track a sine wave in torque of 100Nm at 5Hz.

In order to determine if the actuator had sufficient force and power capability to power the human and exoskeleton, a test was performed where the actuator was commanded to track a trajectory similar to the human hip trajectory in walking. The test was performed on the bench with an equivalent mass on the end of the arm. A digital PD control loop was used for the controller where the gains were tuned experimentally. It can be seen that the arm was capable of tracking the human hip trajectory with an equivalent leg inertia.

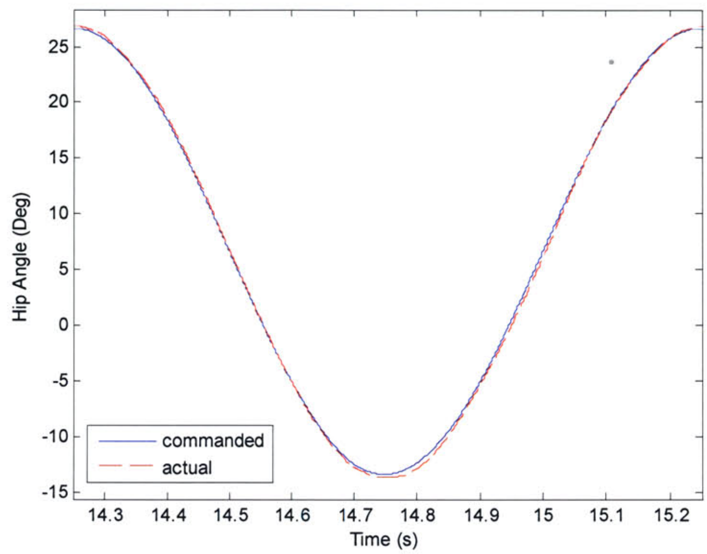

Figure 3.21 Closed loop position control testing. The actuator was commanded to track a trajectory similar to that of the human hip joint in walking.

3.6.1.4 Impedance of Actuator

With the motor turned off the force in the spring due to load motion can be derived. It can be seen that at lower frequencies the impedance has an equivalent mass characteristic because it is rising at 40db/dec. At higher frequencies the impedance is the spring constant of the sensor. At the high frequencies shock loads are filtered through the spring.

3.6.2 Knee Magnetorheological Damper

During slow human walking, the knee largely dissipates energy where minimal positive power is exerted as was seen in Section 2.3.2. The knee of the exoskeleton was implemented with a magnetorheological damper with the fluid used in the shear mode similar to that of Herr and Wilkenfeld (2003). In order to determine the maximum braking torque of the damper a number of weights were hung off a lever arm at various levels of commanded current and the braking torque of the damper was recorded for each case. It was found that the device could exert a maximum braking torque of approximately 50Nm as can be seen from Figure 3.22.

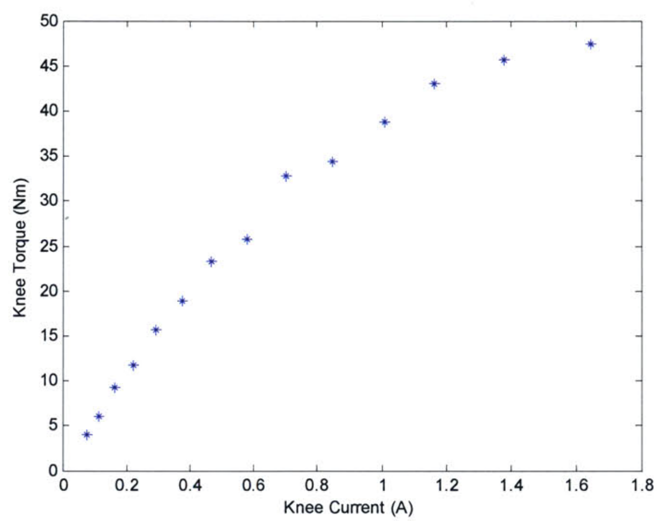

Figure 3.22 Braking torque of the magnetorheological damper vs. commanded current to the damper.

A current command sent to the knee powered an electromagnet that created a magnetic field across the plates in the knee and the magnetorheological fluid between them. The fluid consisted of iron particles and the blades of the knee were steel. When a magnetic field was applied to these materials some magnetism remained within their structure. This is called residual magnetism (hysteresis) and is defined as the flux density remaining in a material after the magnetizing force has been removed. The intensity of the residual magnetism depends upon various factors such as the metallurgy of the steel, the intensity of the magnetic field source, the magnetic circuit and the material temperature.

Any residual magnetism in the magnetorheological damper created a residual torque that impeded the swinging of the human leg during the swing phase of the gait cycle. As a result the damper had to be demagnetized before the swing phase. One method of demagnetizing a structure is to carry out a special demagnetization approach after the normal de-energize operation, i.e. current command of zero. One such demagnetization cycle is to cycle the commanded current to the electromagnet through gradually decreasing values. This can be done by having an exponentially decaying sine wave in current that decays to zero. However, the time available for demagnetization during the gait cycle was approximately 250ms and so due to this time constraint and the relatively slow electromechanical time constant of the knee another method of demagnetization was required. The method used was to send a pulse in current of opposite sign to the current that previously magnetized the knee. For the magnetorheological damper a pulse with an amplitude of 1A and a duration of 50ms was used and a comparison of this to an exponential demagnetization over 5 seconds is shown in Figure 3.23.

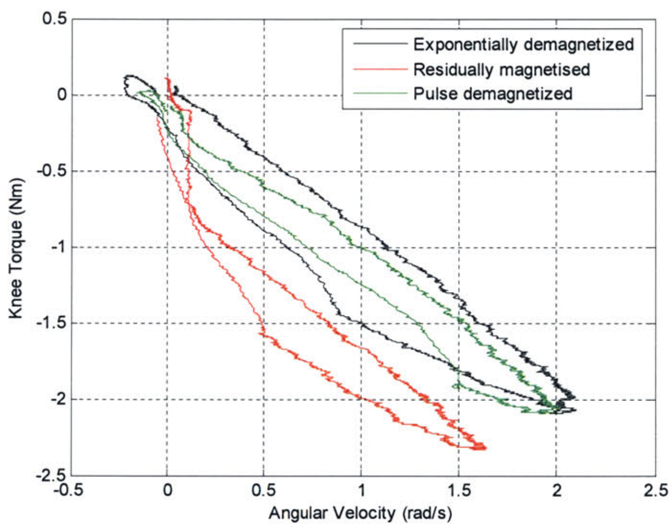

Figure 3.23 Comparing pulse demagnetized knee with the exponentially demagnetized and the residually magnetized cases.

The torque on the knee and the angular velocity shown in Figure 3.23 were recorded as the exoskeleton leg swung freely through ninety degrees. The results show residual magnetization in the damper due to the fact that when the knee was exponentially demagnetized (black) the torque was much less than the case without demagnetization (red). The green data shows the resulting torque-velocity data for the case of pulse demagnetization and it can be seen that this demagnetization result was comparable to that when exponential demagnetization was performed.

3.6.3 Passive Ankle Spring

For slow walking, it has been shown that the ankle behaves like a spring (Palmer 2002). Initial bench level testing revealed that restricting controlled plantarflexion made it uncomfortable to walk. This was a result of the fact that the knee flexing moment at early stance is significantly higher with a locked ankle than that with a plantar free ankle. A high knee flexing moment results from the fact that in order to achieve foot flat with a locked ankle, greater knee and hip flexion occur during the stance phase. The effect of this is to push the knee joint center further forward.

For the exoskeleton, a linear spring located at the ankle joint was designed to capture the negative energy during controlled dorsiflexion. This energy was subsequently released to assist the exoskeleton foot in plantarflexion as the foot came off the ground. This rotary ankle spring was implemented by having a lever compress a linear urethane spring as illustrated in Figure 3.24.

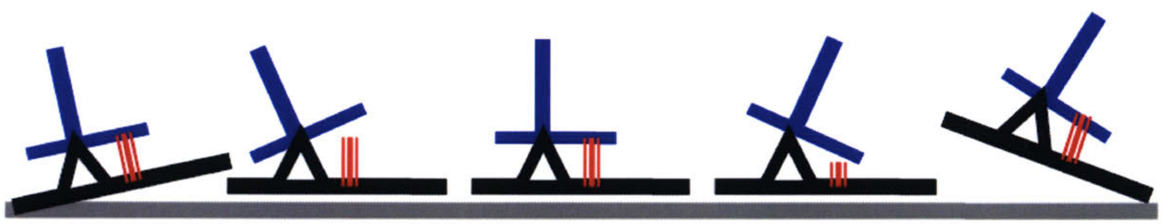

Figure 3.24 Energy is stored in the red uni-directional ankle spring as it is engaged in mid-stance and the shin rocks forward. The energy in the spring is released to assist power plantar flexion.

The implementation of the unidirectional spring is shown below in Figure 3.25. Urethane was used for the spring material as it is lightweight. The linear spring was seen at the ankle joint as an effective rotary stiffness and the linear spring constant was transformed through an effective transmission due to the lever. The spring constant was 247kN/m and the lever arm was 0.0381m (1.5 in) which gave a joint rotary stiffness of 356 Nm/rad. The ankle joint of the exoskeleton was 1.5 inches below the human ankle joint which was not ideal. The exoskeleton foot was attached to the shoe by means of two spring steel pieces located at the front and the back of the shoe. The heel of the exoskeleton foot and the shoe were aligned so that on heel strike both 'feet' came into contact with the ground at the same time.

Figure 3.25 Exoskeleton foot and the shoe worn by the wearer. The urethane compression spring is shown that is used to store the negative energy during dorsiflexion that is released during powered plantarflexion.

3.6.4 Hip Passive Adduction Spring

When the exoskeleton wearer stood on one leg, a moment was created by the backpack load since it was off center from the biological hip joint. This moment was undesirable and caused discomfort. To solve this problem a linear compression spring was placed at the hip joint of the exoskeleton so that it would compress to counter this moment during hip adduction. It was unidirectional so it allowed the hip to freely abduct. The design for the adduction spring is shown in Figure 3.26. The spring was kept in place by means of a keeper that was attached to the exoskeleton hip joint assembly. The keeper was attached to the sagittal plane bearing so that the keeper rotated with the exoskeleton leg. A brass plunger fitted through a hollow spring that was kept from falling out by means of a nut that threaded on to the end of the plunger.

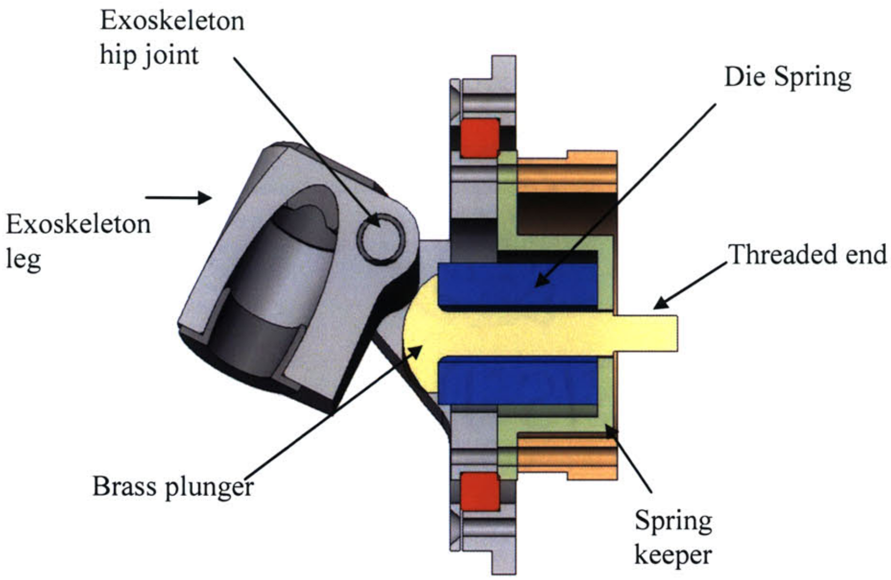

Figure 3.26 Section view of the adduction spring assembly at the hip joint.

The rotary spring constant for adduction was obtained by using a free body diagram of the exoskeleton leg during single support to calculate the moment felt at the hip joint. This was calculated to be 8Nm. Then by examining human walking data it was assumed that the human leg undergoes approximately five degrees of adduction during normal walking. From these two values an effective rotary stiffness of 96Nm/rad was calculated. This was achieved by means of a linear spring of value 425kN/m compressed by a lever arm of 15mm.

3.7 Exoskeleton Prototype Improvements

After initial testing of the exoskeleton two major changes were made to the design. The first was a new design for the foot and ankle joint and the second was a flexible spine to attach the backpack to the harness.

3.7.1 Foot and Ankle Revision

The initial design allowed the payload of the exoskeleton to be transferred to the ground but it significantly increased the foot print of the wearer and did not collocate the human and exoskeleton ankle joints. The revised design improved on the initial design by collocating the exoskeleton and human ankle joints. Also, the exoskeleton foot was integrated into a standard military boot greatly, reducing the footprint to that of a standard military boot. As well as this, the military boot had its standard rubber heel removed and replaced with a tuned carbon composite leaf spring. This spring acts to store energy on heel strike that is later released to help the human foot come off the ground. Another benefit of the heel spring is that it adds improved shock absorption on heel strike and this minimizes shock loads on the human joints.

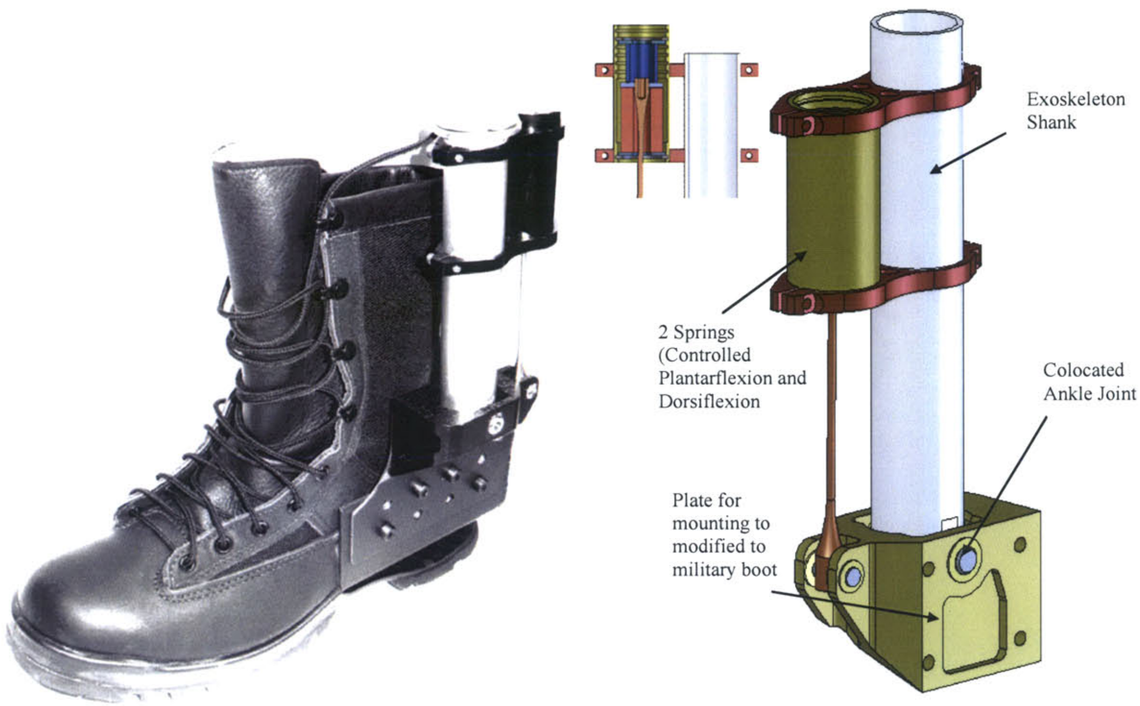

Figure 3.27 Revised foot and ankle design.

In the previous exoskeleton foot design an elastomeric bumper was placed at the ankle to store energy during dorsiflexion and release this energy to assist in powered plantar flexion. The figure below shows the location of the springs in the new ankle design. Two springs, one for controlled plantarflexion (blue) and one for dorsiflexion (red) are placed in the green spring holder. A lightweight rod compresses the appropriate spring during the gait cycle. Analysis showed that the rod will not break in tension or buckling with factors of safety of 4.4 and 2.7 respectively.

3.7.2 Biomimetic exoskeleton spine

The motions of the legs are coordinated with motions of the spine, shoulders, and arms. Spine, shoulder and arm motions make walking efficient by reducing braking motions transmitted through the legs and pelvis to the upper body. Energy expenditure in walking is increased if the back is immobilized and rotational motions of the pelvis and shoulders are eliminated. It has been shown that this kind of restriction of the motions associated with walking requires a higher metabolic rate for walking (Carlsoo, 1972). To allow more freedom for the subject during walking, the backpack frame, which was rigidly attached to the hip harness in the exoskeleton, was replaced by a flexible spine, see Figure 3.28. The backpack is supported by the top horizontal shaft of the spine. This shaft joins with a deformable tube that allows the exoskeleton spine to align with the arch of the subject's spine. A coupler joins the deformable tube to a flexible shaft. The coupler contains a V-groove in order to adapt to various shafts of different diameters and stiffnesses. The flexible shaft fits into a yaw coupler that rotates freely about the vertical axis. A second horizontal shaft clamps onto the yaw coupler.

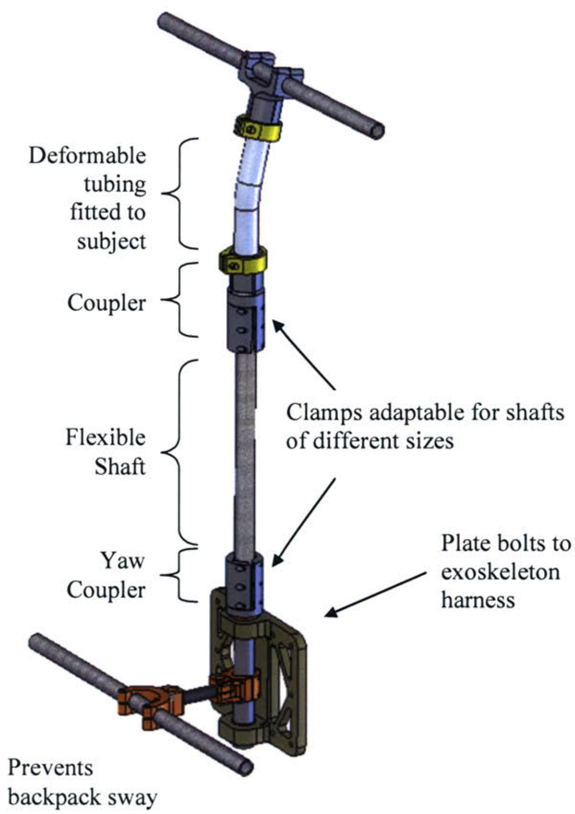

Figure 3.28 Exoskeleton spine to attach the backpack to the harness.

The human pelvis rotates during normal walking. The yaw joint at the base of the spine of the exoskeleton that is connected to the pelvic harness allows the spine (and the backpack that is attached to it) to rotate as the human pelvis rotates. As well as this the flexible shaft bends during walking allowing pelvic obliquity and tilt. By minimally constraining normal human movement the metabolic effect the exoskeleton has on the wearer can be minimized

4 Controller Implementation

The exoskeleton was controlled by reading various sensor values into a central computer mounted on the exoskeleton. Based on these sensor values the appropriate actuation was applied by the hip series elastic actuator and knee variable-damper mechanism. This chapter outlines the electronics hardware used on the exoskeleton and also describes the control strategies at the hip and knee.

4.1 Electronics Test Bed

The exoskeleton was made autonomous by means of an onboard computer with a data acquisition card, power supply and motor amplifiers. The system was powered by a 48V battery pack. Custom signal conditioning boards amplified sensor readings and provided a differential input to the data acquisition board, in order to minimize common mode noise from pick-up in the system. A custom breakout board interfaced the sensors to the D/A board on the PC104 as well as provided power to the signal conditioning boards. The amplifiers for the actuator and variable damper mechanism were 48V digital amplifiers from Copley Controls.

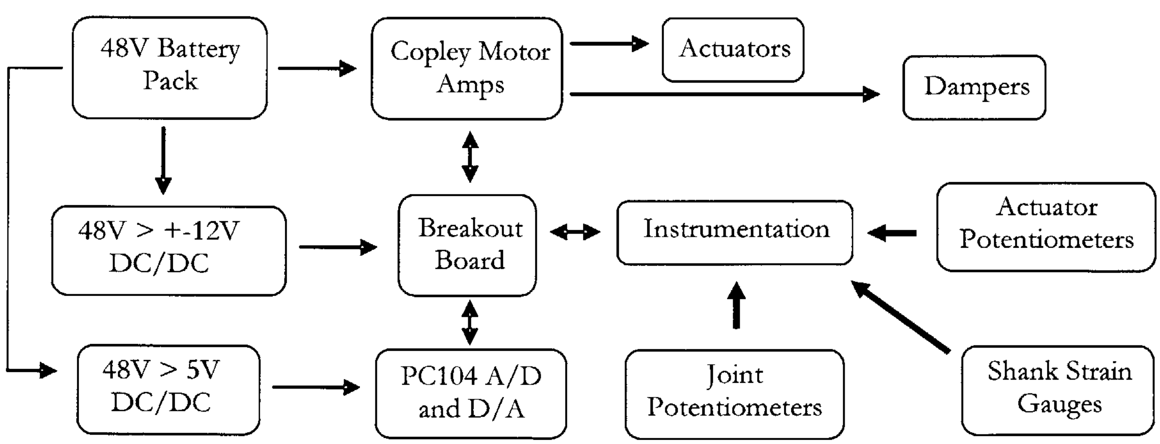

Figure 4.1 Schematic of the electronic components. The system consisted of two actuators at the hip and two dampers at the knee but only one of each is shown here for clarity.

4.1.1 PC 104 and Data Acquisition

The PC used was a MICROSPCACE PC/104 from Digital Logic. It was a miniature modular device that incorporated most of the major elements of a PC compatible computer in a small form factor. It was fitted with a PENTIUM III 700 MHz processor. A PC/104 format data acquisition board, Diamond-MM-32-AT, from Diamond Systems was connected to the PC/104. It had 32 total analog inputs and 4 analog outputs. The board was configured for 16 differential analog inputs in software and on the board with jumpers.

Matlab xPC Target was used to run the algorithm for real-time control and data acquisition. The Matlab xPC real-time kernel was installed and run on the PC/104 (remote PC) which was attached to the exoskeleton. A model was created using Simulink Matlab xPC Target, which allowed I/O blocks to be added to the model. The model was compiled on the host PC using Matlab Real-Time Workshop and a C++ compiler created executable code. The executable code was downloaded from the host PC to the target PC via TCP/IP and the code was run on the target in real-time. Data were recorded by using the xPC host scopes in the Simulink model. After running the experiment the host PC was connected to the target PC to download the data.

4.1.2 Actuator Amplifier Boards

The amplifiers used in the system were general purpose digital servo amplifiers from Copley Controls. They can be used in brushed and brushless mode and offer current, position and velocity control modes, the latter two based on encoder input from the motor to the amplifier. For controlling the series elastic actuators the Accelus model ASP-090-18 was used. It is rated for a continuous current of 6 Amps and a peak current of 18 Amps. This model was chosen based on the maximum continuous current for the RE40 motor being 3.33 amps. The Accelnet Micro Module was used to control the knee variable-damper mechanism and it is similar to the Accelus model but it comes in a PCB mount version which has a much smaller form factor. A custom PCB breakout board interfaced to the Accelnet board. The amplifiers were programmed via RS232 using the CME 2TM software from Copley. After entering the motor specifications into the software, the current loop P and I control gains were determined by using the current loop auto-tune feature in the software. The continuous and peak current limits were entered in the software to protect the actuators while tuning the closed loop force gains in the early stages. The amplifier control parameters were then saved to flash memory and the RS232 connection was terminated.

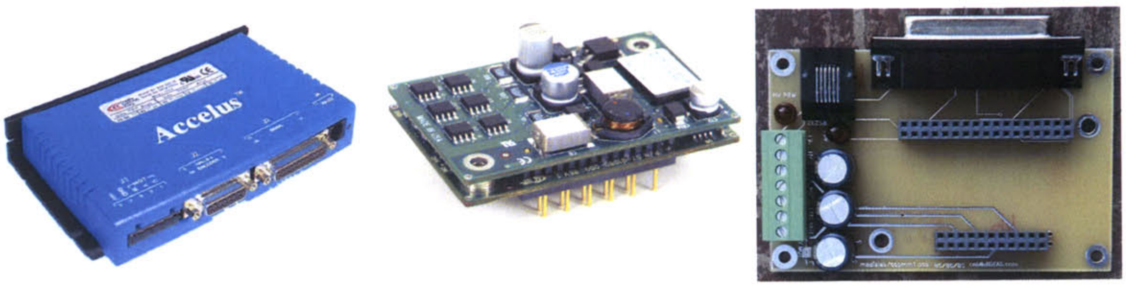

Figure 4.2 In a), the Accelus digital amplifier used at the hip is shown. In b), the PCB mount Accelnet mico-module used at the knee required a breakout board. In c), the custom breakout board for the Accelnet

4.1.3 Signal Conditioning

The sensors on the exoskeleton were read into the computer as analog voltage signals. There was significant noise pick-up on the relatively long connection cables from the sensors on the exoskeleton due to the amplifiers, motors and dampers. In order to achieve a good signal to noise ratio the sensor raw voltage readings were amplified with a differential line driver and the signal was also filtered with an analog low pass filter with a cut off at 1.5kHz.

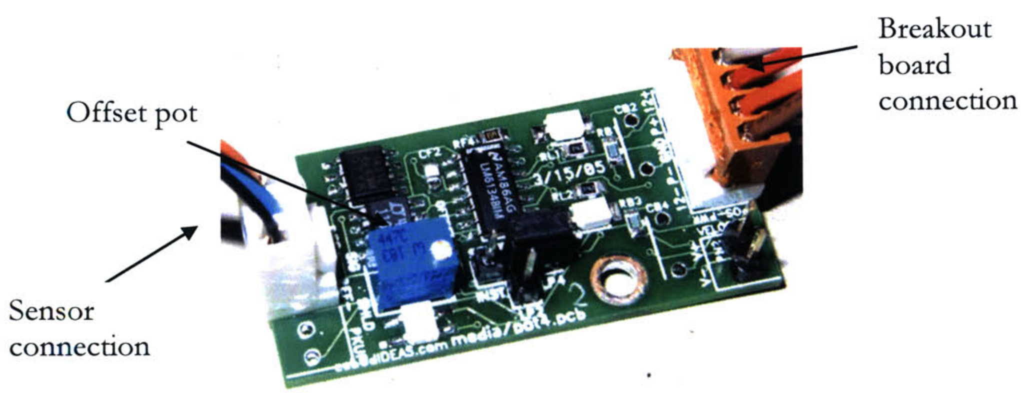

Figure 4.3 Signal conditioning board. One side reads in the voltage from a strain gauge bridge or potentiometer. The other connector differential power to the board and sends an amplified differential signal to the breakout board that gets read by the D/A board.

4.2 Sensing

The exoskeleton was instrumented with sensors in order to detect state transitions for real time control of actuation at the hip and knee. The angles of the exoskeleton hip and knee joints as well as the hip torque were recorded. Strain gauges on the structure of the exoskeleton shank measured the bending moment of the shank as well as the vertical force borne by exoskeleton leg.

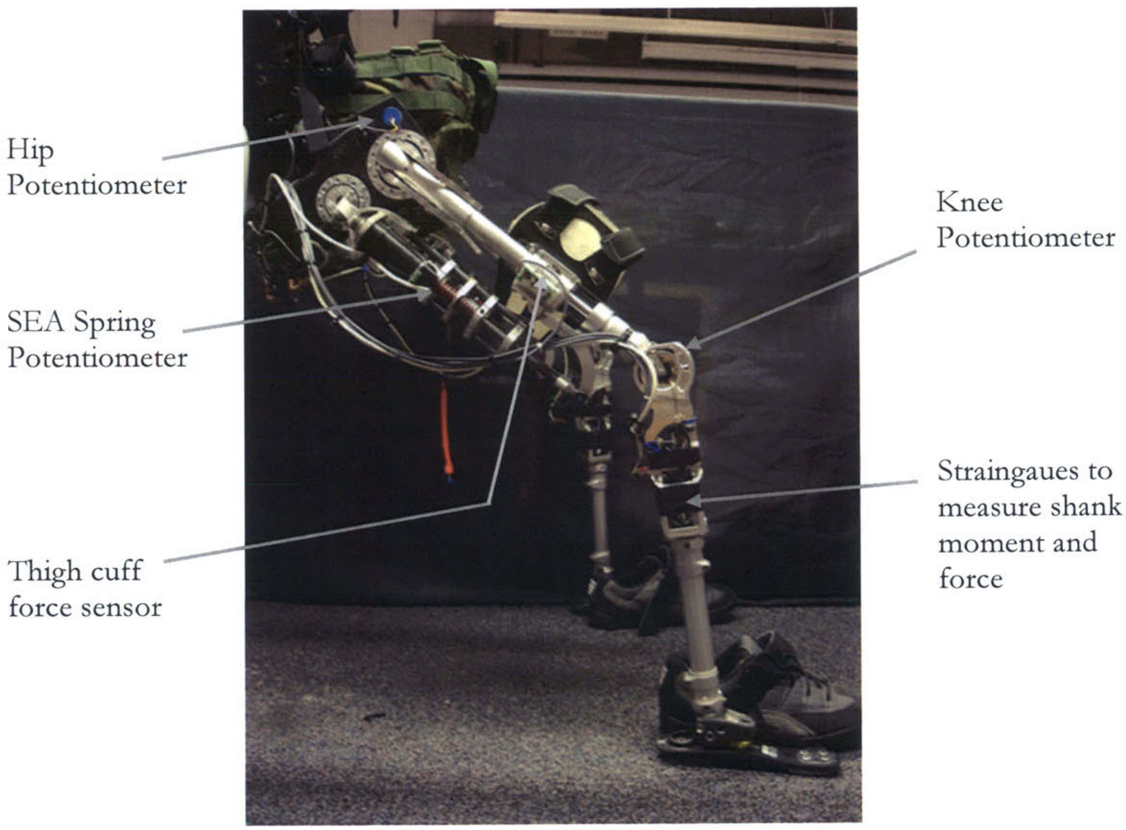

Figure 4.4 Sensors on the exoskeleton leg.

4.2.1 Angle Sensing

The angle of the hip (thigh relative to pelvic harness) and the knee (shank relative to the thigh) were measured using rotary potentiometers. The signals from these potentiometers were amplified and filtered using the signal conditioning board in potentiometer configuration, with a gain of 1.

Figure 4.5 Hip angle sensing was done by means of a timing belt and pulley with a 2:1 reduction on a Bournes rotary pot. The belt system was attached to the hip joint on the inside of the harness as shown.

4.2.2 Hip Torque Measurements

The hip torque produced by the actuator was acquired by measuring the deflection of the spring pack of the series elastic actuator. The torque at the hip joint was calculated by multiplying the linear force measured with the potentiometer by the moment arm of the actuator. This measurement was used for the closed loop control of the actuator.

4.2.3 Ground – Exoskeleton interaction sensing

Strain gauges placed on the structure of the exoskeleton shank were used to measure the bending moment of the shank as well as the vertical force in the exoskeleton leg. The signals from the strain gauges were amplified and filtered using the signal conditioning board in the strain gauge configuration with a gain of 500. The moment in the shank was calculated by subtracting the signals from the two bridges and the vertical load was calculated by adding the two signals. Figure 4.6 illustrates this and equations 4.1 and 4.2 were used to calculate the force and moment respectively. The gains, k_f and k_m were determined experimentally by calibrating the raw voltage with known weights.

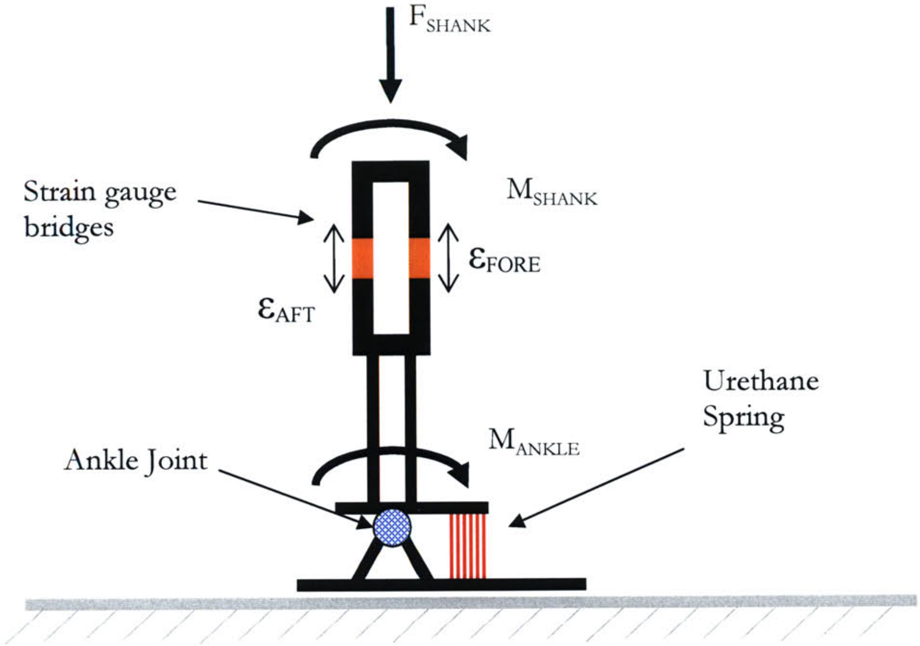

Figure 4.6 Schematic of exoskeleton shank and foot.

$$F_{SHANK} = (\varepsilon_{AFT} + \varepsilon_{FORE}) * k_f \quad \textbf{(4.1)} \qquad M_{SHANK} = (\varepsilon_{AFT} - \varepsilon_{FORE}) * k_m \quad \textbf{(4.2)}$$

4.2.4 Human – Exoskeleton interaction sensing

For the purpose of measuring the interaction force between the human thigh and exoskeleton leg, a custom sensor was built. The sensor consisted of a spring pack and the deflection of the springs was measured with a spring loaded linear potentiometer. The device, shown in Figure 4.7, consisted of die springs, shown in orange, that get compressed due to relative movement of the two parts (one attached to the exoskeleton leg and the human leg) and the displacement was measured with a potentiometer, giving a reading of the force.

One reason for measuring the force at the thigh was that a control strategy could be implemented whereby a motor at the hip could servo the exoskeleton to zero the force felt at the thigh. This would effectively make the exoskeleton get out of the way of the wearer. Additionally, the measured interaction force at the thigh could be used with the thigh velocity to estimate the power transfer between the exoskeleton and the wearer. The velocity at the thigh could be calculated by differentiating the angular position of the hip joint.

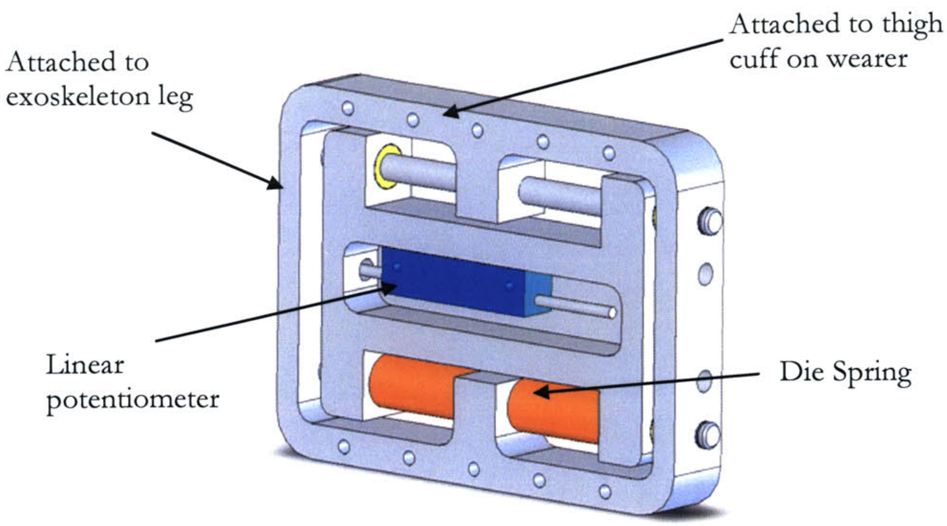

Figure 4.7 Thigh cuff sensor for measuring the force between the exoskeleton and human thigh.

4.3 Control Strategies

The controller for the exoskeleton was required to perform actuation at the hip and knee based on knowledge of the current phase of the gait of the wearer. A state machine control strategy was implemented based on angle and force sensor readings of the exoskeleton. Human walking kinematic and kinetic data motivated the actuation to be commanded in the individual states. Figure 4.8 outlines the desired actuation as a function of gait cycle.

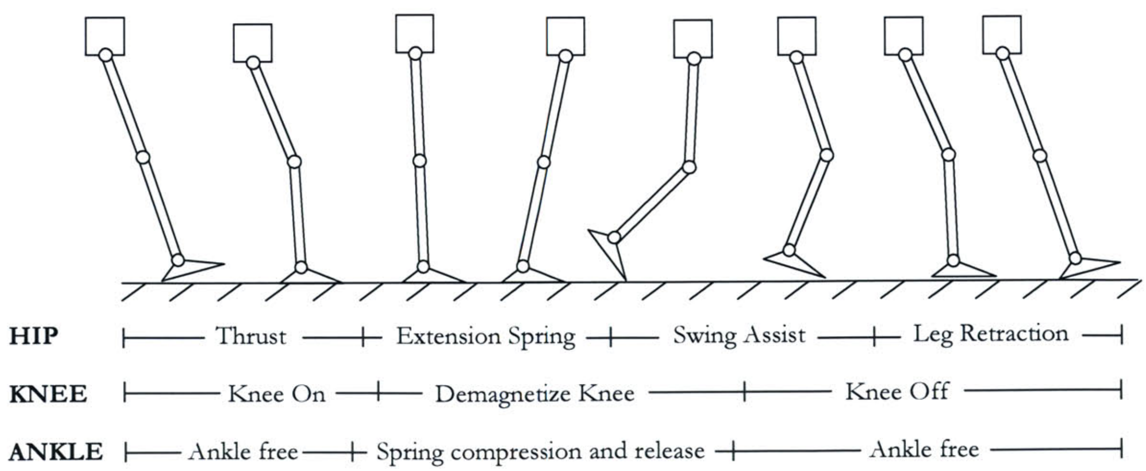

Figure 4.8 Summary of the actuation control of the exoskeleton leg as a function of gait cycle with an actuator at the hip and a variable-damper mechanism at the knee. The ankle is completely passive but is included for completeness.

1) Hip

For the *Thrust* phase, the actuator at the hip exerted a torque to help raise the center of mass of the exoskeleton and human. During the next phase, *Extension Spring,* a virtual spring was programmed that was 'compressed' as the center of mass of the exoskeleton moved forward. As the leg changed direction the *Swing Assist* phase was entered where the energy was 'released' from the virtual spring, and a torque was applied to assist in swinging the leg forward. *Leg Retraction* was entered after full hip flexion and a torque was applied to assist in foot placement and weight acceptance.

2) Knee

Knee On occurred at heel strike and the variable-damper mechanism was programmed to exert a torque proportional to the rotational velocity of the knee joint. Two different gains were used, depending on the velocity sign, to control knee rotation for knee flexion and extension. After the knee was turned off there was a residual magnetic field, and hence a resistive torque, that impeded the swinging of the wearer's leg. The knee was turned off and demagnetized when the knee joint was locked at full extension during the late stance phase. The demagnetization procedure was described in section 3.6.2. After this phase the variable-damper mechanism was turned off throughout the entire swing phase.

4.3.1 Knee Controller

The state-machine controller for the knee processed knee angle and force and moment in the exoskeleton leg to define four stages of the walking cycle. Knowledge of these states provided periods of the gait cycle when the desired action of the variable-damper mechanism at the knee was known. Table 4.1 lists the states and the sensor readings that were used as triggers to switch between states and Figure 4.9 graphically shows the state-machine operation. An *Off* state was implemented so that any time the leg was raised off the ground, and the load in the exoskeleton leg approached zero, the variable-damper mechanism was turned off, allowing the knee to bend freely.

State	Description	Trigger
0	Not walking and leg is unloaded	Load in exoskeleton leg
1	Stance Flexion and Extension	Load in exoskeleton leg
2	Pre-swing	Knee angle and moment in exoskeleton leg
3	Swing Flexion	Load in exoskeleton leg
4	Swing Extension	Knee angle

Table 4.1 Description of states and their respective triggers for the state-machine of the knee controller.

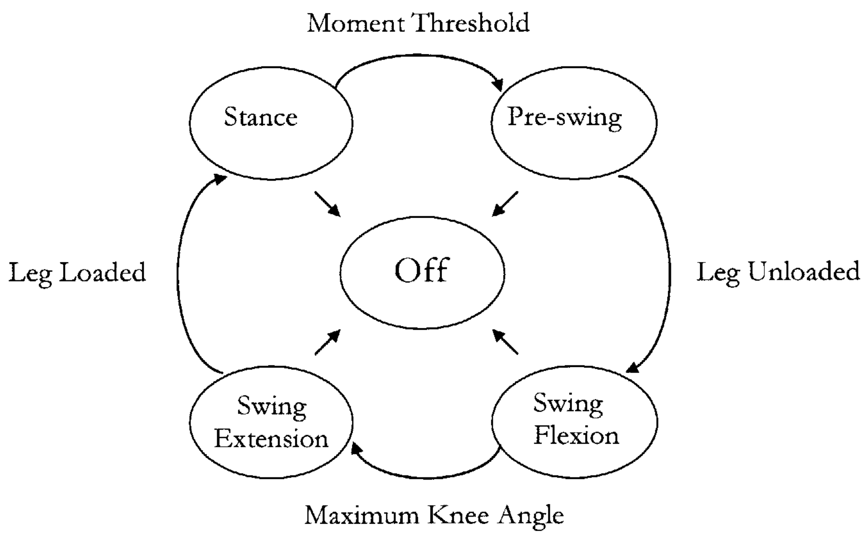

Figure 4.9 State-machine diagram for the knee controller.

Figure 4.10 shows data collected from the exoskeleton leg as a function of gait cycle. It shows the knee angle as well as the force and moment in the exoskeleton shank. The states of the knee controller are superimposed on the plot in grey. The data are plotted vs. percent gait cycle and it goes from heel-strike to next heel-strike of the same limb. It can be see that on initial heel-strike the force in the shank rises rapidly. When this force passed a set threshold, the knee entered the first state where a virtual damper was implemented. *Pre-swing* can be seen to be entered when the moment in the shank reached a certain threshold and it is in this state that demagnetization of the knee occurred. As the leg left the ground as the swing phase began, the load in the exoskeleton shank dropped to near zero triggering *Swing Flexion.* The knee state-machine entered the final state *Swing Extension* when maximum knee flexion was reached.

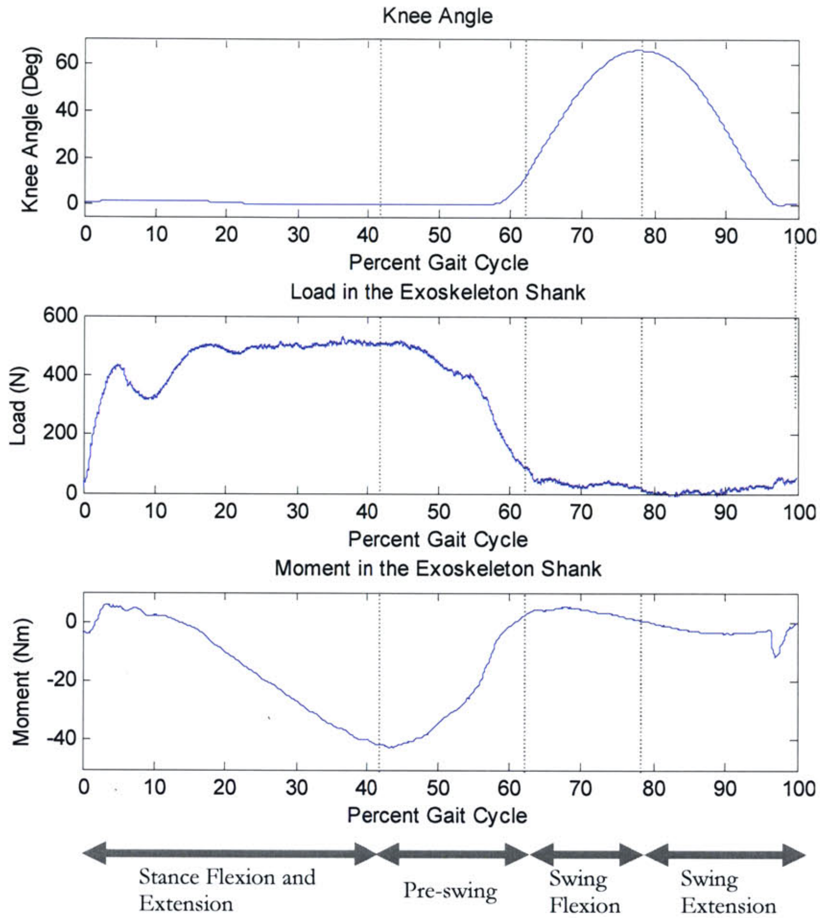

Figure 4.10 Sensor data from the exoskeleton leg for a single gait cycle. States 1 to 4 of the controller are superimposed on the plot.

For steady state walking, the state machine cycled through states 1 to 4 as shown in Figure 4.11. The figure shows real-time data for an 18 second period of a walking trial. The state is superimposed in red. It was found that the controller worked robustly for all the experimental walking trials performed for subject testing. The figure also shows the state-machine operation while the person is no longer walking but shuffling or turning around. The controller goes back and forth between state zero, where the leg is off the ground, and state one, where the leg is on the ground. Once walking resumed the controller began cycling through the states associated with walking in less than one gait cycle.

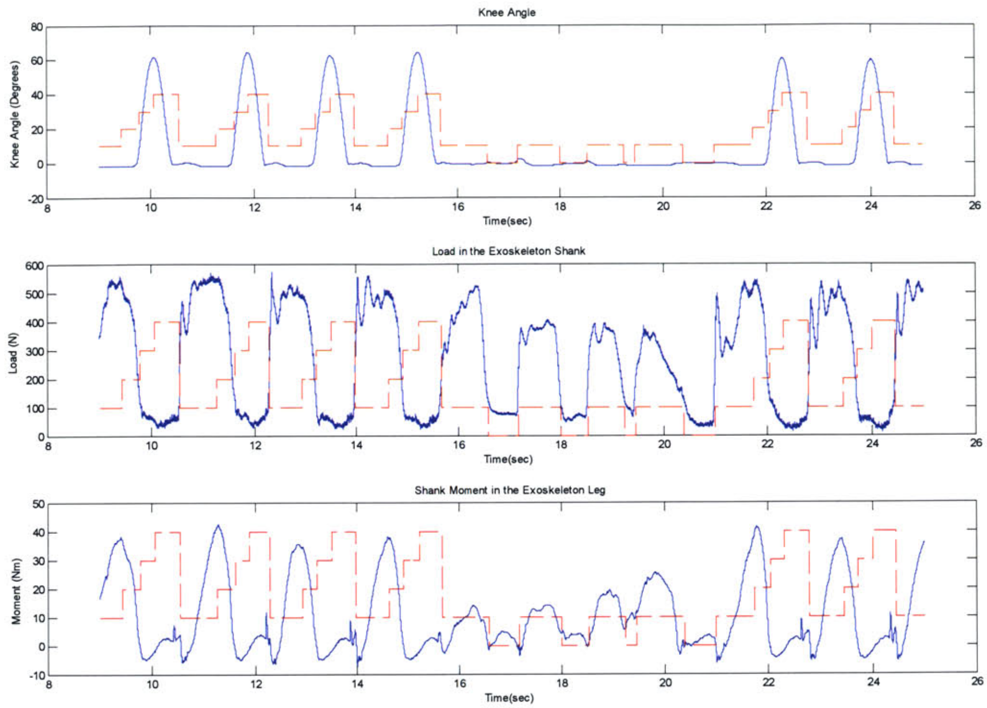

Figure 4.11 The state machine for the exoskeleton knee in operation. The data shows the person walking normally, then shuffling as they turn around and then walking some more.

4.3.2 Hip Controller

The state-machine controller for the hip used the hip angle and the force in the exoskeleton leg to define five stages of the hip during the walking cycle. Figure 4.12 illustrates these states as well as the triggers used to switch between states. State 1 is *Late Stance Extension* as this was deemed to be the most repeatable trigger to determine that walking had started.

State	Description	Trigger
0	Not Walking	Timeout
1	Late Stance Extension	Negative velocity when angle is less than zero
2	Early Swing Flexion	Change in sign of velocity
3	Late Swing Flexion	Angle is greater than some threshold
4	Leg Retraction	Change in sign of velocity
5	Early Stance Extension	Force threshold in leg

Table 4.2 Description of states for hip controller.

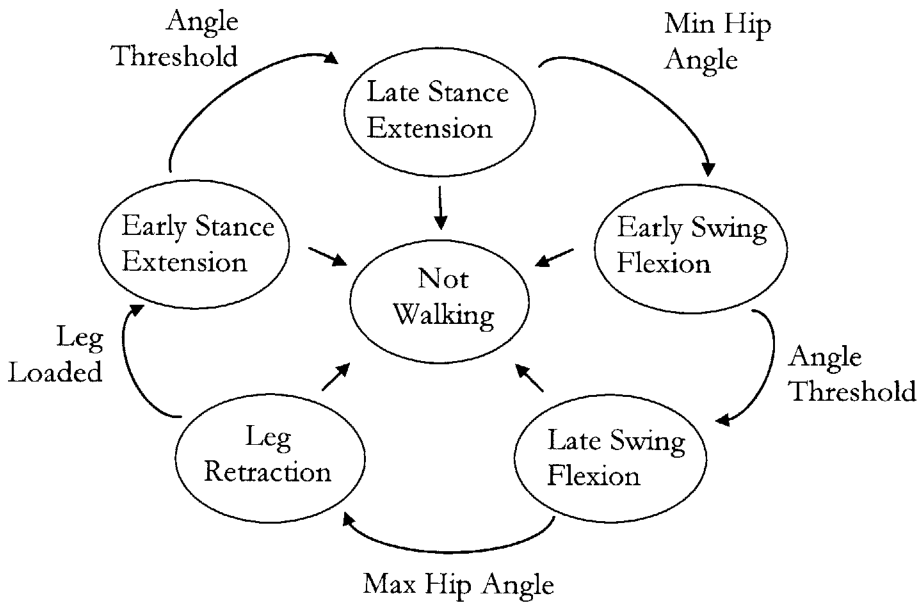

Figure 4.12 State machine diagram for the hip controller.

Figure 4.13 shows data collected from the exoskeleton leg as a function of gait cycle. The states of the hip controller are superimposed on the plot. The controller for the hip entered the first state, *Late Stance Extension,* as the hip angle dropped to a certain threshold. The controller remained in this state until it reached a minimum value. This minimum value was detected when the velocity of the hip joint went to zero and the *Early Swing Flexion* state was then entered. The velocity was calculated by means of a band-limited differentiator so as not to differentiate the high frequency noise component of the angle signal. *Late Swing Flexion* was entered as the hip angle rose to the same angle threshold as that which triggered *Late Stance Extension.* The next state, *Leg Retraction,* was entered when the velocity was again zero; this was when the angle reached a maximum value. The final state, *Early Stance Extension,* was triggered when the load in the exoskeleton leg rose above a pre-determined threshold.

For steady state walking, the state machine cycled through states 1 to 5 as shown in Figure 4.14. Like the knee controller, walking trials proved that the state machine worked robustly. The figure illustrates that as the subject stopped and turned around the controller entered, and remained in, the *Not Walking* state until walking resumed. Once walking did begin the controller detected it in less than one gait cycle.

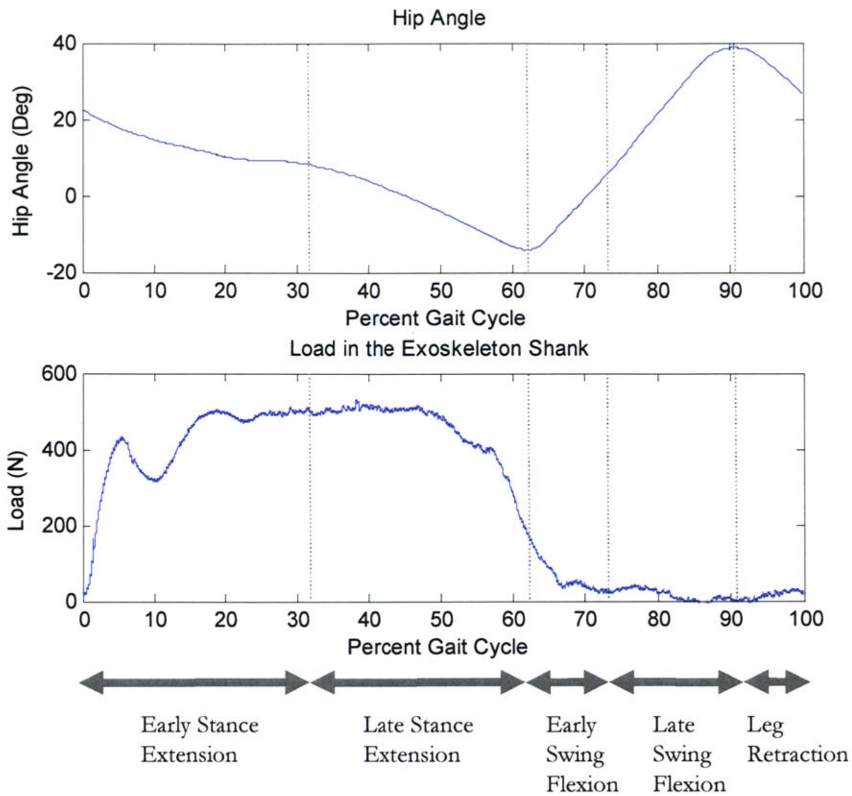

Figure 4.13 Sensor data from the exoskeleton leg for a single gait cycle. The exoskeleton hip angle and load in the exoskeleton leg are shown. States 1 to 5 of the hip controller are highlighted.

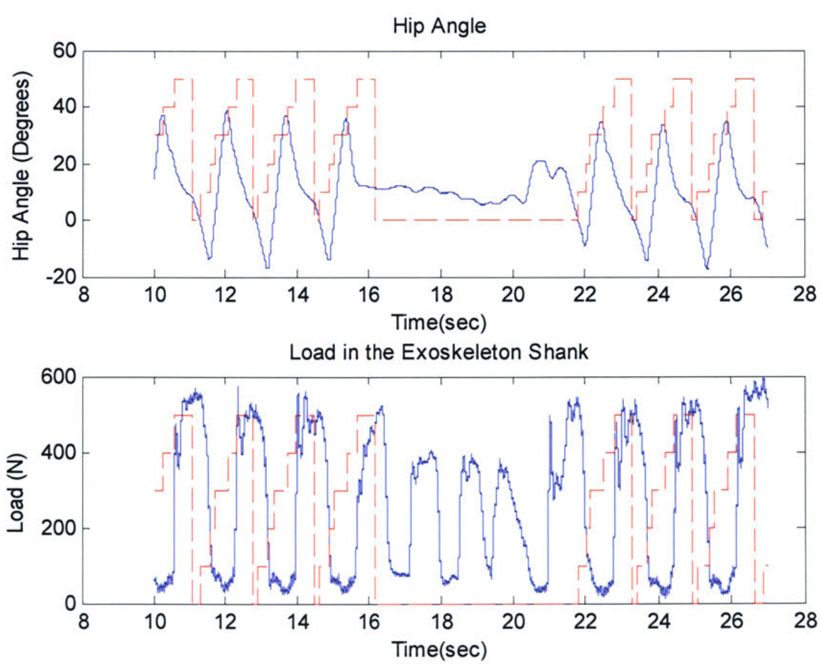

Figure 4.14 The state machine for the exoskeleton hip in operation. The data shows the person walking normally, then shuffling as they turn around and then walking some more.

The control strategy for the hip was discussed at the start of Section 4.3. During the different states an appropriate torque was produced by the actuator at the hip to assist in walking. This was implemented by having the actuator apply a force in proportion to an error from a desired angle, thereby simulating springs during different periods of the gait cycle. A GUI is shown in Figure 4.15 that was used to experimentally tune the values for the various phases of the gait cycle. A different virtual spring constant was used for each of the different phases of the gait cycle defined by the state-machine. The output force was filtered through a low-pass filter to smooth the torque output applied by the actuator. The GUI also allowed for easy configuration of the force and angle thresholds set for the state-machine controllers of the hip and knee.

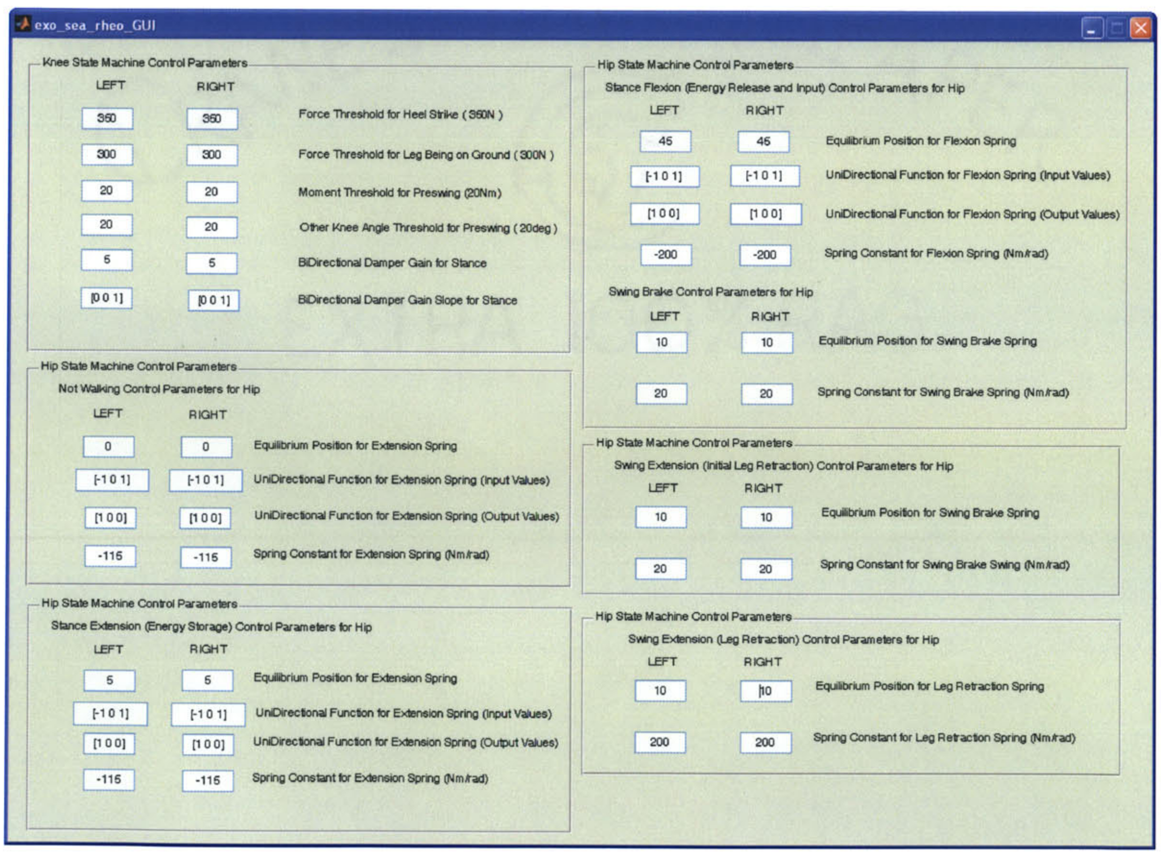

Figure 4.15 GUI used to vary the parameters for gait cycle state-machine tuning.

5 Experimental Methods

This chapter describes the detailed methodology of the human experiments and outlines the experimental methods and metrics for quantifying the metabolic cost. Data collection was spread over a number of days to avoid fatigue effects. Experiments were performed for a number of actuation methods for the exoskeleton as well as a control where a subject walked with a backpack load of 75lbs.

5.1 Experimental Subjects

The subject for the metabolic experiments was the author of this thesis. The subject's relevant information and anthropometric measurements can be found in Table 5.1.

[n]	Participant	Age [yr]	Sex [M/F]	Mass [kg]	Leg Length [m]	Walking Speed [m/s]
1	Author	23	M	76	0.93	

Table 5.1 Experimental participant data.

5.2 Data Collection

Metabolic data were collected during a set of walking experiments where walking speed was controlled by means of a modified golf caddy. Metabolic cost was quantified by measuring the volume of oxygen (VO_2) that the human consumed while performing an experiment. Measuring metabolic cost is appropriate since there is a proportional relationship between the mechanical work done by the human and metabolic cost (Donelan, 2002). Kinematic and kinetic data of the exoskeleton were also recorded.

5.2.1 Measurement of Energy Cost

The energy cost was estimated from O_2 consumption and CO_2 production measured with a portable K4 telemetric system (Cosmed, Italy) (Hausswirth *et al.*, 1997). The K4 system included a portable unit worn by the subject and a base station where the data was recorded. The portable unit weighted 1.5kg and consisted of a silicon mask containing a flow-rate turbine which was fixed to the subject's face. A processing unit containing the O_2 and CO_2 analyzers was placed on the subject's chest and a transmitter/battery pack was placed in the backpack. The day of each trial the turbine was calibrated with a 3l syringe, and a two point calibration of the O_2 and CO_2 analyzers was carried out using ambient air and a standard calibration gas mixture (5% CO_2, 16% O_2, 79% N_2).

5.2.2 Measurement of Walking Speed

In order to achieve consistent metabolic data it was important that the subject walked at a constant known walking speed. The speed for a trial was set with an electric, speed adjustable golf caddy. The cart's motor was instrumented with a voltmeter and the voltage applied to the motor was measured. This voltage was calibrated to speed by setting the applied voltage to the motor and recording the time to travel a known distance. The calibration curve was shown in Figure 5.1.

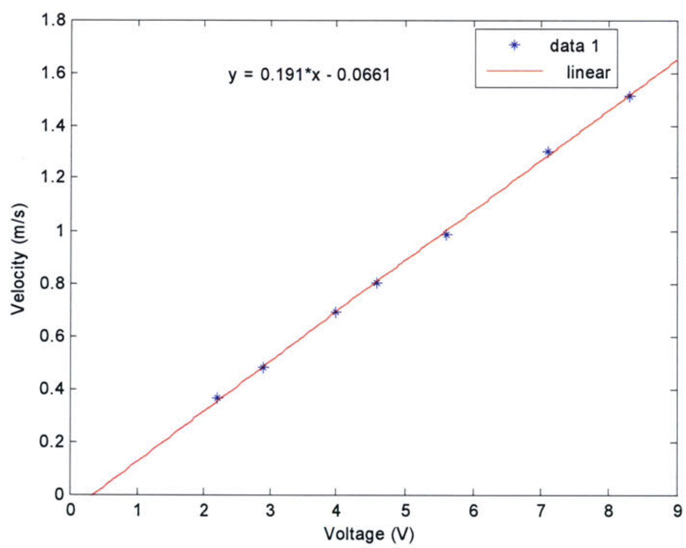

Figure 5.1 Caddy velocity calibration.

5.2.3 Kinematic and Kinetics Measurement

The relative angle between the harness and the thigh (hip angle) and the thigh and the shank (knee angle) were recorded. This kinematic data was used to examine the gait of the exoskeleton (e.g. peak flexion and extension angles) and differences between the exoskeleton gait and normal human walking were noted. The load and the moment in the shank of the exoskeleton leg were also recorded and plotted as a function of gait cycle.

By recording the load in the leg it was possible to determine the percentage of the exoskeleton load plus payload that was transferred through the exoskeleton leg to the ground. The moment measurement in the shank recorded the maximum moment that was seen by the ankle spring as it was compressed during walking. Knowing the stiffness of the ankle spring, the maximum deflection and hence energy storage at the exoskeleton ankle during walking was estimated.

5.3 Experimental Protocol

Experiments were performed at Massachusetts Institute of Technology (MIT) at the Johnson Indoor Track. The subject walked around the track and individual trials lasted 10 minutes.

5.3.1 Human Use Approval

The exoskeleton and backpack experiments were approved by MIT's Committee on the Use of Human as Experimental Subjects (COUHES). The subject was a volunteer and was permitted to withdraw from the study at any time for any reason. Before participating in the study, the subject read and signed a statement acknowledging informed consent. Appendix B includes a copy of the subject consent form.

5.3.2 Subject Preparation

The subject was advised of the following guidelines for behavior before experiments

1. No intense or prolonged exercise for 24 hours
2. No caffeine for 3 hours
3. No heavy meals for 3 hours
4. Stay hydrated
5. No talking when wearing the VO_2 mask
6. Maintain a consistent walking speed and walking cadence

5.3.3 Test Procedure

The order of events of the experiment and a brief description of each are outlined below.

1. Acclimating to the exoskeleton or backpack

The subject walked wearing the exoskeleton for a few minutes to acclimatize to the hardware and to find a self-selected walking speed and cadence.

2. VO_2 system worn

The Cosmed VO_2 mask was fastened tightly to the subjects face to prevent any air leakage. The Cosmed portable unit was strapped to the subject's chest.

3. Pre-Test resting metabolic rate

The subject was seated and 5 minutes of resting metabolic rate was recorded.

4. Testing metabolic measurement

The walking test (either with the backpack or the exoskeleton) was performed by walking around the Johnson Indoor track at MIT on the inside lane.

5. Post-Test resting metabolic rate

The subject was seated for 5 minutes and the resting metabolic rate was measured again.

6. Resting

The subject took a small break and drank some water.

5.4 Data Analysis

Walking trials lasted 10 minutes and the average Vo_2 (ml O_2/min) and Vco_2 (ml CO_2/min) values for steady state (the last 3 minutes of the trial) were calculated. Rest measurements were taken while the subject was seated for 5 minutes before and after each walking trial and the average resting value was calculated. For all experiments performed for this thesis, the respiratory exchange ratios were less than or equal to 1.0, indicating that energy was supplied primarily by oxidative metabolism in all test conditions. The gross metabolic rate for each walking trial was calculated using the following standard equation (Brockway, 1987).

$$\dot{E}_{\text{metab, gross}} = 16.58\frac{W \cdot s}{ml\,O_2}\overline{\dot{V}o_2} + 4.51\frac{W \cdot s}{ml\,CO_2}\overline{\dot{V}co_2} \qquad \textbf{(5.1)}$$

Where $\dot{E}_{\text{metab, gross}}$ is gross metabolic rate, W is watts and $\overline{\dot{V}o_2}$ and $\overline{\dot{V}co}$ are mean values. For the experiments, the net metabolic rate of performing a trial was calculated by subtracting the metabolic rate while resting (sitting) from the gross metabolic rate.

$$\dot{E}_{\text{metab, net}} = \dot{E}_{\text{metab, gross}} + \dot{E}_{\text{resting}} \qquad \textbf{(5.2)}$$

To quantify the metabolic advantage of the exoskeleton $\dot{E}_{\text{metab, net}}$ was obtained for a number of trials which are outlined in the chapter 6.

6 Results and Discussion

Initial walking experiments were conducted with the exoskeleton loaded with a 75lb payload. Kinematic and kinetic data were recorded and analyzed. Metabolic data from a number of experiments of various exoskeleton configurations as well as a control experiment are presented and the results are compared and discussed.

6.1 Kinematic and Kinetic Data

The exoskeleton was instrumented with angle, force and moment sensors to measure real time characteristics of the exoskeleton gait. This information was used to compare the trajectories of the joints of the exoskeleton to that of the human joints in normal walking. The force sensing in the exoskeleton leg allowed the percentage of the weight of the exoskeleton and payload being transferred through the exoskeleton leg to be determined.

6.1.1 Hip and Knee Trajectories

It was found that the hip and knee angles in the sagittal plane followed similar trajectories to that of normal human gait kinematics, indicating that the exoskeleton gait was similar to that of normal human walking. Figure 6.1 shows the measured angles as a function of gait cycle as the subject walked with the exoskeleton. The range of motion of the exoskeleton hip joint for a typical gait cycle was found to be approximately fifty five degrees which agrees well with the fifty degrees for the human hip data in Figure 2.7. However the trajectory of the exoskeleton hip was not as close to a sinusoid as the normal human walking hip trajectory. It can be seen that, when wearing the exoskeleton, leg retraction began earlier (before heel strike). This is likely due to the increased mass attached to the human leg which limited maximum hip flexion and caused leg retraction to begin earlier. Maximum knee flexion of the exoskeleton was on average sixty degrees, a value which is similar to that of human knee flexion at slow to moderate walking speeds as seen in Figure 2.10. However, at heel strike the knee of the exoskeleton did not exhibit a similar amount of initial knee flexion and extension. This is due to the fact that the exoskeleton knee exerted high damping on heel strike in order to bear load.

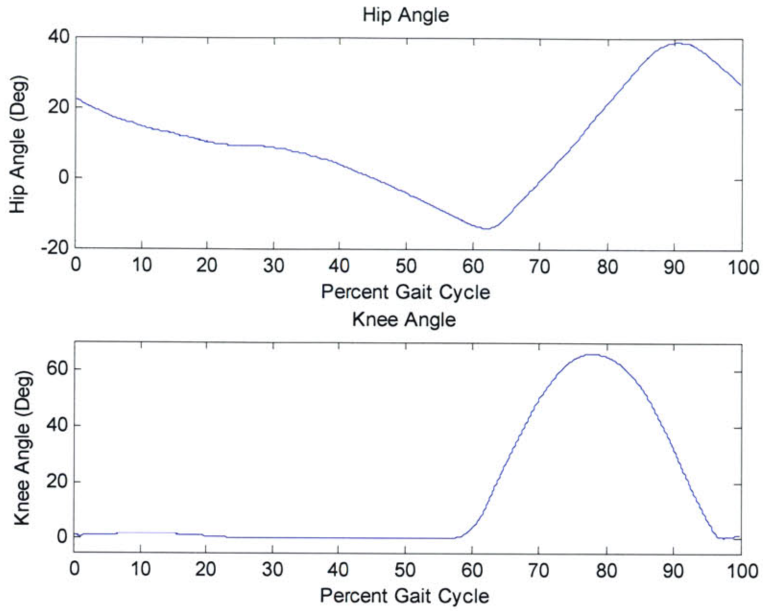

Figure 6.1 Hip and knee angle data of the exoskeleton as a function of gait cycle. The data are shown from heel strike to heel strike.

6.1.2 Load in the exoskeleton shank as a function of gait cycle

The function of the exoskeleton leg was to transfer the payload weight as well as the weight of the exoskeleton to the ground during the stance phase of the walking cycle. The force and moment in the exoskeleton shank were recorded as the subject walked with the exoskeleton. Figure 6.2 shows the load in the exoskeleton leg as a function of the gait cycle.

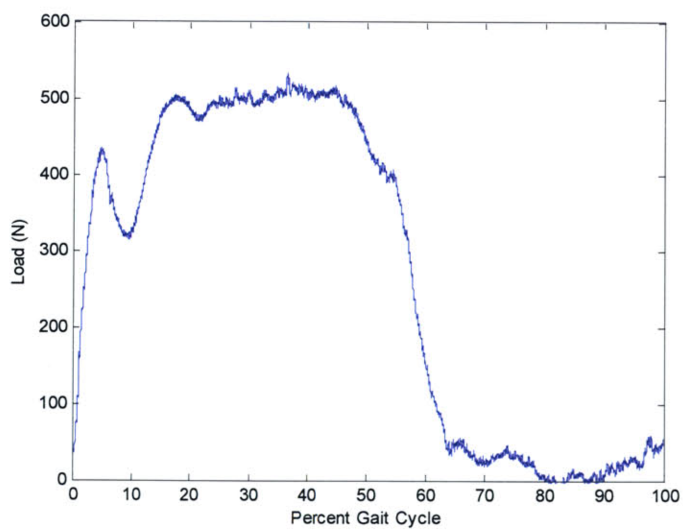

Figure 6.2 Load in the exoskeleton leg shank as a function of gait cycle. Heel strike is evident by a large increase in measured force level. During the swing phase it can be seen that there is minimal load in the exoskeleton leg.

It was determined that approximately 90% of the weight of the payload and exoskeleton mass was transferred through the exoskeleton leg structure to the ground. This result demonstrates that the under-actuated leg exoskeleton presented in this thesis is capable of transferring the weight to the ground. One reason that 100% of the weight was not transferred to the ground is that some of the weight was born through the interface between the exoskeleton and the wearer, i.e. the shoulder straps, waist belt and thigh cuffs.

6.1.3 Moment in the exoskeleton shank as a function of gait cycle

During controlled dorsiflexion in walking, the muscles about the ankle joint help to control the body falling forward. The spring at the ankle joint of the exoskeleton was compressed during controlled dorsiflexion and this can be seen by the increasing moment in the shank of the exoskeleton leg as a function of gait cycle in Figure 6.3. The spring constant value along with the maximum moment seen in the exoskeleton shank allowed the amount of energy stored by the spring to be estimated at 2.3J. This is approximately four times lower than that observed from the biological gait data shown in Figure 2.15 and this is due to the fact that the maximum peak moment observed for the exoskeleton was half that of normal human walking.

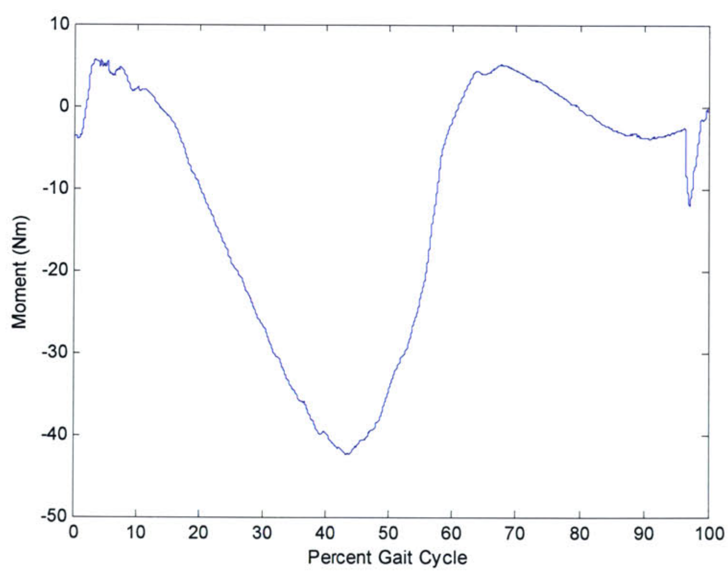

Figure 6.3 Moment in the exoskeleton shank as a function of gait cycle. It is seen that during controlled dorsiflexion the moment is increasing. During powered plantarflexion this moment goes to zero as the energy stored in the ankle spring is released. During the swing phase the moment is close to zero.

6.2 Metabolic Measurements

A summary of the metabolic data taken during the experiments performed at MIT is shown in Table 6.1. $\overline{\dot{V}o_2}$ and $\overline{\dot{V}co}$ data are shown for all walking tests as well the average rest data from before and after each walking trial. For all experiments the respiratory exchange ratio (RER) was less than 1. The self selected walking speed while wearing the exoskeleton was 0.8m/s and walking speed was controlled so that tests were performed at approximately this speed. A number of tests were also performed with and without payload at 0.59, 0.8 and 0.9m/s. Data were also collected with the subject wearing a non-actuated exoskeleton (no motor, variable-damper, or spring) with and without payload.

Description	Load	Speed	Vo_2 [ml/min]			Vco_2 [ml/min]			RER
	[lbs]	[m/s]	Walk	Rest	Net	Walk	Rest	Net	
Backpack (Alice military pack)	0	0.80	780	250	530	610	174	436	0.82
	0	0.90	806	350	456	778	271	507	0.98
	75	0.59	961	223	738	808	194	614	0.83
	75	0.80	1106	280	826	849	194	655	0.79
	75	0.90	1181	285	896	975	213	763	0.82
Exo with Rheo and Ankle Spring	75	0.80	1330	280	1050	1285	274	1012	0.96
Exo with SEA, Rheo and Ankle Spring	75	0.76	1595	202	1394	1445	156	1289	0.93
Exo with no actuation (light pin joints)	0	0.77	976	207	769	829	177	652	0.85
	75	0.77	1545	264	1282	1507	239	1269	0.99

Table 6.1 Summary of metabolic data from experiments.

Using the $\overline{\dot{V}o_2}$ and $\overline{\dot{V}co}$ data from Table 6.1 the net metabolic cost for the walking trials was calculated using equations 5.1 and 5.2 and the results are listed in Table 6.2. As described in Chapter 5, $\dot{E}_{metab,\,net}$ gives a measure of the power required to walk. The resting metabolic rate can be seen to vary slightly over the trials and the average value was 85W. In the following sections, the exoskeleton is evaluated by comparing the power required to walk from the results of the different experiments performed.

Description	No	Load	Speed	$\dot{E}_{metab,\,gross}$	$\dot{E}_{metab,\,resring}$	$\dot{E}_{metab,\,net}$
		[lbs]	[m/s]	[W]	[W]	[W]
Backpack (Alice military pack)	1	0	0.80	261	82	179
	2	0	0.90	281	101	181
	3	75	0.59	326	76	250
	4	75	0.80	369	92	277
	5	75	0.90	400	86	313
Exo with Rheo and Ankle Spring	6	75	0.80	464	98	366
Exo with SEA, Rheo and Ankle Spring	7	75	0.76	549	67	482
Exo with no actuation (light pin joints)	8	0	0.77	332	71	262
	9	75	0.77	540	91	449

Table 6.2 Metabolic cost for the various exoskeleton and control experiments performed.

6.2.1 Speed dependence on metabolic cost for load carrying

Metabolic data were collected for a number of walking speeds while carrying the backpack. The results are shown in Figure 6.4 below. The increase in net metabolic rate with speed agrees with the exponential increase reported in the literature (Bastien *et al.*, 2005).

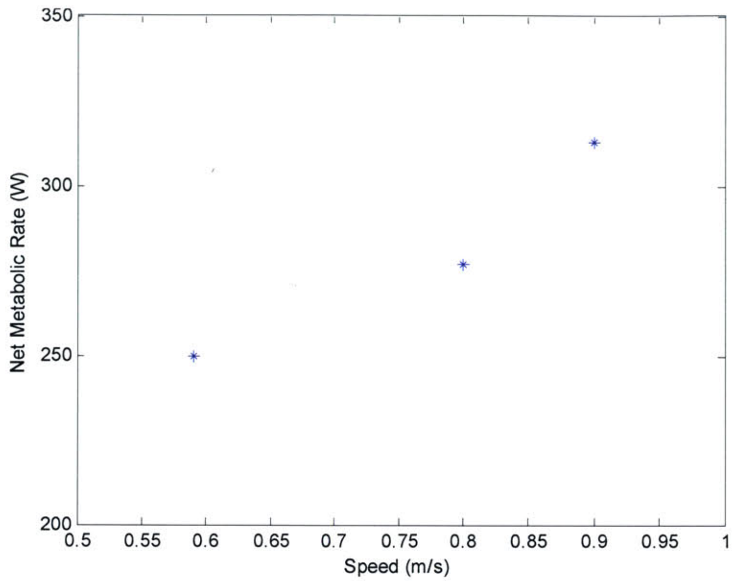

Figure 6.4 Increasing metabolic cost of carrying 75lbs with increasing walking speed.

6.2.2 Exoskeleton with actuation vs. walking

In order to quantify the advantage that the exoskeleton achieved when carrying a payload, metabolic data are compared to a control experiment where the subject carried a backpack unassisted. Two configurations of the exoskeleton were tested. The first was the exoskeleton with a non-conservative actuator at the hip, variable-damper mechanism at the knee and a uni-directional spring at the ankle. For the second case the actuator at the hip joint was removed.

Configuration with 75lb payload	**Speed [m/s]**	**E_{net} [W]**	**Advantage [%]**
Backpack	0.80	277	-
Exo with hip motor, knee damper and ankle spring	0.76	482	-74
Exo with knee damper and ankle spring	0.80	366	-32

Table 6.3 Comparison of walking with 75lbs with and without the exoskeleton. Two configurations of the exoskeleton were tested.

From Table 6.3 it can be seen that for both configurations more effort was required to walk with the exoskeleton compared to unassisted load carrying. Factors that likely contributed to the increased metabolic rate are the mass of the exoskeleton, the kinematic constrainment of the exoskeleton and non-collocation of the exoskeleton and human joints. Another possible reason for the increase in metabolism is that the exoskeleton knee joint had some intrinsic damping. During the swing phase the human may have had to do extra work to overcome this resistance. The amount of energy stored in the ankle spring was estimated to be 2.3J and this compares to approximately 9J based on biological data. An increase in the amount of energy stored at the ankle would assist the exoskeleton foot come off the ground thus reducing the effort exerted by the wearer. The results also show that adding actuation at the hip has a negative effect. This could be due to the fact that the weight of the actuators and battery pack out way the benefit of the power added.

6.2.3 Effect of increased mass for actuation at knee and ankle

By comparing distinct exoskeleton configurations, the relative effect of the exoskeleton components was determined. In this case the exoskeleton with variable-damper mechanism at the knee and spring at the ankle is compared to a non-actuated exoskeleton where the joint components were replaced with pure pin joints. Metabolic data show that the variable-damper knee and ankle spring mechanisms increase metabolism by only 32%, whereas a non-actuated exoskeleton (no motor, variable-damper, or spring) increases walking metabolism by 62% as can be seen in Table 6.4. This result highlights the benefit of ankle elastic energy storage and knee variable-damping in exoskeleton design.

Configuration with 75lb payload	**Speed [m/s]**	**$E_{metab,net}$ [W]**	**Advantage [%]**
Backpack	0.80	277	-
Exo with knee damper and ankle spring	0.80	366	-32
Exo with pin joints	0.77	449	-62

Table 6.4 The effect of increased mass for actuation at the ankle and knee.

6.2.4 Metabolic cost for wearing exoskeleton with no load

In order to quantify the metabolic cost a non-actuated exoskeleton imparted on the subject, metabolic data were recorded with the subject wearing an exoskeleton with a payload of 5lbs (weight of electronics) where the actuation at the joints was replaced with lightweight pin joints. The total weight of this system, including the backpack, was 29.4lbs. This is 17.8% of the mass of the subject. It has been shown that metabolic cost increases by 15% if a load of 10% of body weight is carried (Griffen *et al.*, 2003). If we assume a linear relationship between increase in load and metabolic cost and extrapolate this result, we can estimate that a load of 17.8% will increase the metabolic rate by 26.7%.

Configuration	**Speed [m/s]**	**$E_{metab,net}$ [W]**	**Incremental [W]**	**Advantage [%]**
Backpack with 0lbs	0.80	179	-	-
Exo with pin joints and 5lbs	0.77	262	83	-46
Backpack with 75lbs	0.80	277	98	-55

Table 6.5 The metabolic cost of wearing the exoskeleton with no load.

Table 6.5 it can be seen that wearing the non-actuated exoskeleton, the metabolic rate increased by 46% (83W). The fact that this is higher than 26.7% is expected because the weight of the exoskeleton was distributed along the human leg and it has been shown that distal mass is more metabolically costly than proximal mass (Royer *et al.*, 2005). Another possible reason for the higher value may be the fact that the exoskeleton affected the gait of the wearer. McMahon *et al.* (1987) showed that changes in gait increase the physiological energy expended during locomotion. For comparison, it can be seen that the increase in net metabolic rate for carrying 75lbs unassisted was 55% (98W). This is not much more than the case for the non-actuated exoskeleton with 5lbs payload. Further reducing the weight of the exoskeleton as well as reducing the affect on normal gait would likely reduce metabolism while wearing the exoskeleton.

6.2.5 Incremental cost of load carrying

The incremental cost for carrying a load was calculated by subtracting the net metabolic rate with no load from the net metabolic rate while carrying 75lbs.

Configuration	Speed [m/s]	$E_{metab,net}$ 0lbs	$E_{metab,net}$ 75lbs	Incremental Cost [75lbs – 0lbs]
Backpack	0.80	179	277	98
Exo with knee damper and ankle spring	0.77	262	366	104

Table 6.6 Incremental cost of load-carrying for walking with and without the exoskeleton.

Table **6.6** shows the incremental cost for carrying a load for the unassisted case and the case while wearing the exoskeleton with a variable-damper mechanism at the knee and a spring at the ankle. It can be seen that the increase in net metabolic rate was approximately 100W for both the unassisted case and the case when wearing the exoskeleton. This result suggests that the increase in metabolic rate when wearing the exoskeleton is more involved than simply the additional mass of the exoskeleton.

7 Conclusion

Metabolic studies have shown that there is a metabolic cost associated with carrying a load (Griffin *et al.*, 2003). Further studies have shown that by applying forward propulsive forces a person can walk with a reduced metabolic rate (Farley and McMahon, 1992; Gottschall and Kram, 2003). In this thesis, a lightweight, under-actuated exoskeleton is presented that runs in parallel to the human leg and transmits payload forces to the ground. The exoskeleton component design is based on the kinematics and kinetics of human walking. The joint components of the exoskeleton in the sagittal plane consist of a force-controllable actuator at the hip, a variable-damper mechanism at the knee and a passive spring at the ankle. A state-machine control strategy for the hip and knee is implemented and is based on joint angle and ground-exoskeleton force sensing. Data are collected from the sensors in real time and the controller for the hip and knee is shown to robustly work during walking trials.

It is demonstrated that the exoskeleton does transfer load to the ground with a 90% and higher load transfer depending on the phase of gait. Further, exoskeleton wearers report that the exoskeleton greatly reduces the stress on the shoulders and back. However, although a significant fraction of the payload is transferred through the exoskeleton structure, the exoskeleton is found to increase metabolic economy by 74%. By comparing distinct exoskeleton configurations, the relative effect of each exoskeleton component is determined. Metabolic data show that the variable-damper knee and ankle spring mechanisms increase metabolism by only 32%, whereas a non-actuated exoskeleton (no motor, variable-damper, or spring) increases walking metabolism by 62%. These results highlight the benefit of ankle elastic energy storage and knee variable-damping in exoskeleton design, and further the need for a lighter, more efficient hip actuator. In addition to augmenting the load carrying capacity of the human, the advancement of leg exoskeletons can contribute to the science of bipedal walking and lead to a better understanding of locomotory biomechanics, energetics and control.

8 Future Work

This section presents a number of possible areas to focus on gong forward.

Hip Actuator Redesign

It is clear that the actuator used in this thesis had a negative effect on metabolic rate. A more efficient, lightweight actuator requiring a smaller power supply used in conjunction with a spring at the hip could add sufficient power with minimal mass.

Minimize Kinematic Constraints

The results showed that the kinematic constraints from the exoskeleton on the gait of the wearer may have a negative effect on metabolic cost. Improvements to the foot and spine of the exoskeleton are shown in Chapter 3. These improvements may reduce the effect the exoskeleton has on human gait. The effect of these changes will be tested with further metabolic experiments. The medial-lateral rotation of the human and exoskeleton leg are not collocated and this leads to some discomfort in walking so this is another possible area for improvement.

Improved Knee

The knee of the exoskeleton can only dissipate energy. An improved design would be one that stores energy on heel strike that is then released to assist in raising the center of mass of the wearer. Further, the variable–damper mechanism used in the exoskeleton presented had intrinsic damping, even when off, that may have impeded the swinging of the human leg. A knee that would have zero resistance when off would be ideal.

Extensive Testing on Exoskeleton Gait and Effect of Distal Mass

The exoskeleton does affect the gait of the wearer. This could be thoroughly examined by taking measurements while walking in a gait lab with a motion capture system. The effect of the mass of the exoskeleton attached to the human leg could be examined by placing similar mass on the human leg and examining its affect on metabolic rate.

References

Bastien, G.J, Willems, P.A., Schepens, B., Heglund, N.C., (2005) 'Effect of load and speed on the energetic cost of human walking', *European Journal of applied Physiology,* 94: 76-83

van den Bogert, A.J. (2003), 'Exotendons for assistance of human locomotion'. *Biomedical Engineering Online*, 2:17.

Brockway JM. (1987) 'Derivation of formulae used to calculate energy expenditure in man', *Human Nutrition: Clinical Nutrition* 41: 463-471

Carlsoo, S. (1972) 'How man moves' *London: Heinemann*

Chu, A., Kazerooni, H. and Zoss, A., (2005) 'On the Biomimetic Design of the Berkeley Lower Extremity Exoskeleton', *Proceedings of the 2005 IEEE International Conference on Robotics and Automation, Barcelona, Spain,* pp. 4356 – 4363 (April)

Collins, S., Ruina, A., Tedrake, R., Wisse, M. (2005) 'Efficient Bipedal Robots Based on Passive-Dynamic Walker', *Science*, Vol. 307. no. 5712, pp. 1082-1085

Crowell, H., (1995) 'Human Engineering Design Guidelines for a Powered, Full Body Exoskeleton', *Army Research Laboratory, Technical Report*

Dalen, A., Nilsson, J. and Thorstensson, A. (1978) 'Factors influencing a prolonged foot march', *Stockholm Sweden: Karolinska Institute, FOA Report C50601-H6*

Deffenbaugh, B., Herr, H., Pratt, G., & Wittig, M. (2001) 'Electronically Controlled Prosthetic Knee', *US Patent 6,764,520.*

Donelan J.M., Kram, R., & Kuo, A.D. (2002), 'Mechanical work for step-to-step transitions is a major determinant of the metabolic cost of human walking', *Journal of Experimental Biology* pp. 205; 3717–372.

Farley, C.T. & Ferris, D.P. (1998), 'Biomechanics of Walking and Running: from Center of Mass Movement to Muscle Action', *Exercise and Sport Sciences Reviews* pp. 26:253-285.

Farley, C. & McMahon, T. (1992), 'Energetics of walking and running: insights from simulated reduced-gravity experiments', *The American Physiological Society* pp. 2709-2712.

Fletcher, C. (1974), 'The Complete Walker', *Alfred Knopf, New York*

General Electric Co., (1968) 'Hardiman I Prototype Project, Special Interim Study', *General Electric Report S6-68-1060*, Schenectady, NY 1968

Gottschall, J.S. & Kram, R. (2003) 'Energy cost and muscular activity required propulsion during walking', *Journal Applied Physiology* pp. 94: 1766–1772, 2003.

Griffen, T. M., Roberts, T. J., Kram, R. (2003) 'Metabolic cost of generating muscular force in human walking: insights from load carrying and speed experiments', *Journal Applied Physiology* 95: 172-183

Harman, E., Han, K., Frykman, P., Pandorf, C. (2000), 'The Effects of Backpack Weight on the Biomechanics of Load Carriage', *USARIEM Technical Report* pp. T100-17, Natick, Massachusetts.

Hausswirth C, Bigard AX, Lechevelier JM (1997), 'The Cosmed K4 telemetry system as an accurate device for oxygen uptake measurement during exercise', *International Journal of Sports Medicine* 18:449-453

Herr, H. & Wilkenfeld, A. (2003), 'User-Adaptive Control of a Magnetorheological Prosthetic Knee', *Industrial Robot: An International Journal* pp. 30: 42-55.

Huang, G.T. (2004), 'Demo: Wearable Robots', *Technology Review, July/*August

Inman, V.T., Ralston, H.J., & Todd., F. (1981), 'Human Locomotion', in: *Human Walking*, Rose, J. & Gamble, J. G., eds., Williams and Wilkins, Baltimore.

Jansen, J., Richardson, B., Pin, F., Lind, R. & Birdwell, J. (2000), 'Exoskeleton for soldier enhancement systems feasibility study', *Technical Report TM-2000/256,* Oak Ridge National Laboratory.

Jones, B.H., (1983) 'Overuse injuries of the lower extremities associated with marching, jogging and running: a review', *Military Medicine* 148, 783-788.

K4B2 User manual, X Edition (2004) 'COSMED' Srl., Rome, Part N. C01508-02-91, pp 14.

Kazerooni, H., Racine, J.L., Huang, L., & Steger, R. (2005), 'On the Control of the Berkeley Lower Extremity Exoskeleton (BLEEX)', *IEEE International Conference of Robotics and Automation* pp. 4364-4371.

Kirtley, C. (1998) 'CGA Normative Gait Database', *Hong Kong Polytechnic University, 10 Young Adults*, Available http://guardian.curtin.edu.au:16080/cga/data/

Kirtley, C. (1998) 'CGA Normative Gait Database', *Hong Kong Polytechnic University, 10 Old Adults*, Available http://guardian.curtin.edu.au:16080/cga/data/

Knapik, J., Harman, E., Reynolds, K., (1996). 'Load carriage using packs: a review of physiological, biomechanical and medical aspects', *Applied Ergonomics* 27, 207-215.

Knapik, J., Reynolds, K., Staab, J., Vogel, J.A. and Jones, B., (1992) 'Injuries associates with strenuous road marching', *Military Medicine* 157, 64 - 67

Linskell, J. (1997) 'CGA Normative Gait Database', *Limb Fitting Centre, Dundee, Scotland, Young Adult*, Available http://guardian.curtin.edu.au:16080/cga/data

Liu, X., Low, K. H., Yu, H. Y., (2004) 'Development of a Lower Extremity Exoskeleton for Human performance Enhancement', *IEEE Conf. On Intelligent Robots and Systems*, Sendai, Japan

Llyod R., & Cooke C.B. (2000) 'Kinetic changes associated with load carriage using two rucksack designs' *Ergonomics* 43(9), 1331-1341

Louhevaara, V., Smolander, J., Tuomi, T., Korhonen, O. and Jaakkola, J., (1985) 'Effects of an SCBA on breathing pattern, gas exchange, and heart rate during exercise' *J Occupational Medicine* 27, 213-216

McMahon, T. A., Valiant, G. & Frederick, E.C. (1987) 'Groucho Running', *Journal of Applied Physiology*, 62(6) 2326-2337

Oberg, E., Jones, F.D. & Horton, J.H. (2000), *Machinery's Handbook, 26th ed.* New York: Industrial Press, pp. 239.

Pandolf, K. B., B. Givoni , and R.F. Goldman (1978) 'Predicting energy expenditure with loads while standing or walking very slowly.', *J Applied Physiology* 43, 577-581

Palmer, M. L., (2002) 'Sagittal Plane Characterization of Normal Human Ankle Function Across a Range of Walking Gait Speeds', *MS Thesis*, MIT

Perry, J. (1992). *Gait Analysis: Normal and Pathological Function,* SLACK Inc., New Jersey.

Pratt, G. A., Williamson, M. M., (1995) 'Series Elastic Actuators', *IEEE RSJ International conference on Intelligent Robots and Systems*, PA

Pratt, J., Krupp, B., Morse, C., Collins, S., (2004) 'The RoboKnee: An Exoskeleton for Enhancing Strength and Endurance During Walking', *IEEE Conf. On Robotics and Automation*, New Orleans

Robinson, D., (2000) 'Design and analysis of series elasticity in closed-loop actuator force control', *PhD Thesis*, MIT

Royer, T.D. & Martin, P.E (2005) 'Manipulations of Leg Mass and Moment of Inertia: Walking', *Medicine & Science in Sports & Exercise*, pp. 37(4): 649-656

Sankai, Y., (2004) 'Hybrid Assistive Limb', http://sanlab.kz.tsukuba.ac.jp/HAL/

Sutherland, D.H., Kaufman, K.R., Moitoza, J.R. (1994), 'Kinematics of Normal Human Walking,' in: *Human Walking*, Rose, J. & Gamble, J. G., eds., Williams and Wilkins, Baltimore, pp. 38.

Tilley, A.R. (1993), 'The measure of man and woman,' in: *Human Factors Design*, Henry Dreyfuss Associates, New York, pp. 22–23.

Valiente, A., (2005), 'Design of a Quasi-Passive Parallel Leg Exoskeleton to Augment Load Carrying for Walking', *MS Thesis*, MIT

Vukobratović, M., Borovac, B., Surla, D., Stokić, D. (1990), *Biped Locomotion: Dynamics, Stability, Control, and Application*, Springer-Verlag, Berlin, pp. 321-330.

Wisse, Martijn (2004), 'Essentials of Dynamic Walking, Analysis and Design of two-legged robots', *PhD Thesis*, Technical University of Delft

Appendix A: Carbon Fiber Harness Construction

This appendix details briefly the procedure for the construction of the carbon fiber harness. Once the design of the harness was complete and modeled in CAD the next step was to cut 2D slices of the harness out of foam using the waterjet. The foam was cutting using just high pressure water on the waterjet cutter so as to provide a relatively smooth finish to the mount for layering over the carbon fiber. These 2D sections were then assembled to make a mold for the harness.

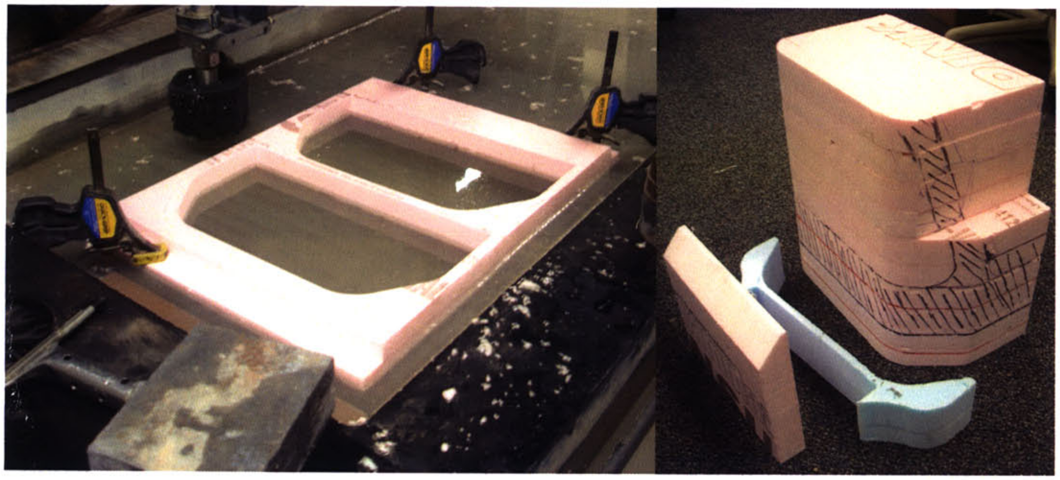

Figure A1 In a), cutting foam using the waterjet and b), the foam sections before being layered.

The figure below shows the assembled mold with carbon fiber layered over it. This part of the process was carried out by working with Bob Emerson. The carbon fiber was then trimmed to give the final harness as shown in Chapter 3.

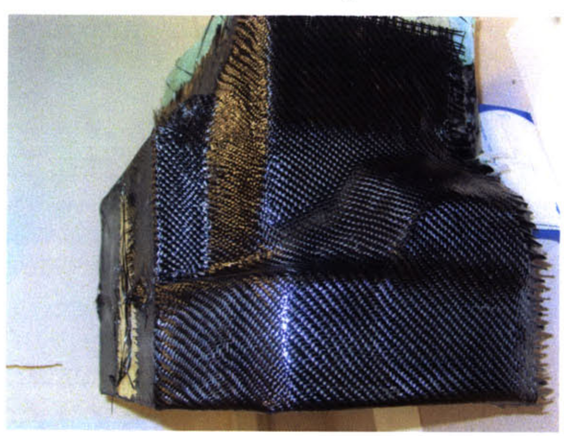

Figure A2 Assembled mold with carbon fiber layer over it.

Appendix B: Subject Consent Forms

CONSENT TO PARTICIPATE IN BIOMEDICAL RESEARCH

Leg Orthoses for Locomotory Endurance Amplification

You are invited to participate in a research study conducted by Dr. Hugh Herr, Ph.D., Dan Paluska, B.S.E, Conor Walsh, B.S.E, Andrew Valiente, B.S.E, and William Grand, B.S.E from the Media Lab: Biomechatronics Group at the Massachusetts Institute of Technology (M.I.T.). You have been invited to participate in this study because you are a member of the MIT Biomechatronics Group and are involved in the design of the orthosis. You will be invited to be one of four subjects in this study. You should read the information below, and ask questions about anything you do not understand, before deciding whether or not to participate.

· PARTICIPATION AND WITHDRAWAL

Your participation in this research is completely VOLUNTARY. If you choose to participate you may subsequently withdraw from the study at any time without penalty or consequences of any kind. If you choose not to participate, that will not affect your relationship with M.I.T. or your right to health care or other services to which you are otherwise entitled or will not cause you to lose your research compensation.

· PURPOSE OF THE STUDY

We would like permission to enroll you as a participant in a research study. The purpose of this study is to develop a robust, low-power, stable, and lightweight leg orthosis that will dramatically increase the locomotory endurance of walking and running. The orthosis system will run parallel to your body, transmitting forces between the ground and your leg, thigh and torso as you stand, walk and run. Orthosis forces will effectively reduce the fraction of your body weight borne by your stance legs. As well as this the device will be attached to a backpack loaded up to a maximum of 75lbs and the orthosis will reduce the fraction of this load borne by your stance legs. Instead of your leg actively stiffening to support the weight throughout each locomotory step, the parallel orthosis will offer that support, deactivating your leg muscles and dramatically lowering metabolic demands. Your opinion is needed regarding the comfort level of the system. We also want to measure your rate of oxygen consumption using a VO2 machine while you walk/run to see if wearing the exoskeleton decreases your metabolic rate.

· DEVICE DETAILS

The leg orthosis will comprise motor and variable- impedance systems previously developed for robotic and human rehabilitation applications. To augment hip movements, a series-elastic actuator (SEA), previously developed for legged robots, will be employed to power hip flexion-extension actions during walking and running..Variable-damping

and variable-spring mechanisms will be placed in parallel to the knee to augment leg impedance. During level ground ambulation, knee damping will be controlled during the swing phase to dissipate energy and to decelerate the swinging leg.
In distinction, throughout early to midstance, knee damping will be minimized and a variable spring mechanism will be engaged to resist the knee buckling moment of early stance. Similar to the knee, the orthotic ankle will act primarily as variable-impedance device during ambulation.
The orthosis will be custom fit and will consist of several rigid carbon fiber sections. The rigid sections, which look like body armor, are needed so that the springs and mechanical devices can be mounted. The rigid sections will be custom fit and made by a professional orthotist from Next Step Inc. at North Andover, MA. The orthotist will need to cast your lower body in plaster to make a mold for the rigid carbon fiber harness that would be used. The rigid sections will have a layer of protective material such as silicon between the rigid sections and the skin for comfort.

· **PROCEDURES**

If you volunteer to participate in this study, we would ask you to do the following things:
A professional orthotist will make you a customized carbon fiber orthosis, by first casting you in plaster from the torso down. This casting would be done at Next Step Inc. of North Andover, MA. The casting process typically takes several hours.
You will be asked to wear the soft- lined rigid orthosic interface structure during walking and running. This is so we can know if the orthosis interface is comfortable and that we can correct any discomfort locations before we proceed with anymore testing. This should take about two hours.
Once walking and running is comfortable with the orthotic interface, we will proceed with your permission to test the hypothesis of our experiment – to see if the orthosis does, in fact, reduce the metabolic cost of walking and running. You will be asked to wear a Cosmed Oxygen Consumption (V_{O2}) mask which will measure the rate with which you consume oxygen and will determine your metabolic rate. Two hours prior to testing, you will be asked not to eat. The procedure will be as follows:

Walking:
You will wear the V_{O2} system and walk for 8 minutes on the treadmill to establish a control metabolic rate. After resting for 8 minutes, you will wear the orthosis and get acclimated to the device by walking for 5 minutes. You will then walk on the treadmill for 8 minutes as we measure your metabolic rate with the device. You will then rest for another 8 minutes. This protocol will be repeated two additional times, and the entire experiment will take approximately 2 hours.

Throughout the study, you will be videotaped and photographed to document the affect that the orthosis has on walking and running. This video would be used in conferences and may be published on the internet. If you volunteer to this study you ARE giving consent to be videotaped and photographed and that this media may be published at the discretion of the investigators involved.

· POTENTIAL RISKS AND DISCOMFORTS

Falling:
1. As with any orthotic walking, there is a small risk of falling during the trials. This will be minimized by having parallel bars and by having a safety harness attached to the ceiling. If a backpack is being used then there will be a safety harness attached between the backpack and the ceiling.
2. The electronics will have two kill switches, one on the operator and one remote so that either the subject or the investigator can immediately disable the device.
3. If you become too fatigued you may ask to rest or stop the study at any time.
4. Since the orthosis is mechanical, there is a risk of malfunction. The developers will make every effort to reduce this risk, but if a malfunction occurs, you will have standard parallel bars to catch you. If you fail to catch yourself with the parallel bars, a safety harness will hold you upright.
Orthosis discomfort:
5. As with any orthotic device, there is also potential physical discomfort from wearing the orthosis. This will be minimized by having a professional orthotist design and modify a customized orthotic for your use.
Other:
6. This device is investigational and it may involve risks that are currently unforeseeable.
7. Your participation in this study may be terminated by the investigator if they feel there are excessive risks from the device being tested.

· ANTICIPATED BENEFITS TO SUBJECTS

The potential benefits may include:
1. There are no known direct benefits for participating in this experiment. The orthosis being developed is a prototype and will not be immediately available.
2. You should not expect your ambulation to improve as a result of participating in this research

· ANTICIPATED BENEFITS TO SOCIETY

1. The orthosis may help reduce the metabolic cost of walking and running. This device may also help those with weak legs or other physical disabilities.

· ALTERNATIVES TO PARTICIPATION

This research is a study to augment normal human endurance and decrease normal human metabolic cost in waling and running using an assistive device. Your alternative is to not participate in the study.

· PAYMENT FOR PARTICIPATION

Subjects will not be paid for participating in this study. The subject would however receive research compensation for the design of the orthosis which is independent of involvement in this study.

· POSSIBLE COMMERCIAL PRODUCTS

The orthosis may be become a commercial product as an assistive device for running and walking. It may have both military and rehabilitative applications.

· FINANCIAL OBLIGATION

Neither you nor your insurance company will be billed for your participation in this research.

· PRIVACY AND CONFIDENTIALITY

The only people who will know that you are a research subject are members of the research team and, if appropriate, your physicians and nurses. No information about you, or provided by you during the research will be disclosed to others without your written permission, except: if necessary to protect your rights or welfare, or if required by law. When the results of the research are published or discussed in conferences, no information, other than the photographs or videos, will be included that would reveal your identity. If photographs, videos, or audio-tape recordings of you will be used for educational purposes, your identity will be protected in that your name or other identifiers will not be mentioned. Your face however may be recognizable in the photograph or video.

The videotapes and photos will be under the control of the MIT Media Laboratory's Biomechatronics Group. After the results are published, a copy of the photos and videos will be kept on file in the laboratory for future reference. A video clip or some photographs may be published on the group's website, available to the general public, as a sample of the work that has been developed.

· WITHDRAWAL OF PARTICIPATION BY THE INVESTIGATOR

The investigator may withdraw you from participating in this research if circumstances arise which warrant doing so. If you experience any of the following side effects extreme tiredness or irregular breathing or if you become ill during the research, you may have to drop out, even if you would like to continue. The investigator, Hugh Herr, will make the decision and let you know if it is not possible for you to continue. The decision may be made either to protect your health and safety, or because it is part of the research plan that people who develop certain conditions may not continue to participate.

· **NEW FINDINGS**

During the course of the study, you will be informed of any significant new findings (either good or bad), such as changes in the risks or benefits resulting from participation in the research or new alternatives to participation, that might cause you to change your mind about continuing in the study. If new information is provided to you, your consent to continue participating in this study will be re-obtained.

· **EMERGENCY CARE AND COMPENSATION FOR INJURY**

In the unlikely event of physical injury resulting from participation in this research you may receive medical treatment from the M.I.T. Medical Department, including emergency treatment and follow-up care as needed. Your insurance carrier may be billed for the cost of such treatment. M.I.T. does not provide any other form of compensation for injury. Moreover, in either providing or making such medical care available it does not imply the injury is the fault of the investigator. Further information may be obtained by calling the MIT Insurance and Legal Affairs Office at 1-617-253-2822.

· **IDENTIFICATION OF INVESTIGATORS**

In the event of a research related injury or if you experience an adverse reaction, please immediately contact one of the investigators listed below. If you have any questions about the research, please feel free to contact Hugh Herr at (617) 258-6574 or at Building E15, Room 419, 20 Ames Street, Cambridge, MA.

· **RIGHTS OF RESEARCH SUBJECTS**

You are not waiving any legal claims, rights or remedies because of your participation in this research study. If you feel you have been treated unfairly, or you have questions regarding your rights as a research subject, you may contact the Chairman of the Committee on the Use of Humans as Experimental Subjects, M.I.T., Room E32-335, 77 Massachusetts Ave, Cambridge, MA 02139, phone 1-617-253 6787

SIGNATURE OF RESEARCH SUBJECT OR LEGAL REPRESENTATIVE

I have read (or someone has read to me) the information provided above. I have been given an opportunity to ask questions and all of my questions have been answered to my satisfaction. I have been given a copy of this form.

BY SIGNING THIS FORM, I WILLINGLY AGREE TO PARTICIPATE IN THE RESEARCH IT DESCRIBES.

____
Name of Subject

____
Name of Legal Representative (if applicable)

____ _______________
Signature of Subject or Legal Representative Date

SIGNATURE OF INVESTIGATOR

I have explained the research to the subject or his/her legal representative, and answered all of his/her questions. I believe that he/she understands the information described in this document and freely consents to participate.

____
Name of Investigator

____ ______________________________
Signature of Investigator Date (must be the same as subject's)

SIGNATURE OF WITNESS (If required by COUHES)

My signature as witness certified that the subject or his/her legal representative signed this consent form in my presence as his/her voluntary act and deed.

____
Name of Witness

____ ______________________________